Performance Enhancement of Power System Operation and Planning through Advanced Advisory Mechanisms

by

Jonghwan Kwon

A Dissertation Presented in Partial Fulfillment
of the Requirements for the Degree
Doctor of Philosophy

Approved October 2017 by the
Graduate Supervisory Committee:

Kory Hedman, Chair
Gerald Heydt
Vijay Vittal
Jiangchao Qin

ARIZONA STATE UNIVERSITY

December 2017

ABSTRACT

This research develops decision support mechanisms for power system operation and planning practices. Contemporary industry practices rely on deterministic approaches to approximate system conditions and handle growing uncertainties from renewable resources. The primary purpose of this research is to identify soft spots of the contemporary industry practices and propose innovative algorithms, methodologies, and tools to improve economics and reliability in power systems.

First, this dissertation focuses on transmission thermal constraint relaxation practices. Most system operators employ constraint relaxation practices, which allow certain constraints to be relaxed for penalty prices, in their market models. A proper selection of penalty prices is imperative due to the influence that penalty prices have on generation scheduling and market settlements. However, penalty prices are primarily decided today based on stakeholder negotiations or system operator's judgments. There is little to no methodology or engineered approach around the determination of these penalty prices. This work proposes new methods that determine the penalty prices for thermal constraint relaxations based on the impact overloading can have on the residual life of the line. This study evaluates the effectiveness of the proposed methods in the short-term operational planning and long-term transmission expansion planning studies.

The second part of this dissertation investigates an advanced methodology to handle uncertainties associated with high penetration of renewable resources, which poses new challenges to power system reliability and calls attention to include stochastic modeling within resource scheduling applications. However, the inclusion of stochastic modeling

within mathematical programs has been a challenge due to computational complexities. Moreover, market design issues due to the stochastic market environment make it more challenging. Given the importance of reliable and affordable electric power, such a challenge to advance existing deterministic resource scheduling applications is critical. This *ongoing* and *joint* research attempts to overcome these hurdles by developing a stochastic look-ahead commitment tool, which is a stand-alone advisory tool. This dissertation contributes to the derivation of a mathematical formulation for the extensive form two-stage stochastic programming model, the utilization of Progressive Hedging decomposition algorithm, and the initial implementation of the Progressive Hedging subproblem along with various heuristic strategies to enhance the computational performance.

DEDICATION

This dissertation is dedicated with love to my parents, Taeju Kwon and Soonjeong Kim. They were always providing all sorts of tangible and intangible support and encouraging me with their best wishes.

My lovely wife, Soyeon Joo, received the greatest appreciation. She has assisted me in innumerable ways, whatever I might say here cannot do full justice to the extent and the value of her contribution. Lastly, this dissertation is dedicated to my two sons, James and Jason, who brought many beautiful stories to my life. Words cannot express how much I love you all.

ACKNOWLEDGMENTS

I would like to express the deepest appreciation to my advisor, Dr. Kory W. Hedman (Associate Professor, School of Electrical, Computer, and Energy Engineering), for the advice, mentoring, and providing me with an excellent atmosphere for doing research. Without his guidance and persistent help this dissertation would not have been possible. I would like to thank Dr. Vijay Vittal for his advice and valuable insights during the Pserc projects. I would also like to thank Dr. Gerald Heydt for his valuable feedback on this research. In addition, a thank you to Dr. Jiangchao Qin for his time and effort to review this dissertation.

I would like to thank the Power Systems Engineering Research Center (PSerc) as well as the Advanced Research Projects Agency-Energy (ARPA-E) with the U.S. Department of Energy (DOE) for the financial contributions.

My appreciation also extends to my colleagues and friends for their encouragement and support. Xingpeng Li and Nikita Singhal, your help in my research was imperative. Thank you for your friendship.

TABLE OF CONTENTS

Page

CHAPTER Page

CHAPTER Page

LIST OF TABLES

Table Page

Table Page

LIST OF FIGURES

NOMENCLATURE

ACCR	Aluminum Conductor Composite Reinforced
ACOPF	Alternating Current Optimal Power Flow
ACSR	Aluminum Conductor Steel Reinforced
B_k	Electrical susceptance for line *k.*
c	Index for generator contingency $c \in C$.
c_{kt}	Degradation cost for line k in period t.
C_g^{NS}	Non-spinning reserve cost of generator g.
C_g^{NL}	No-load cost of generator g.
C_g^{op}	Production cost of generator g.
C_{gi}^{op}	Production cost of generator g for segment i.
$C_g^{reg\_dn}$	Cost of regulation down reserve of generator g.
$C_g^{reg\_up}$	Cost of regulation up reserve of generator g.
C_g^{SD}	Shutdown cost of generator g.
C_g^{SP}	Spinning reserve cost of generator g.
C_g^{SU}	Startup cost of generator g.
C_k^{ED}	End of service cost for line *k.*
C_{wi}	Operational cost of renewable generator w for segment i.
CAISO	California ISO
$Collect_k^j$	Collected conductor degradation cost for line k at iteration j.
CR	Constraint Relaxation

d	Index for day types.
d_{kt}	Degradation effect for line k in period t.
di	Conductor diameter [inches].
D_i	Operating duration at relaxation point i.
D_i^{eq}	Operating duration at relaxation point i.
D_{nt}	Real power demand at node n in period t.
D_{nt}^0	Initial real power demand at node (bus) n in period t.
D_{T_c}	Operating duration at temperature T_c [Hours].
DCOPF	Direct Current Optimal Power Flow
Deg_{al}^+	Maximum degradation level of aluminum strands.
Deg_T	Loss of tensile strength of a whole conductor [%].
Deg_T^+	Maximum degradation level of a whole conductor.
D_{zt}^{Supp}	Supplemental reserve deployment factor for the largest contingency event in zone z during time t.
D_{zt}^{Spin}	Spinning reserve deployment factor for the largest contingency event in zone z during time t.
$Expect_k^j$	Expected conductor degradation cost for line k at iteration j.
f_{kt}	Pre-contingency real power flow on line k in period t.
F_{kt}^0	Initial pre-contingency real power flow on line k in period t.
$F_{kt}^{\mathrm{a}+}$	Real power maximum limit (rate A) for line k in period t.
$F_{kt}^{\mathrm{c}+}$	Real power maximum emergency limit (rate C) for line k in period t.
f_{kt}^{over}	Slack variables for line overloading on line k in period t.

FMP	Flowgate Marginal Price
FTR	Financial Transmission Rights
g	Index for generator, $g \in \Omega_G$.
G^{AGC}	Subset of generators with AGC capability, $G^{AGC} \subset \Omega_G$.
G^{fast}	Subset of generators with fast-start capability, $G^{fast} \subset \Omega_G$.
G^n	Subset of generators at node (bus) n, $G^n \subset \Omega_G$.
G_k	Electrical conductance for line *k*.
GDF_{gt}^c	Generator loss distribution factors.
h_{kt}	Line temperature variable for line *k* [°C].
h_{kt}^+	Positive segments of overloaded temperature on line *k* in period t.
h_{kt}^-	Negative segments of overloaded temperature on line *k* in period t.
H_k^{tr}	Overheating threshold for line *k* [°C].
H_k^+	Maximum temperature for line *k* [°C].
H_∞	Room temperature [°C].
HTLS	High Temperature Low Sag Conductors
i	Index for segments, $i \in I$.
i_{kp}	Line investment decision on investment option *p* for line *k*.
is_{kyp}^{st1}	Investment status of option *p* in investment subproblem for line *k* in year *y*.
is_{kyp}^{st2}	Investment status of option *p* in production cost subproblem for line *k* in year *y*.
I_p	Capital cost of investment option *p* [$/Mile].
ISO	Independent System Operator

k	Index for transmission asset (line or transformer) $k \in K$.
ℓ	Index for transmission contingency $\ell \in L$; $\ell = 1$ means loss of line 1.
l^{+}_{ktdy}	Total losses on line *k* represented at the 'from bus'.
l^{-}_{ktdy}	Total losses on line *k* represented at the 'to bus'.
l_{nt}	Total losses on all lines connected and delivering power to bus *n* in period t.
L_k	Length of line *k*, [Mile].
LMP	Locational Marginal Price
LODF_{lk}	Line outage distribution factor for the loss of transmission asset (line or transformer) ℓ and the resulting impact on transmission asset k.
LR	Lagrange Relaxation
LS_k^{Temp}	Temperature effect term in the degradation decomposition model for line *k*.
LS_k^{Time}	Time effect term for in the degradation decomposition model for line *k*.
mC_P	Total heat capacity of conductor [J/(m-°C)].
M	Big M values.
M_t	Time interval length for period t.
MIP	Mixed Integer Programming
MISO	Midcontinent ISO
n	Index for node (bus) $n \in N$.
N^c	Number of candidate lines.
N_d	Number of days for day type *d*.
NERC	North American Electric Reliability Corporation
NYISO	New York ISO

OMC	Out-of-Market Correction
OPF	Optimal Power Flow
p	Index for investment candidates.
p_{gt}	Real power output of generator g in period t.
p_{gti}	Real power output for segment i of generator g in period t.
p_{gtis}	Real power output for segment i of generator g in period t for scenario s.
p_{gts}	Real power output of generator g in period t for scenario s.
p_{nt}^{inj}	Net power injection at node n.
p_{wt}	Renewable real power dispatch for renewable generator w in period t.
p_{wti}	Renewable real power dispatch for segment i of renewable generator w in period t.
p_{wtis}	Renewable real power dispatch for segment i of renewable generator w in period t for scenario s.
p_{wts}	Renewable real power dispatch for renewable generator w in period t for scenario s.
p_{wts}^{slack}	Renewable real power dispatch for slack segment of renewable generator w in period t for scenario s.
P_g^-	Real power minimum output of generator g.
P_g^+	Real power maximum output of generator g.
P_{gt}^0	Initial real power output of generator g in period t.
P_{gt}^W	Real power output of wind farm g.

P_k^j	Transmission thermal constraint relaxation penalty price for line k at iteration j.
P_{wt}^0	Initial renewable real power dispatch for renewable generator w in period t for the base case.
$\overline{P_{wt}}$	Renewable real power forecast for renewable generator w in period t.
P_{wti}^+	Renewable real power maximum segment i bid for renewable generator w in period t.
$\overline{P_{wts}}$	Renewable real power forecast for renewable generator w in period t for scenario s.
PH	Progressive Hedging
PJM	Pennsylvania-New Jersey-Maryland Interconnection
PTDF_{nk}^R	Power transfer distribution factor for an injection at n sent to the reference bus, for flow on line k.
$PTDF_{zk}^{res}$	Aggregated sensitivity of the flow on transmission element k to the requirement for deployed reserve type (i.e., regulation up/down, spinning or non-spinning) in zone z and a corresponding withdrawal at the reference bus.
$PTDF_{zk}^{TRIP}$	Aggregated sensitivity of the flow on transmission element k to the largest generator contingency in zone z
PYOMO	Python optimization modeling objects
q_{kt}	Reactive power flow in line k in period t.
q_{gt}	Reactive power output of generator g in period t.
Q_C	Forced convection heat loss [W/m].

Q_g^+ Reactive power maximum output of generator g.

Q_g^- Reactive power minimum output of generator g.

Q_n Reactive power demand at node n.

Q_R Radiated heat loss [W/m].

Q_S Solar heat gain [W/m].

r_{gt}^{sp} Spinning reserve provided by generator g.

r_{gt}^{ns} Non-spinning reserve provided by generator g.

$r_{gt}^{reg_{dn}}$ Regulation reserve down for generator g in period t.

$r_{gt}^{reg_{up}}$ Regulation reserve up for generator g in period t.

$r_{gt}^{spin_{dn}}$ Spinning reserve down for generator g in period t.

$r_{gt}^{spin_{up}}$ Spinning reserve up for generator g in period t.

$r_{gt}^{w_{dn}}$ Renewable (spin) reserve down for generator g in period t.

$r_{gt}^{w_{up}}$ Renewable (spin) reserve up for generator g in period t.

r_{gtc} Activated (deployed) ten-minute reserve from generator g in response to generator contingency c for the base case renewable scenario in period t.

r_{gtcs} Activated (deployed) ten-minute reserve from generator g in response to generator contingency c during renewable scenario s in period t.

$r_{gts}^{reg_{dn}}$ Regulation reserve down for generator g in period t for scenario s.

$r_{gts}^{reg_{up}}$ Regulation reserve up for generator g in period t for scenario s.

$r_{gts}^{spin_{dn}}$ Spinning reserve down for generator g in period t for scenario s.

$r_{gts}^{spin_{up}}$	Spinning reserve up for generator g in period t for scenario s.
r_t^{req}	Required level of operating reserve.
R_g^5	Five-minute ramp rate of generator g.
R_g^{10}	Ten-minute ramp rate of generator g.
R_g^{dn}	Inter-temporal ramp rate down limit of generator g.
R_g^{HR}	Maximum ramp up and down rate of generator g.
R_g^{SD}	Maximum shutdown ramp rate of generator g.
R_g^{SU}	Maximum startup ramp rate of generator g.
R_g^{up}	Inter-temporal ramp rate up limit of generator g.
R_t^{cont}	Contingency reserve requirement in period t; fixed discretionary input.
$R_t^{reg_{dn}}$	Regulation reserve down requirement in period t; fixed discretionary input.
$R_t^{reg_{up}}$	Regulation reserve up requirement in period t; fixed discretionary input.
r_{zt}^{Spin}	Spinning reserve scheduled from zone z in time t.
r_{zt}^{Supp}	Supplemental reserve scheduled from zone z in time t.
ROW	Rights-of-Way
RS_{al}	Residual tensile strength of an aluminum strand [%].
RTS	Reliability Test System
s	Index for renewable scenario $s \in S$.
s_{gt}	Startup variable for generator g in period t.
$st2$	Index for sub problems.
S_i^L	Slope of segment *i* for loss approximation.

S_i^T	Slope of segment *i* for line temperature approximation.
S_k^+	Apparent power maximum limit for line *k*.
SCED	Security Constrained Economic Dispatch
SCUC	Security Constrained Unit Commitment
$\overline{SL_\iota}$	Length of each relaxation point i.
SLAC	Stochastic Look-Ahead Commitment
SOPF	Stochastic Optimal Power Flow
SPP	Southwest Power Pool
STR_{al}	Initial strength of aluminum strands [lb_f]
STR_{st}	Initial strength of a steel core [lb_f]
STR_T	Initial strength of a whole conductor [lb_f]
t	Index for time periods, $t \in$ T.
T^+	Predetermined maximum line temperature [°C].
T_a	Air temperature [°C]
T_i	Anticipated line temperature at relaxation point i.
T_k^+	Length of allowable overheating for line *k*.
TCDC	Transmission Constraint Demand Curves
TCR	Transmission Thermal Constraint Relaxation
TEP	Transmission Expansion Planning
u_{gt}	Unit commitment variable for generator g in period t.
$\overline{U_{gt}}$	Scheduled commitment status for generator g in period t.
v_{gt}	Startup variable for generator g in period t.

v_n	Voltage variable at node n.
V_n^-	Minimum bus voltage at node *n*.
V_n^+	Maximum bus voltage at node *n*.
w	Index for renewable generator, $w \in \Omega_G^W$.
w_{gt}	Shutdown variable for generator g in period t.
W^n	Subset of renewable generators at node n, $W^n \subset \Omega_G^W$.
W_s	Wind speed [ft/s]
WECC	Western Electricity Coordination Council
X_k	System operating condition.
y	Index for years, $y \in$ Y.
$Y(\varphi)$	Conductor temperature states in weather condition φ.
z	Index for reserve zones, $z \in Z$.
z_{ktdyi}^+	Binary variable of positive segment *i* for line *k*.
z_{ktdyi}^-	Binary variable of negative segment *i* for line *k*.
α_t^{dn}	Regulation reserve down requirement relative to net load for period t [%].
α_t^{up}	Regulation reserve up requirement relative to net load for period t [%].
β	Shape parameter of a Weibull distribution.
γ	Scale parameter of a Weibull distribution.
$\overline{\delta_i^+}$	Length of segment *i*.
δ_{kti}^+	Length of positive segment i on line *k* in period t.
δ_{kti}^-	Length of negative segment i on line *k* in period t.
θ^+	Maximum voltage angle difference.

θ^-	Minimum voltage angle difference.
θ_{nt}	Voltage angle at node n.
κ_y	Discount factor in year y.
μ	Adjustment factor for the degradation decomposition model.
π_s	Probability of renewable scenario s.
σ	Shape parameter a Normal distribution.
τ_y	Salvage factor in year y.
υ	Scale parameter a Normal distribution.
φ	Joint weather condition.
Ω^{LC}	Set of frequently congested critical transmission lines.
Ω_D	Set of day types, $d \in \Omega_D$.
Ω_G	Set of generators, $g \in \Omega_G$.
Ω_G^H	Set of hydro units, $\Omega_G^H \in \Omega_G$.
Ω_G^n	Set of generators connected to bus n.
Ω_G^W	Set of wind farms, $\Omega_G^W \in \Omega_G$.
Ω_K	Set of transmission lines, $k \in \Omega_K$.
Ω_K^-	Set of lines need decomposition routine.
Ω_K^C	Set of candidate lines, $\Omega_K^C \in \Omega_K$.
Ω_K^F	Set of existing lines, $\Omega_K^F \in \Omega_K$.
Ω_K^{n+}	Set of lines specified as 'from' bus n.
Ω_K^{n-}	Set of lines specified as 'to' bus n.
Ω_N	Set of buses, $n \in \Omega_N$.

CHAPTER 1. INTRODUCTION

1.1. Motivation and Research Objectives

Power systems are among the largest and most complex systems in the world. Independent system operators (ISOs), regional transmission operators, or vertically integrated utilities, which will be referred as ISOs throughout this dissertation, must maintain a reliable and economical supply of electric energy continuously. To do this, system planners and operators manage various simulation tools, which include market optimization models, for long-term capacity expansion planning as well as short-term operational planning. This research aims to investigate the possible room for improvement of the contemporary power system operational practices and to enhance the system reliability as well as market transparency. Particularly, this research proposes innovative algorithms, methodologies, and tools to provide operational guidance to system planners, operators and market models.

First, the research focuses on constraint relaxation (CR) practices. ISOs solve market optimization models, such as security constrained unit commitment (SCUC) or security constrained economic dispatch (SCED), to manage generation scheduling economically while respecting complex operational and reliability requirements as well as strict physical restrictions of the system. All ISOs in the US already employ CR practices, which allow certain constraints to be relaxed for penalty prices, in their market models. That is, instead of strictly adhering to all the approximated system conditions, operators treat certain constraints as soft constraints by adding slack variables into the constraints and penalty terms into the objective function. Although ISOs employ CR practices on a much broader basis,

this research only focuses on transmission thermal constraint relaxations (TCR) that allow a line flow to exceed its flow rating, based on a predefined penalty price. Due to the influence that penalty prices have on generation scheduling and market settlements, it is important to ensure that ISOs set penalty prices such that economic (price) signals avert market inefficiencies. The research motivation emerged from the fact that the existing industry practices for defining penalty prices are neither transparent nor systematic; rather, the contemporary processes rely on the operators' judgment and stakeholder negotiations. Thus, it is crucial to develop a systematic penalty price determination methodology. This research introduces penalty price determination methodologies for TCR while considering a reduced service life of an asset from the relaxations. This work investigates the importance of acknowledging the existing operational practices, TCR, along with the proposed methodologies in short-term operational planning and long-term transmission expansion planning (TEP) studies. The results show that exercising TCR with a proper selection of penalty prices can provide net benefits to market participants. Particularly, the first part of this dissertation focuses on the following areas:

(1) A linearization method for the conductor temperature and degradation effect estimation.

(2) A static TEP model that determines optimal conductor size and path for a large wind farm integration while considering TCR along with the linearized conductor temperature and degradation estimation model.

(3) A dynamic TEP model that considers various methods, including TCR, to increase transmission capacity while preserving existing rights-of-way (ROW).

(4) An offline risk-based penalty price determination model for TCR that provides fixed penalty prices based on the degradation risk while considering probabilistic weather conditions.

(5) An online penalty price determination model for TCR that provides staircase penalty prices based on the marginal degradation effect.

The second part of this dissertation investigates an advanced methodology to secure the system reliability at least cost based on stochastic optimization. Recently, significant attention has been given to renewable energy technologies, such as wind and solar, to meet the grand challenge of power system sustainability and to achieve power system security. In addition to the frequently changing system operating conditions due to load forecasting deviations and system resource contingencies, the uncertainty and variability associated with the increasing penetration of renewable resources pose new challenges to power system reliability. However, combining uncertainty modeling within resource scheduling applications, such as SCUC and SCED, presents two practical barriers: (1) computational complexity of the resulting stochastic optimization algorithm, and (2) market objections primarily due to the complications associated with pricing in a stochastic market environment. As a result, most of the contemporary power system operational frameworks use operating reserves in a deterministic manner along with various approximations to handle the uncertainties. However, with such inherent approximations, the existing industry practices can cause unreliable operating state and require expensive out-of-market corrections (OMCs) to adjust resource schedules to account for modeling inaccuracies. This ongoing and joint research attempts to overcome hurdles above by developing a stochastic look-

ahead commitment (SLAC) tool, which is a stand-alone advisory tool. The proposed SLAC tool has two main modules. The first module is a two-stage stochastic programming model, for stochastic resource scheduling applications, which leverages statistical information of an ensemble of scenarios and their respective likelihoods. The second module is proposed to be a solution translation tool that processes the output from the first module and generates information to be communicated with system operators and market models. This dissertation contributes to the derivation of a mathematical formulation for the extensive form two-stage stochastic programming model, the utilization of Progressive Hedging (PH) decomposition algorithm, and the initial implementation of the PH subproblem along with various heuristic strategies to enhance the computational performance.

1.2. Main Contribution

The main contributions of this dissertation are summarized as follows:

In Chapter 5, this study proposes a linearization approach for the conductor temperature and degradation effect estimation. The work evaluates the proposed method with two long-term TEP models. The Lagrange relaxation (LR) based decomposition algorithm is applied to solve the mixed integer programming (MIP) problems in a parallel computing environment.

In Chapter 6, this research proposes an offline-based penalty price determination model for TCR; the model determines fixed penalty prices for a set look-ahead period. The model captures the cost of violating transmission thermal limits based on the conductor degradation risk. The conductor degradation risk quantification considers probabilistic weather conditions.

In Chapter 7, this work introduces an online-based penalty price determination model for TCR; the model determines staircase penalty prices based on the marginal degradation effect along with the conductor temperature anticipation. The model simultaneously captures the impact of magnitude and duration of the relaxations and provides penalty prices to a real-time SCED model at each execution interval.

In Chapter 8, this thesis presents a two-stage stochastic programming model for the SLAC tool. A horizontal decomposition technique, PH, is used along with various heuristic techniques to preserve the scalability of the model. Also, an actual large-scale PJM test system is used to evaluate the computational performance of the PH subproblem.

1.3. Dissertation Organization

This dissertation is organized into nine chapters. Chapter 2 provides background and technical details of power system operation and planning, which are helpful to understand later chapters. Chapter 3 presents the literature review on TCR and TEP.

Chapter 4 focuses on the conductor degradation effect. The chapter introduces the thermal dynamics of overhead conductors, current-temperature relationship of the overhead conductor, and the effect of elevated temperature operation.

Chapter 5 presents a linearization approach for conductor temperature and degradation effect estimation. The proposed method was applied into the two long-term TEP models as a set of constraints. First, the chapter introduces a static TEP model, which provides an optimal conductor size and path for a large wind farm integration, while employing TCR combined with the linearized conductor degradation model. Second, the chapter presents a

dynamic TEP model, which can consider various means to increase transmission capacity, while preserving existing ROW.

Chapter 6 introduces an offline-based penalty price determination model for TCR; the model determines fixed penalty prices for a set look-ahead period while considering the conductor degradation risks.

Chapter 7 presents an online-based penalty price determination model for TCR. The model provides staircase penalty prices, which are defined based on the marginal degradation effect, to a real-time SCED model at each execution interval.

Chapter 8 introduces a core description of the research approach to handle the uncertainties associated with the increasing penetration of renewable resources through a stochastic optimization technique. Moreover, the chapter includes the main contribution of this dissertation.

Chapter 9 devoted to concluding remarks and future work.

CHAPTER 2. POWER SYSTEM OPERATIONS AND PLANNING

This chapter provides the background knowledge necessary to understand the technical details in the subsequent chapters. The information in this chapter also provides context for this dissertation. First, this chapter reviews the modeling of optimal power flow (OPF), SCUC and SCED. Second, the chapter introduces CR practices. Lastly, the chapter describes the TEP concept and the means of increasing transmission system capacity.

2.1. Power System Scheduling

2.1.1. Alternating Current Optimal Power Flow Studies

The OPF problem, generally, minimizes the total production cost subject to the system and resource constraints. These constraints include power flows, bus voltage magnitudes, bus voltage angles as well as generator capacities.

The alternating current optimal power flow (ACOPF) problem uses the AC power flow equations in the constraints. Due to the nonconvexity of the problem, obtaining a solution for large-scale ACOPF problems is challenging even with an advanced algorithms for non-linear problems. The general mathematical formulation of the ACOPF problem takes the following form,

$$\text{Min } \sum_g (C_g^{op} p_g) \tag{2.1}$$

$$\sum_g p_g + \sum_{\forall \Omega_K^{n-}} f_k - \sum_{\forall \Omega_K^{n+}} f_k = D_n \qquad \forall n \tag{2.2}$$

$$\sum_{\forall \Omega_G^{n}} q_g + \sum_{\forall \Omega_K^{n-}} q_k - \sum_{\forall \Omega_K^{n+}} q_k = Q_n \qquad \forall n \tag{2.3}$$

$$\| f_k^2 + q_k^2 \| \le S_k^+ \qquad \forall k \tag{2.4}$$

$$P_g^- \le p_g \le P_g^+ \qquad \forall g \tag{2.5}$$

$$Q_g^- \leq q_g \leq Q_g^+ \qquad \forall g \qquad (2.6)$$

$$V_n^- \leq v_n \leq V_n^+ \qquad \forall n \qquad (2.7)$$

$$\theta^- \leq \theta_n - \theta_m \leq \theta^+ \qquad \forall k \qquad (2.8)$$

where the complex power flow equations for a line *k*, connecting bus *n* and *m* can be derived as following equations [1].

$$f_k = v_n^2 G_{ik} - v_n v_m (G_{ik} \cos(\theta_n - \theta_m) + B_{ik} \sin(\theta_n - \theta_m)) \qquad (2.9)$$

$$q_k = -v_n^2 B_{ik} - v_n v_m (G_{ik} \sin(\theta_n - \theta_m) - B_{ik} \cos(\theta_n - \theta_m)) \qquad (2.10)$$

In the above formulation for the ACOPF, the optimization variables are the active and reactive power generations, bus voltage magnitude, and angles. The total production cost is usually used as the objective function. The equality constraints (2.2) and (2.3) represent the power balance at each bus. It is important to note that, in the above formulation, the power generation is represented by power injection to the grid, and the bus loads are in the receiving reference. The inequality constraints (2.4) represent limits on the apparent power flow in the line. The active and reactive power generation is bounded by (2.5) and (2.6) respectively. The proxy of power system stability bounds are enforced in (2.7) and (2.8) as the voltage magnitude and angle constraints.

2.1.2. Direct Current Optimal Power Flow

The DC formulation of the OPF problem (DCOPF) is a linearized version of the ACOPF model, which uses the linearized power flow equations. The DCOPF assumes fixed bus voltage magnitudes, negligible reactive power, and negligible network losses. Thus, the original non-convex ACOPF problem can be transformed into a linear

programming model, as long as the objective function is linear. The general mathematical formulation of the DCOPF problem takes the following form:

$$\text{Min } \sum_g (C_g^{op} p_g) \tag{2.11}$$

$$\sum_{\forall g \epsilon \Omega_G^n} p_g + \sum_{\forall k \epsilon \Omega_K^{n-}} f_k - \sum_{\forall k \epsilon \Omega_K^{n+}} f_k = D_n \qquad \forall n \tag{2.12}$$

$$f_k - B_k(\theta_n - \theta_m) = 0 \qquad \forall k \tag{2.13}$$

$$F_k^+ \leq f_k \leq F_k^+ \qquad \forall k \tag{2.14}$$

$$P_g^- \leq p_g \leq P_g^+. \qquad \forall g \tag{2.15}$$

Another simpler way to approximate AC power flow without using voltage angle variables, θ, is using shift factors. In particular, power transfer distribution factors (PTDFs) are widely used in system scheduling applications to represent how much power flow will be distributed to a particular transmission line as a result of power exchanges between two nodes. That is, $PTDF_{k,n}^R$, represents the power flow on line k as a result of power injection at bus n and withdraw at the reference bus R. One notable benefit of using PTDF formulations is that it allows to monitor only critical lines, which could be selected in an off-line study, instead of considering all bus voltage angles and power flow variables. On the other hand, the primary drawback of using the PTDF formulations is that PTDF values should be updated whenever the network topology changes [1]. The above DCOPF formulation can be rewritten by replacing (2.12)-(2.14) with (2.16)-(2.17).

$$\sum_{\forall g} p_g = \sum_{\forall n} D_n \tag{2.16}$$

$$F_k^+ \leq \sum_{\forall n} PTDF_{k,n}^R \left(\sum_{\forall g \epsilon \Omega_G^n} P_g - D_n \right) \leq F_k^+ \qquad \forall k \tag{2.17}$$

2.1.3. Modeling Network Losses on the DC Model: Piecewise Approximation

Power flow analysis is an essential part of system planning and operation. The ACOPF is a nonlinear and non-convex problem. Thus, linear approximation of the ACOPF, the DCOPF, has been applied widely in system planning and operation studies to avoid the computational complexity. However, traditional DCOPF formulations do not reflect the effect of real power losses.

Diverse loss approximation methods have been studied. Reference [2] presents a Taylor series expansion to linearize the loss formulation. Losses are represented as fictitious loads in [3]. One can intrinsically capture the real power losses by using the piecewise linear loss approximation as well [4]-[5]. The line loss between bus *n* and *m* can be expressed as a mathematical form in (2.18). By applying one of the assumptions used in the DC approximation, i.e., by assuming all voltages are 1 pu, (2.18) can be simplified as (2.19). The nonlinear part of (2.19), along with a piecewise linear curve approximation, is shown in Figure 2.1.

$$l_k = G_k(v_n^2 + v_m^2) - 2G_k v_n v_m \cos(\theta_n - \theta_m) \tag{2.18}$$

$$l_k = 2G_k(1 - \cos(\theta_n - \theta_m)) \tag{2.19}$$

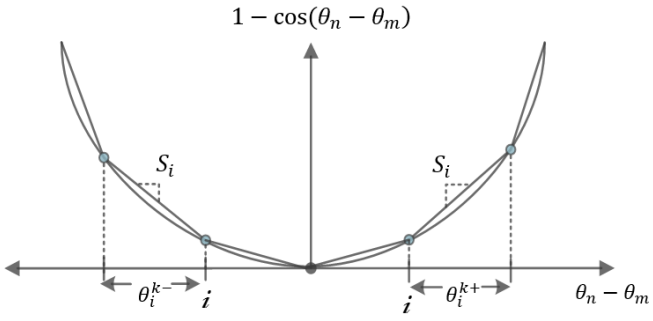

Figure 2.1 Overview of the piecewise linearized loss approximation.

In order to linearize the simplified loss equation, the bus angle difference can be expressed as a summation of multiple segments δ_{ki}^{+} and δ_{ki}^{-} in (2.20). The slope of segments are used to represent the nonlinear part, i.e., $1-\cos(\theta_n-\theta_m)$ accordingly in (2.21). Finally, $2G_k$ is multiplied to fully approximate the line loss equation in (2.22). The length of bus angle difference segments is limited by (2.23) and (2.24). Note that the number and the length of segments may affect accuracy of the approximation and computational complexity. Additional information on the lossy DCOPF and the alternative way to model it using MIP to avoid fictitious losses can be found in [4].

$$\theta_n-\theta_m=\left(\sum_{\forall i}\delta_{ki}^{k+}-\sum_{\forall i}\delta_{ki}^{k-}\right) \qquad \forall k \qquad (2.20)$$

$$1-\cos(\theta_n-\theta_m)=\left(\sum_{\forall i}S_i^L\delta_{ki}^{+}-\sum_{\forall i}S_i^L\delta_{ki}^{-}\right) \qquad \forall k \qquad (2.21)$$

$$l_n=\sum_{\forall k(n,;)}2G_k\left(\sum_{\forall i}S_i^L\delta_{ki}^{+}\right)+\sum_{\forall k(;,n)}2G_k\left(\sum_{\forall i}S_i^L\delta_{ki}^{-}\right) \qquad \forall n \qquad (2.22)$$

$$0\le\delta_{ki}^{+}\le\overline{\delta_i^{+}} \qquad \forall i \qquad (2.23)$$

$$0\le\delta_{ki}^{k-}\le\overline{\delta_i^{+}} \qquad \forall i \qquad (2.24)$$

2.1.4. Security Constrained Unit Commitment

Unit commitment (UC) is a resource scheduling process to determine the most cost-effective commitment status for generators and obtain an optimal dispatch solution while satisfying the system and resource requirements. The commitment means that a generating unit is turned on and synchronized with the system to deliver power to the network [1]. Security constrained unit commitment (SCUC) further ensures the system reliability by, typically, acquiring reserves. Generators could provide regulation, spinning, and non-spinning reserves based on their commitment status and physical availability. A common rule

to procure the reserves is the *N*-1 reliability requirement, which requires the system-wide reserve to cover the loss of any bulk power system element, set forth by the North American Electric Reliability Corporation (NERC) and the Western Electricity Coordination Council (WECC). In addition, most ISOs use a zonal reserve model to distribute the reserves across the system.

ISOs solve SCUC problems on a daily basis within a day-ahead market clearing process. An SCUC problem is modeled as an MIP problem with several constraints that include power balance constraint, reserve constraint, generation limit constraint and minimum up-time and down-time constraints. An explicit formulation of an SCUC model is presented in Chapter 6.

2.1.5. Stochastic Security Constrained Unit Commitment

Most of the contemporary SCUC models being used by ISOs rely on a deterministic approach, by procuring reserves, to handle uncertain events, such as system resource contingencies, load forecasting deviations, and variability associated with the increasing penetration of renewable resources. However, with inherent rough approximations, the scheduling of the reserves in the system may not ensure reliable operation of the system. That is, there is no guarantee that reserves will be deliverable without causing security violation in the post-disturbance realization state. Moreover, such deterministic approaches also require expensive OMCs to adjust resource schedules to account for modeling inaccuracies.

Stochastic SCUC models address the uncertain events directly by explicitly incorporating a set of uncertain scenarios. Stochastic programs minimize expected cost

over a set of scenarios. Most stochastic SCUC models are formulated as a two-stage stochastic program. Typically, in a two-stage stochastic SCUC, the first-stage decision variables are generation commitment status and dispatch set point. The second stage includes recourse decision variables that compensate any negative effect that uncertain events may have [6]. An explicit formulation of a stochastic SCUC model is presented in Chapter 8.

2.2. Constraint Relaxation

System operators must manage generation scheduling while considering complex operational requirements and strict physical restrictions, to ensure a reliable supply of electric energy. To do this, system operators solve various market models, which are typically optimization problems. Moreover, system operators employ CR practices, which allow certain constraints to be relaxed for penalty prices, in their market model. That is, instead of strictly adhering to all the approximated system conditions, market operators treat certain constraints as soft constraints by adding slack variables into the constraints and penalty term into the objective function. Reference [7] presents a summary of CR practices in the industry and investigates the impacts of CR practices on markets and system security.

CR practices provide several benefits to market operators and participants. First, CR practices help market operators to obtain a solution within given time limits even if one or more of original (non-relaxed) constraints cannot be satisfied by available resources. Secondly, CR practices provide an opportunity to achieve possible gains in market surplus

by not strictly adhering all the approximated constraints; at times, strictly enforcing a constraint can substantially increase the operating costs while the enforcement of that constraint to such a stringent requirement may serve a minimal purpose [7]. Lastly, CR practice allows market operators to limit market prices (shadow prices). The electric energy markets in the US use shadow prices, such as locational marginal prices (LMPs) or flowgate marginal prices (FMPs), for market settlements. Originally, many ISOs employed bid caps to limit market prices; however, this practice does not place a maximum cap on the dual variables (e.g., LMPs). Instead, by employing CR practices, the shadow prices are capped by the assigned penalty price [7]. For instance, when a node balance constraint is relaxed, its LMP will be limited by the assigned penalty price.

This research only focuses on TCR that allows a line flow to exceed its flow rating, based on a predefined penalty price. Although such a TCR concept is not new, limited work has been done to propose a systematic methodology to determine associated penalty prices. Reference [8] presents a penalty function-based TCR method for an OPF model. The proposed method investigates the dual of transmission thermal constraints and determines lower bounds of penalty prices such that constraint violations will only be exercised when the original OPF is infeasible; for the application of only handling infeasibilities, an intuitively large enough price is sufficient. Reference [9] proposes a risk-based CR process for SCED to cope with the model infeasibility, without exogenously selecting penalty prices. However, the proposed method added complexity into the SCED model along with an iterative process. System operators can achieve the same goal (and more benefits),

without adding such complexities to the optimization model, by exercising TCR with properly selected penalty prices.

2.3. Transmission System Planning

2.3.1. Overhead Conductors

Aluminum Conductor Steel Reinforced (ACSR) cable is commonly used overhead conductor in existing transmission systems and has thermal limits due to either the maximum sag or the loss of tensile strength. High Temperature Low Sag (HTLS) conductors have been developed to overcome such limits by improving thermal expansion characteristic and tensile strength with temperature. Therefore, HTLS conductors can dissipate more heat, without incurring excessive sag and this increases the thermal power rating of the line typically by a factor of two. For limited time emergencies, ACSRs may be operated at temperatures as high as 125 °C. At the same time, an HTLS conductor with the same diameter as the ACSR could be operated at temperatures as high as 240 °C with less thermal elongation than the ACSR; however, at the maximum line rating, utilizing HTLS conductors bring higher losses [10]. HTLS conductors can replace conventional conductors without extensive alteration of existing structures and new ROW [11]. Low conductor sags are another advantage of HTLS conductors [12].

The performance of HTLS conductors depends on the mechanical and electrical properties of the aluminum strand and reinforcing cores. Most of the electrical current flows in Aluminum strands that surround a reinforcing core. The reinforcing core supports most of the tension load at high temperatures and under high loads. There are many

commercially available HTLS conductors. Aluminum Conductor Steel Supported has fully annealed aluminum strands over a conventional steel core. Gap-type Thermal Resistant Aluminum Alloy Conductor Steel Reinforcement has high-temperature aluminum alloy strands over a low-thermal elongation steel alloy. Thermal Resistant Aluminum Alloy Conductor Invar Reinforced has an oil-filled gap between wires and a conventional steel core. Aluminum Conductor Composite Core has thermal resistant aluminum alloy wires over a low-thermal elongation metal matrix composite core. Aluminum Conductor Composite Reinforced (ACCR) has fully annealed Aluminum strands over a low-thermal elongation polymer matrix composite core. Also, Carbon Fiber Reinforced Aluminum and Composite Reinforced Aluminum Conductors are in a stage of development [11], [13].

2.3.2. Transmission Expansion Planning Overview

The TEP problem determines the time, location, and size of new lines that should be installed to serve future loads and improve both the economic efficiency and reliability of the power system [14]. Generally, the TEP problem is represented as a MIP. Diverse objective functions can be considered, such as investment cost, reliability cost, and congestion cost. Reference [15] classified TEP problem constraints into two sections: mandatory constraints, such as power system operational constraints, and optional constraints, such as environmental concerns. The combination of these diverse objective functions and constraints allows for flexibility in the design of the formulation for the TEP problem.

2.3.3. Increasing Transfer Capability

Political obstacles and environmental issues often impede construction of a new transmission line, especially when a new right of way is required. As a result, recent academic studies, as well as those by utility companies, have been given considerable attention to new means of transporting more power through existing transmission corridors. In this section, power flow limits of the transmission system are investigated first, then diverse means to increase the transmission systems ampacity, without needing new ROW, are introduced.

The maximum allowable conductor temperatures and the assumed "worst-case" conditions, such as ambient weather conditions or ground clearance requirements, determine the thermal rating of an overhead transmission line. The maximum allowable conductor temperature, which can be converted to the amount of power that can be transferred over the line, is specified to avoid excessive sag or loss of tensile strength. For example, temperature limits on ACSR conductors ranges from 50 °C to 150 °C based on the maximum sag or loss of tensile strength in the aluminum strands [16].

In addition, non-thermal system restrictions, such as system stability problems, can also limit the maximum power flow. Generally, system modifications cannot resolve such problems. For instance, the limits on voltage drop require a lower power flow for long overhead lines. Typically, the power flow is restricted by the thermal limit for shorter lines (up to 50 miles). Longer lines (50 to 200 miles) have voltage regulation problems, and very long lines (more than 200 miles) are limited by stability issues [17].

Moreover, the transmission system consists of electrical equipment, which is typically specified to have certain power flow limits for safe and reliable operation. The maximum allowable power flow over the whole transmission system may be limited by any one of the system elements. Reference [18] presents that only 41 % of the power flow limits are set by the line thermal limits while 59 % were limited by other system elements.

There are several different means to increase transmission capability. The optimal way may depend on various factors such as system structure, environmental concerns, and existing component conditions. In addition, it is necessary to know how much and how often one needs increased capability. Diverse alternatives to increase transmission line capacity can be divided into two groups based on needs and conditions: investment options for modifying physical structures and operational options by improving control of system status [11].

When the overloading magnitude and occurrence rate is small, conductor retensioning may be a possible way to reduce sag at high temperatures and, therefore, increase the line rating. Increasing tower height may also be an efficient investment option. However, the corresponding increases in rating are modest. On the other hand, when overloading occurs frequently at high magnitude, a possible investment option is reconductoring with a conductor, which has a higher thermal capacity, such as a HTLS conductor. The corresponding transmission capability may increase by more than 100 %. All of the options above preserve the existing system structure, with the exception of replacing conductors. Also, the environmental impact is normally low and the extended out-of-service period during construction is rare [19]-[21].

Parallel line addition is another option that one may consider. The advantage of this method is a reduced power losses over the line. However, transmission tower replacements may be required since most of them do not support parallel line installation. Also, it may need more out of service time than a reconductoring option [11]. Moreover, HTLS parallel line addition, installing two HTLS lines in parallel, is another option that brings a thermal rating increase over 200 %, while taking advantage of parallel line addition option, reduced power losses.

Large transmission capacity increases, which require replacing the whole transmission structure, would be the most dramatic option among other investment options. Also, this is the most expensive and time consuming process, but it only preserves the existing ROW [55].

In addition to system configuration changes by investments, there are operational based options available for increasing transmission line capability. The dynamic line rating utilizes real-time adjusted line ratings based on the ampacity under ambient circumstances such as weather parameters and other conditions. Transmission systems are commonly operated at much less than their thermal capacity under steady state operation. Implementing dynamic line rating may allow the use of less conservative assumptions that rely on worst-case conditions. The real-time rating can be determined by line temperature measurements along with the use of methods to determine line ratings. Reference [19] studied different means to utilize the dynamic line rating.

TCR is another operational based option that allows a line flow to exceed the steady state line ratings for a certain penalty price. TCR in this study aims to increase the line

ampacity by utilizing the asset more flexibly. It is clear that there is a cost associated with flexible operations at elevated temperature. These high temperature effects on the conductor, as well as the degradation model for capturing the penalty price, are discussed in detail in Chapter 4.

2.4. Lagrange Relaxation and Decomposition

Prior studies investigated various decomposition-based solution methods for complex multi-stage optimization problems. There are mainly two classes of decomposition techniques: vertical decomposition and horizontal decomposition. Vertical decomposition methods decompose a model by stages. On the other hand, horizontal decomposition techniques decompose a model by scenarios. Lagrange relaxation and decomposition is one type of vertical decomposition technique. Lagrange relaxation solves complex optimization problems by relaxing certain constraints and adding these relaxed constraints with a 'penalty factor' in the objective function [22]. For example, the second constraint (2.27) in the primal problem can be dualized with the Lagrangian multiplier, λ, in (2.29).

The primal problem:

$$\text{Min } c^T x \tag{2.25}$$

$$A_1 x = b_1 \tag{2.26}$$

$$A_2 x = b_2 \tag{2.27}$$

$$x \geq 0 \tag{2.28}$$

The Lagrange relaxation:

$$L(\lambda) = \text{Min } c^T x + \lambda^T (b_2 - A_2 x) \tag{2.29}$$

$$A_1 x = b_1 \tag{2.30}$$

$$x \geq 0 \tag{2.31}$$

Solving Lagrangian:

$$\max_{\lambda} L(\lambda) = \max_{\lambda}[\text{Min } c^T x + \lambda^T (b_2 - A_2 x)] \tag{2.32}$$

$$A_1 x = b_1 \tag{2.33}$$

$$x \geq 0 \tag{2.34}$$

The Lagrangian, $L(\lambda)$, is a relaxation of the primal problem. Based on optimization theory, the Lagrangian is a lower bound to the solution of primal problem. Note that Lagrange relaxation provides a lower bound when the original problem is a minimization problem and it provides an upper bound when the original problem is a maximization problem; for this discussion, this section focuses on minimization problems. Instead of solving the primal problem, one can solve the Lagrangian dual by maximizing the Lagrangian function with respect to the Lagrangian multipliers. The Lagrangian dual finds the Lagrangian multipliers with the tightest lower bound that enforce $(b_2 - A_2 x)$ term into zero at optimality. However, the tightest lower bound may be below the optimal solution for non-convex problems. The gap between the lower bound and the optimal solution is known as a duality gap. Thus, the Lagrange relaxation does not guarantee an optimal solution for non-convex problems, but Lagrange relaxation generally can provide a decent lower bound. However, this lower bound solution is infeasible whenever the duality gap is not zero. To achieve a feasible solution, one can repair the infeasibility or find a possible feasible solution with proper techniques. Thus, the lower bound can still be used to provide a path to find a "good" feasible solution.

Lagrange decomposition is one special case of Lagrange relaxation, which is based on the dual optimization theory. That is, one can decompose the original problem into several independent subproblems by choosing proper coupling constraints and relax them using Lagrange relaxation. Then, one can solve the subproblems independently while sharing the same Lagrangian multiplier during each iteration. In addition, parallel computing techniques can be applied to solve independent subproblems. In [23], generator outputs are treated as coordination variables to form coupling constraints. In [24], the coupling constraints contain the voltage and bus angle variables along with tie-lines to decompose operating areas into independent sub-areas. Reference [25] shows that relaxing two kinds of constraints were more beneficial.

The performance of Lagrange decomposition is dependent on the parameter tuning process. For example, the initialization and updating strategies of the Lagrangian multipliers influence algorithm efficiency in the optimization process. Reference [26] introduced three algorithms in determining of the Lagrangian multipliers: the sub-gradient method, various versions of the simplex-based method, and multiplier adjustment methods.

2.5. Progressive Hedging Decomposition

The Progressive Hedging algorithm, proposed by Rockafellar and Wets [27], is a widely used horizontal decomposition technique for multi-stage stochastic optimization programs. Although PH is a heuristic method and does not guarantee a global optimal solution for non-convex optimization models, Watson et al. [28] showed that PH is an effective heuristic for large-scale mixed integer stochastic programs. A simple extensive form two-stage stochastic optimization problem can be represented as follows,

$$Minimize\ c \cdot x + \sum_{s \in S} \Pr(s)(f_s \cdot y_s) \tag{2.35}$$

$$(x, y_s) \in \Omega_s \qquad \forall s \in S \tag{2.36}$$

where x is a first stage decision variable with c as a cost coefficient vector. Also, y_s is a second stage decision variable with the cost coefficient vector f_s. $\Pr(s)$ denotes the probability of occurrence of each scenario $s \in S$. The requirement $(x, y_s) \in \Omega_s$ represents the problem constraints.

PH algorithm decomposes the extensive form two-stage stochastic optimization problem into smaller subproblems by scenarios. For each scenario $s \in S$, the PH subproblem can be expressed as follows,

$$Minimize\ c^T x + f_s \cdot y_s \tag{2.37}$$

$$(x, y_s) \in \Omega_s. \tag{2.38}$$

Each PH subproblem is solved independently. Then PH algorithm seeks an agreement of the hedging variables, e.g., the first stage decision variable x, between solutions from each subproblem by iteratively updating the weights to be added to the objective function of each subproblem. The added weights penalize the lack of agreement of the hedging variables using a sub-gradient estimator and a squared penalty term [29]. Figure 2.2 presents a flow chart of PH algorithm.

1. $k \leftarrow 0$

2. For all scenario $s \in S$: $x_s^{(k)} \leftarrow \text{argmin } f_s(x, y_s) : (x, y_s) \in \Omega_s$

3. $\bar{x}^{(k)} \leftarrow \sum_{s \in S} \Pr(s) x_s^{(k)}$

4. For all scenario $s \in S$: $w_s^{(k)} \leftarrow \rho(x_s^{(k)} - \bar{x}^{(k)})$

5. $k \leftarrow k + 1$

6. For all scenario $s \in S$:

$x_s^{(k)} \leftarrow \text{argmin } f_s(x, y_s) + w_s^{(k-1)} x + \rho/2 \left\| x - \bar{x}^{(k-1)} \right\|^2 : (x, y_s) \in \Omega_s$

7. $\bar{x}^{(k)} \leftarrow \sum_{s \in S} \Pr(s) x_s^{(k)}$

8. For all scenario $s \in S$: $w_s^{(k)} \leftarrow w_s^{(k-1)} + \rho(x_s^{(k)} - \bar{x}^{(k)})$

9. $g^{(k)} \leftarrow \sum_{s \in S} \Pr(s) \left\| x_s^{(k)} - \bar{x}^{(k)} \right\|$

10. If $g^{(k)} > \epsilon$, then go to step 5. Otherwise, terminate.

Figure 2.2 Flow chart of the Progressive Hedging decomposition algorithm [28].

CHAPTER 3. LITERATURE REVIEW

3.1. Thermal Behavior of Overhead Conductors

Operating an overhead conductor at an elevated temperature can cause damage to the aluminum wires cumulatively and that prolonged high temperature operation can significantly reduce the expected service life of the conductor. The conductor temperature is the fundamental parameter that affects the degradation of an overhead conductor. A combination of heating and cooling effect contributes to the conductor temperature.

The IEEE has published a mathematical model to predict conductor temperature [30]. This model provides a standard method for calculating conductor temperature and the thermal capacity in the steady and dynamic states. The CIGRE working group has also proposed a calculation method for conductor thermal behavior in [31]. Reference [32] examined the differences between the IEEE standard model in [30] and CIGRE model in [31]. Also, W. Z. Black and R. L. Rehberg [33] proposed a simplified conductor temperature model by approximating the radiation term as a linear function of conductor temperature.

The material tensile strength of aluminum wires decreases with continuous operation at elevated temperature due to an annealing effect. The annealing effect is a temperature and time dependent phenomenon. The American Society for Testing and Materials and the International Engineering Consortium Standards specify the minimum tensile strength of aluminum and copper wires. Likewise, the National Electrical Safety Code sets the standards of the ground clearance [16].

Harvey [34] used experimental results to derive the residual tensile strength predict equations, which were adopted in the IEEE standard for determining the effects of high-temperature operation on conductors [35]. Morgan [36] proposed that the percentage reduction in cross-sectional area during wire drawing has more effect on the loss of tensile strength than its diameter.

3.2. Thermal Constraint Relaxation: Industry Practices

TCR allows a line flow to exceed the steady state line rating for a certain penalty price. Typically, exceeding the steady state operating level is only allowed for emergency situations for a limited time. However, many ISOs already implemented similar CR practices in their market models. This section introduces the contemporary industry practices regarding TCR and associated penalty prices.

In sum, each ISO has a different attitude to utilize the CR practices. Also, the contemporary industry practices for determining penalty prices are neither transparent nor systematic; rather, the existing process relies on operator's judgments and stakeholders' agreements. Moreover, few ISOs do not provide information regarding their CR procedures and penalty price parameters which could raise concerns regarding market transparency.

3.2.1. Midcontinent ISO

Midcontinent ISO (MISO) sets marginal value limit of each transmission constraint in both day-ahead and real-time market through the transmission constraint demand curves (TCDC). First, MISO grouping transmission lines into two categories. The group one is classified based on the voltage level. A two-step TCDC is used for group one constraints

to consider the impact of relaxation magnitude. Constraints that do not respond well to group one TCDCs are assigned to group two. Moreover, MISO operators can temporarily override group one or two TCDCs based on operating conditions. For example, when overloading is occurring for two or more consecutive dispatch intervals, MISO may temporarily override TCDCs. The shape and magnitude of an override TCDC are determined based on the operating costs and capabilities of available resources that affect the transmission constraint [37].

The TCDCs do not reflect what CR activations would cause to the system or transmission assets. Instead, TCDCs are determined as a mean to control power flows. Also, it is not clear how group one and two TCDCs differ each other. Moreover, the TCDCs do not change with magnitude and duration of the relaxations systematically. Rather, MISO operators manually overrides TCDCs to handle exceptional situations.

3.2.2. Pennsylvania-New Jersey-Maryland Interconnection

Pennsylvania-New Jersey-Maryland Interconnection (PJM) uses a default penalty factor of $2,000/MWh regardless of voltage level of transmission constraints. The determination of the penalty factor is based on a historical constraints control analysis. PJM overrides penalty factor based on system operating condition. However, PJM does not allow the penalty factor to set the shadow price of a constraint. That is, PJM adjusts transmission ratings so that market model itself does not experience any line overloading and, as a result, transmission penalty factors does not affect shadow price of the constraint.

3.2.3. Electric Reliability Council of Texas

Electric Reliability Council of Texas sets a fixed penalty price for TCR in the base case and contingency case as presented in Table 3.1. The penalty prices are determined based on the maximum LMP congestion component and shift factors [39]. However, the fixed penalty price scheme does not provide a meaningful way to capture the magnitude or duration of the relaxations.

Table 3.1 Penalty Prices for TCR in ERCOT ($/MWh)

Base Case/Voltage Violation	*N*-1 Constraint Violation		
	69 kV	138 kV	345 kV
5,000	2,800	3,500	4,500

3.2.4. New York ISO

New York ISO (NYISO) adjusts transmission ratings when power flows exceed the original rating. First, NYISO solves the market model with graduated transmission demand curve for specific transmission constraints and $4,000 for remaining constraints. Then, if any line flow level is greater than the original limit, NYISO adjusts the transmission rating equal to the relaxed flow plus 0.2 MW. In this case, penalty price does not affect market clearing prices since the market model will not experience overloading after operator's adjustment on the transmission ratings. However, when the marginal re-dispatch cost is greater than the penalty price, NYISO sets market clearing prices by the penalty prices [40]. Table 3.2 presents the detailed penalty price information.

Although NYISO has a staircase penalty price scheme, the main purpose is to find a relaxed line flow which could be used to adjust the transmission rating. Also, the penalty

prices do not capture the duration of relaxations. Lastly, the penalty price determination process is not publicly available.

Table 3.2 Penalty Prices for TCR in NYISO ($/MWh)

Graduated Transmission Demand Curve			Penalty Prices for Remaining Constraints
First 5 MWs	next 15 MWs	thereafter	
350	2,350	4,000	4,000

3.2.5. California ISO

California ISO (CAISO) has lowered the real-time scheduling run TCR penalty price factor from $5,000 to $1,500 in 2013 [41]. In 2016, CAISO proposed a new tiered approach for TCR for the scheduling run based on the voltage level and relaxation magnitude as presented in Table 3.3. Setting the lower price at first tier aims to promote efficient real-time market dispatch for small amounts of constraint violation. The two-tiered CAISO's penalty price scheme for TCR seems to capture the magnitude of relaxations; however, the shape of the penalty price scheme does not capture the duration of the relaxations.

Table 3.3 Penalty Prices for TCR in CAISO ($/MWh)

Voltage Level	230 kV and above		115 kV and lower	
Constraint Relaxation Level	below 2 %	2% or more	below 2 %	2 % or more
Penalty Price	750	1,500	500	1,000

3.2.6. Southwest Power Pool

Southwest Power Pool (SPP) utilizes the violation relaxation limits for spinning reserve requirements, operating constraints, resource ramp constraints, global power balance constraint, and resource capacity constraints. SPP has a five-tiered penalty price scheme with

1 % segment length for the first four tiers as presented in Table 3.4 [42]. However, the segment step-size and amount of price increases at each step is exactly same. Although a common belief is that a penalty price scheme with a higher number of segments would provide a better reflection of the actual impact of the relaxations, the process of the penalty price determination is also important. Also, the penalty price scheme of SPP does not capture the duration of constraint relaxations.

Table 3.4 Penalty Prices for TCR in SPP ($/MWh)

Loading Level	100 % - 101 %	101 % - 102 %	102 % - 104 %	103 % - 104 %	thereafter
Penalty Price	500	750	1,000	1,250	1,500

3.2.7. ISO New England

ISO New England does not provide information regarding the penalty prices for TCR. The CR practices can affect the market outcome; therefore, to maintain the market transparency, it is recommended that ISOs provide details regarding their CR procedures as well as the mechanism to derive penalty prices.

3.3. Transmission Expansion Planning

Due to the physical and reliability restrictions of the power system, system planners need to conduct long-term TEP studies to ensure a reliable and stable supply of future forecasted electricity demands as well as improve the operational efficiency. TEP studies determine time, location, and size of new line installations in the power systems [15].

From the planning time horizon point of view, TEP can be classified into static TEP and dynamic TEP [43]. In a static TEP, all investments are considered within a single year;

while a dynamic TEP considers different time horizons. A dynamic TEP will provide more realistic planning solutions; however, it is harder to solve [44].

Diverse models have been proposed to formulate TEP. The models can be classified into two groups based on the assumptions or simplifications of the power flows. The models are either formulated as ACOPF or DCOPF, where the latter is a simplified and linearized model of the former one. The reference [14] discusses the advantages and disadvantages of two models.

Algorithms for solving TEP can be divided into two groups, mathematical optimization method and meta-heuristic (or heuristics) optimization method [44]-[45]. Mathematical optimization method, such as dynamic programming [46], quadratic programming [47], nonlinear programming [48], and mixed integer programming [49]-[50], have frequently been used. These techniques are, at times, exact solution methods depending on the class of the optimization problem. Interior point algorithm [51]-[52] and Benders' decomposition [53] have also been proposed as a mathematical optimization method. On the other hand, meta-heuristic optimization method can solve the problem relatively quickly, but there is no general guarantee that the meta-heuristic will be effective at finding quality solutions nor can they guarantee a global solution. Meta-heuristic optimization method includes genetic algorithm [54], greedy randomized adaptive search procedure [55], tabu search [56], and fuzzy set theory [57].

Two main evaluation factors for TEP are economic assessment and reliability assessment [58]. One of the methodologies of economic assessment is "Transmission Economic Assessment Methodology," which is developed by CAISO [59].

The probabilistic approaches in the TEP model for a large wind farm integration are presented in [60]-[62]. References [60] and [61] reflect the uncertainties on both load and power generation of wind farms in the proposed static *N*-1 reliable TEP model and chance constrained TEP model, respectively. Reference [62] introduces a probabilistic multi-objective TEP model only with the wind farm output uncertainty. Reference [63]-[64] proposes a two-stage TEP model that captures uncertainties within an electricity market; however, uncertainties associated with the wind output were not considered. The above studies mainly focus on the expansion planning problem of existing transmission systems while considering the impact of large wind farm integration.

3.4. Stochastic Security Constrained Unit Commitment

Stochastic resource scheduling applications have received much attention in the recent literature as a way to address the uncertain nature of power system operations. The primary source of uncertainty comes from the load forecasting deviations, the resource contingencies, and the variability of renewable resources. The main focus in the literature on stochastic resource scheduling is on scenario-based stochastic UC problems, which often rely on pre-sampling of discrete uncertainty realizations. The scenarios can be obtained by using Monte-Carlo simulation [65]-[66] or constructing a scenario tree [67]. Zhou et al. [68] present an overview of recent literature on stochastic methods applied to power system operations with renewable energy.

In the scenario-based stochastic UC models, various uncertain events are represented as a set of scenarios. System resource contingencies are modeled as a set of scenarios in [69]-[72]. In [69], the demand uncertainties and the generator contingencies are modeled.

An extensive form of SCUC formulation, which includes an explicit modeling of the transmission contingencies, is presented in [70]. A stochastic SCUC model to handle a preselected set of random generator and transmission contingencies is introduced in [71]-[72]. The variability and uncertainty of renewable resources are addressed in [25], [28], and [73]-[79]. In [25], the authors present a two-stage stochastic program to address the uncertainties associated with the wind output deviations as well as system resource contingencies. Moreover, this work presents a scenario selection algorithm. In [28], the authors utilized PH, to solve a large scale two-stage stochastic programming model to handle the variability of renewable resources; the authors showed that PH is an effective heuristic for large-scale mixed integer stochastic programs. In [73], the authors introduce a two-stage stochastic programming model to determine optimal reserve requirements with a large amount of wind power. In [74], a Benders' decomposition based SCUC model is presented to account for the intermittency and volatility of wind power resources. In [75] and [76], the authors highlight the possible benefit of using stochastic SCUC while considering high penetration of wind power. In [77], a stochastic dynamic programming based stochastic SCUC model is introduced to cover increased variation in wind output in Netherlands. In [78] and [79], stochastic resource scheduling applications that consider uncertainties associated with the load and wind power output deviation is presented.

Solution methods stochastic UC problems can be classified into two groups, direct methods and decomposition-based methods. For small-scale applications, an extensive form stochastic UC models can be solved directly via commercial solvers, such as CPLEX or GUROBI. However, when it comes to larger-scale applications, the extensive form

models are difficult to solve directly. Thus, various decomposition-based methods are introduced in the literature. The decomposition-based methods can be divided into two groups: vertical decomposition and horizontal decomposition. Vertical decomposition techniques decompose a model by time stages. Lagrangian relaxation and decomposition is applied in [22]-[26]. Benders' decomposition is also widely used in the recent research [74], [80]-[81]. Lastly, Progressive Hedging, which is a well-known horizontal decomposition algorithm, is applied in [27]-[29].

CHAPTER 4. THE DEGRADATION EFFECT OF OVERHEAD CONDUCTORS

The operation of overhead conductors at elevated temperatures can cause loss of tensile strength as well as a reduction in the expected service life. Such costs associated with overloading operations can be captured by introducing a degradation model. This chapter introduces the conductor thermal dynamics as well as the degradation effect due to high-temperature operations.

4.1. Thermal Dynamics of Overhead Conductors

Transmission line overflows, which are enabled by TCR, can elevate transmission line temperatures that can cause degradations on conductor materials. The overhead conductor thermal dynamics, which balances heating and cooling, govern overhead conductor temperatures. The main sources of conductor heating are the line flow, radiation from the sun, and reflection from the surroundings. At the same time, the ambient air temperature, wind speed, and radiation of heat from the conductor incur a cooling effect [12]. These heating and cooling effects should be balanced. A generic representation of the conductor thermal behavior is shown in Figure 4.1.

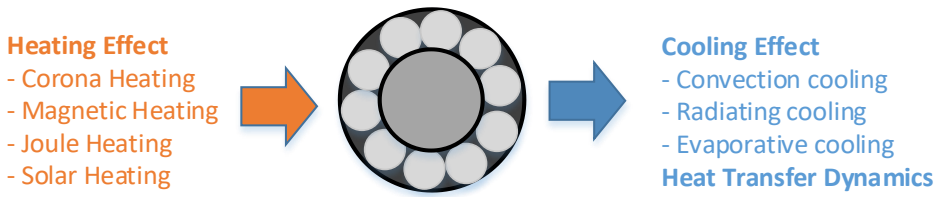

Figure 4.1 Generic Representation of the Conductor Thermal Behavior [82].

However, the aspects that influence overhead conductor temperatures vary along a transmission line and are difficult to measure or predict precisely, due to the inherent

nonlinearity of the conductor thermal dynamics. This research adopts an IEEE standard model in [30], which will be referred as IEEE standard temperature model throughout this thesis, for calculating overhead conductor temperatures and thermal ratings at specific weather conditions. This IEEE standard temperature model provides a method for calculating conductor temperature and the thermal capacity in the steady and dynamic states. In the IEEE standard temperature model, the dynamic heat balance equation is expressed as follows,

$$Q_C + Q_R + mC_P \frac{dT_c}{dt} = Q_S + i^2 R(T_c) \tag{4.1}$$

where Q_C is the forced convection heat loss, Q_R is the radiated heat loss, mC_P is the total heat capacity of conductor, Q_S is the solar heat gain, and $i^2 R(T_c)$ is the joule heating from the line flow at the line temperature T_c. Convection heat loss mainly depends on wind speed and direction. Higher wind speeds directed perpendicular to a conductor gives a greater cooling effect. Solar heat gain is estimated based on the available solar energy as well as the emissivity and absorptivity of a conductor surface. A newly installed conductor typically has a lower emissivity and absorptivity whereas an old conductor has higher values [83]. Therefore, even with fixed line flows, line temperatures can vary based on ambient weather and the conductor physical conditions. The IEEE standard temperature model ignores the corona heating effect, magnetic heating effect, and evaporative cooling effect, which have little impact on the conductor thermal behavior. In addition, this equation normally requires an iterative calculation due to its inherent nonlinearity. Specific methods to calculate each term in (4.1) can be found in [30].

4.2. Effect of High-Temperature Operation on Overhead Conductors

It is clear that the operation of overhead conductors at elevated temperature can cause damage to the aluminum wires cumulatively and that continued high-temperature operation will significantly reduce the expected service life of the conductor. As the current flowing through a conductor increases, a conductor elongates with the increased temperature. This elongation increases the sag of the conductor, which decreases the ground clearance. If the conductor temperature remains high for an extended and consecutive period, the tensile strength of the conductor decreases [84]. Although the loss of tensile strength is gradual, it accumulates over time and increases the probability of outages [85]. Also, the effects of the elevated temperature operation on the aluminum conductor are irreversible and the damages experienced by the conductor are also cumulative. Note that other factors that may incur negative changes in the conductor mechanical and electrical properties, such as wind induced vibration and corrosion, are outside of the scope of this study.

The loss of tensile strength of a conductor is caused by the annealing effect. Annealing is the metallurgical process where applied high temperature softens hardened metal resulting in a loss of tensile strength and is a function of both the magnitude of the temperature and the duration of the overheated time. The loss of tensile strength of an aluminum conductor, such as ACSR, is a function of the loss of tensile strength of the aluminum strands compared to the rated strength of both the aluminum and steel wires. Typically, the steel wires will not anneal at temperatures incurred during steady-state and even for emergency operation of ACSR. The degradation of the aluminum strands only

partially affects the overall conductor strength since ACSR derives half of its strength from the steel wires and remainings from the aluminum strands.

Some conductors are designed to reduce the effect of annealing on conductor strength by increasing the strength percentage of steel core or using already annealed aluminum strands. For those conductors, however, the maximum temperature can be determined by the thermal capability of connectors, as well as by other accessories. The reference [86] presents the maximum operating temperature of different types of conductors.

The loss of tensile strength due to annealing of the aluminum wires is a temperature and time dependent phenomenon. Predicting such loss requires a complex analysis of the metallurgical aspects of the conductor components as well as probability characteristic of ambient factors that affect the conductor temperature. The key to approximate the loss of strength over the expected life of a conductor is to predict a time-temperature series that will result in annealing. The projected remaining strength of the conductor can be determined based on such information [86].

Harvey [34] derived equations that capture the residual tensile strength of an overhead conductor. The IEEE standard model in [35], which will be referred as IEEE standard degradation model throughout this dissertation, adopts the residual conductor strength predictor model for determining the effects of the high-temperature operation on conductors. The IEEE standard degradation model is expressed as follows,

$$RS_{al} = (-0.24T_c + 134)D_{T_c}{}^{-(0.001T_c - 0.095)\left(\frac{0.1}{dt}\right)} \tag{4.2}$$

$$if\ (-0.24T_c + 134) > 100, use\ 100\ for\ RS_{al}$$

$$Deg_T = 100 - (RS_{al}\left(\frac{STR_{al}}{STR_T}\right) + 109\left(\frac{STR_{st}}{STR_T}\right)) \quad (4.3)$$

where RS_{al} is the residual tensile strength of an aluminum strand in percentage with a diameter of di in inches, Deg_T is the loss of tensile strength of a whole conductor in percentage, and D_{T_c} is the duration of operations in hours at temperature T_c in degrees. Also, STR_{al}, STR_{st}, STR_T are the initial strength of aluminum strands, steel core, and a whole conductor in pounds-force, respectively. Conductor degradation effects mainly depend on the magnitude and the duration of elevated temperature exposures. Moreover, the number of aluminium strands, their diameter, and the structure of a conductor are other key factors that influence conductor degradation effects.

Note that the presented IEEE standard degradation model was derived for ACSR. It assumes that the loss of tensile strength of stranded conductors is dependent on the diameter of the strand wires. The factor 109 in the presented model accounts for the increased load carried by the steel core as a result of conductor elongation due to the high-temperature operation. Moreover, in applying these equations, the cumulative strength reduction for multiple exposures at the same conductor temperature can be obtained by simply adding up all the hours and calculating the residual strength. For multiple exposures at different conductor temperatures, all exposures should be expressed as an orderly time series of temperatures and converted to an equivalent duration at the highest temperature [34]. Lastly, this research adopts the IEEE standard degradation model; however, there is no guarantee that a specific method would work perfectly in all cases. Therefore, it would be advisable to investigate different methodologies for given situations.

CHAPTER 5. IMPACT OF THERMAL CONSTRAINT RELXATIONS ON LONG-TERM TRANSMISSION EXPANSSION PLANNING

This chapter introduces a linearization approach for conductor temperature and degradation effect estimation. The proposed degradation model is applied into the two long-term TEP models as a set of constraints. First, this chapter introduces a static TEP model, which able to provide an optimal conductor size and path for the large wind farm integration, while employing TCR combined with the linearized conductor degradation model. Second, the chapter presents a dynamic TEP model, which can consider various means to increase transmission capacity, while preserving existing ROW.

5.1. Linearized Conductor Degradation Model

5.1.1. Degradation Decomposition Model

The IEEE standard degradation model, which is defined in Chapter 4, aims to approximate the final conductor degradation effect based on an ordered series of temperature history. Therefore, the model cannot provide the degradation information at each operating time interval. Also, the nonlinearity in the equations makes it difficult to be applied in an optimization model directly.

The main goal of the linearized conductor degradation model in this chapter is to decompose the degradation effect into two terms so that the model can be incorporated into an optimization model as a set of constraints. Figure 5.1 presents an overview of the decomposition approach.

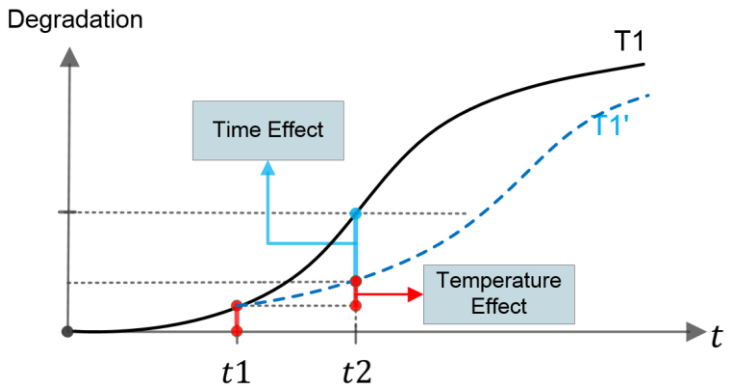

Figure 5.1 Decomposition Approach of the Degradation Effect.

The model decomposes the degradation effect, d_{kt}, into the temperature effect term, Deg_{kt}^{Temp}, and the time effect term, Deg_{kt}^{Time}, as follows,

$$d_{kt} = Deg_{kt}^{Temp} + Deg_{kt}^{Time}. \qquad \forall k, t \qquad (5.1)$$

The work makes several assumptions at this point to carry the analysis further. First, the model assumes a linear relationship between the temperature and degradation effect. Thus, the determination of the temperature effect term is based on the ratio of the present temperature and the predefined maximum temperature. Note that if an actual operational temperature is above the maximum allowable temperature, which can incur a permanent loss of tensile strength, then the first assumption will become less accurate, and one should consider the nonlinear relationship between each temperature and degradation effect. Second, the degradation model considers the only specific number of continuous overheating operations. It is clear that considering a longer time span will provide a better approximation along with computational complexity. Since the marginal effect of additional degradation due to continuous operation decreases as time increases, one can obtain a conservative approximation with a shorter time span.

By applying these assumptions, the temperature effect parameter, LS_k^{Temp}, can be obtained from the IEEE standard degradation model in (4.3). The time effect parameter, LS_k^{Time}, due to continuous overheating operations can be obtained by taking the gap between the temperature effect term and the degradation level in a following consecutive time interval. The maximum temperature, H_k^{tr}, is considered to prevent a permanent damage to the line. At the end, the loss of tensile strength of the conductor at each time, (5.2), and the degradation cost, (5.3), can be expressed as,

$$d_{kt} = \mu\left(\frac{LS_k^{Temp}}{H_k^{tr}-H_k^{+}} h_{kt}^{+} + \frac{LS_k^{Time}}{H_k^{tr}-H_k^{+}} h_{k,t-1}^{+}\right) \qquad \forall k,t \qquad (5.2)$$

$$c_{kt} = C_k^{ED} d_{kt}. \qquad \forall k,t \qquad (5.3)$$

The time effect term is only applied when there is a continuous overloading operation. For simplicity, this work only considers one continuous overloading operation. Figure 5.2 presents the overview of the proposed degradation approximation.

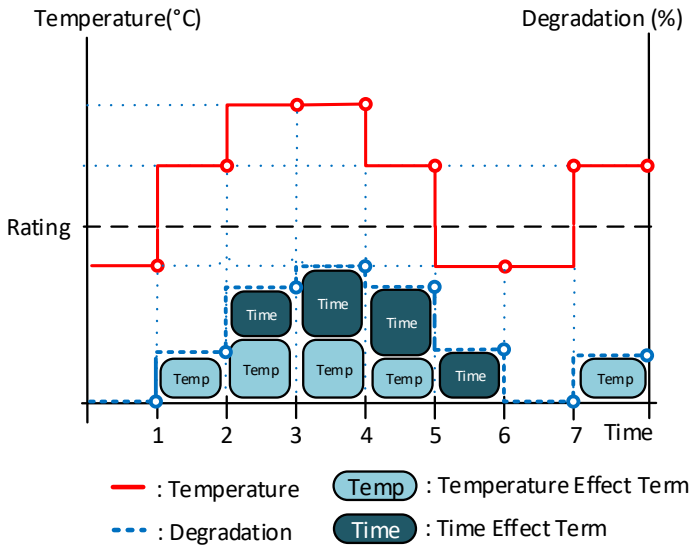

Figure 5.2 Overview of the Linearized Degradation Approximation.

Note that the approximated loss of strength obtained by the proposed method would be overestimated without the adjustment factor, μ, since the marginal degradation effect tends to decrease as time increases. This adjustment factor is used to relate the equation in (5.2) with the IEEE standard degradation model in (4.3) to ensure that the degradation result from the proposed model is consistent with the more complex IEEE standard degradation model. In this work, Monte-Carlo simulations are conducted to obtain the adjustment factor by comparing the degradation results from the proposed method and IEEE standard degradation model. That is, the adjustment factor is updated at each iteration until the gap between the average degradation result from the proposed method and the IEEE standard degradation model for 10,000 random temperature-time series, ranges from the room temperature to the emergency temperature and generated at each iteration, is converged within 2 %. In the numerical study, the average difference between these two methods was 1.76 %.

The end of service time of the conductor is used to determine the degradation cost in (5.3). For instance, the manufacturers of ACSR and ACCR conductors state that each conductor can be operated for 1,000 hours and 1,500 hours at their emergency temperatures in the whole service lifetime, respectively [87]-[88]. This research assumes 10 % loss of tensile strength as the end of service life of each conductor [89]. That is, one should replace the specific line if the loss of strength has reached 10 %; at such a point, this research assumes that the line is replaced at the additional capital cost of that line.

The main advantage of the proposed method is its availability to provide the degradation cost at each operation time interval. However, there are two drawbacks of this

approach. First, the loss of tensile strength is measured whenever the line temperature exceeds its steady-state limits. This may be inaccurate in some cases, e.g., when the temperature is close to the steady-state limits, actual degradation occurs after several continuous operations. Second, this method requires a tuning process, the adjustment factor. The level of the adjustment factor depends on the length of the planning horizon.

5.1.2. Piecewise Linearized Temperature Model

The proposed piecewise linearized temperature model approximates the IEEE standard temperature model, which is defined in Chapter 4, while assuming fixed environmental factors. The bus angle difference along a transmission line can be represented as a summation of linear blocks in (5.4) to apply the piecewise linear approximation. The line susceptance is multiplied to obtain line power flow in (5.5). Finally, one can get the piecewise approximation of line temperature by multiplying the proper slopes of each segment as in (5.6). The length of each bus angle difference segment is limited by (5.7)-(5.8).

$$\theta_n - \theta_m = (\sum_{\forall i} \delta_{ki}^{+} - \sum_{\forall i} \delta_{ki}^{-}) \qquad \forall n \qquad (5.4)$$

$$f_k = (\sum_{\forall i} B_k \delta_{ki}^{+}) + (\sum_{\forall i} B_k \delta_{ki}^{-}) \qquad \forall k \qquad (5.5)$$

$$h_k = (B_k \sum_{\forall i} S_i^T \delta_{ki}^{+}) + (B_k \sum_{\forall i} S_i^T \delta_{ki}^{-}) \qquad \forall k \qquad (5.6)$$

$$0 \le \delta_{ki}^{+} \le \overline{\delta_i^{+}} \qquad \forall i \qquad (5.7)$$

$$0 \le \delta_{ki}^{+} \le \overline{\delta_i^{+}} \qquad \forall i \qquad (5.8)$$

The difference between a line temperature and the steady state temperature rating is captured in (5.9) with two slack variables h_k^{+} and h_k^{-}. The overloading of each line is

restricted in the area between the steady state thermal limit and the presumed maximum overloading temperature to prevent a permanent damage in (5.10)-(5.11).

$$h_k - H_k^+ = h_k^+ - h_k^- \qquad \forall k \qquad (5.9)$$

$$0 \le h_k^+ \le T^+ \qquad \forall k \qquad (5.10)$$

$$0 \le h_k^- \le T^+ \qquad \forall k \qquad (5.11)$$

5.2. Transmission Expansion Planning Model for Optimal Conductor Sizing of Wind Integration

Social concerns on alternative ways to supply clean and sustainable energy bring significant deployment of renewable energy, especially wind power. This research proposes a TEP model for selecting an optimal conductor size and path for a wind farm integration. The model considers TCR along with the linearized conductor degradation model. This research investigates the tradeoff of the savings from choosing a lower capacity conductor while enabling short-term overloading, against the associated degradation cost. Numerical simulations conducted on the modified IEEE 24-bus test case show the effectiveness of the proposed application of TCR.

5.2.1. Background and Motivation

Alternative ways to supply clean and sustainable energy has recently been given considerable attention due to environmental concerns and the depletion of fossil fuel sources. This brings forth significant deployment of renewables. Wind power is the most widely utilized renewable power source, and the worldwide annual growth of installed capacity was over 25 % in the last decade [43]. However, the integration of large wind

farms into electric power systems raises difficulties regarding transmission planning. One major difficulty is that wind generation sites with rich wind energy potentials are usually located at remote areas far from the existing transmission system; therefore, it requires long transmission lines to connect the wind farms to the system. Also, the existing transmission system needs proper expansion to utilize significant amounts of intermittent resources. Expansion planners tried to tackle this problem by incorporating wind power integration into a TEP problem. However, recent studies, which are introduced in Chapter 2, mainly focus on the impact of integrating wind farms into the expansion of existing transmission systems, while assuming that certain wind farms were already or planned to be connected to specific nodes with proper conductor size.

This chapter proposes a static TEP model combined with TCR and the degradation decomposition model, which provides an optimal conductor size and paths for a large wind farm integration while capturing the impacts of flexible line operation. The degradation model is applied to evaluate the associated degradation cost due to the reduced expected service life of the conductor. The TEP model is a MIP problem that includes a lossy DCOPF based SCUC formulation. A LR based decomposition algorithm is used to solve the proposed model while employing a parallel computing environment.

5.2.2. Mathematical Formulation

This section presents a mathematical formulation for the proposed TEP model. Cost savings from choosing optimal conductor size are mainly influenced by the generation dispatch scheduling that determines the power flows and LMPs. Thus, an accurate network modeling shall provide better analytical results at the expense of computational complexity.

The proposed TEP formulation is represented as a MIP problem. The lossy DCOPF is adopted with the SCUC formulation. Since the proposed TEP problem is complicated, a total of six day-types, which represent weekdays and weekends in the spring/fall, summer, and winter, are used. Also, the unit commitment decisions are assumed to be identical for each day type. The model formulation is,

$$Minimize: \sum_y (OC(p,v,w,u,d,c) + IC(i) - SV(i)) \tag{5.12}$$

$Subject\ to:$

Objective function:

$$OC(p,v,w,u,d,c): \kappa_y \sum_d N_d \{\sum_t (\sum_g (C_g^{op} p_{gtdy} + C_g^{SU} s_{gtdy} + C_g^{SD} w_{gtdy} + C_g^{NL} u_{gtdy}) + \sum_{k\in\{\Omega_K\}} C_k^{ED} d_{ktdy} + \sum_{k\in\{\Omega_C\}} \sum_p c_{ktdyp})\} \tag{5.13}$$

$$IC(i): \kappa_y \sum_{k\in\{\Omega_C\}} \sum_p (L_k i_{kp} I_p) \tag{5.14}$$

$$SV(i): \kappa_y \sum_{k\in\{\Omega_C\}} \sum_p (\tau_y L_k i_{kp} I_p) \tag{5.15}$$

Network constraints:

$$\sum_{\forall \Omega_K^{n-}} f_{ktdy} - \sum_{\forall \Omega_K^{n+}} f_{ktdy} + \sum_{\forall \Omega_G^n}^{g\in\Omega_G} p_{gtdy} - l_{ntdy} = D_{ntdy} - \sum_{\forall \Omega_G^n}^{g\in\Omega_W} P_{gtdy}^W \qquad \forall n,t,d,y \tag{5.16}$$

$$f_{ktdy} - B_k(\theta_{ntdy} - \theta_{mtdy}) = 0 \qquad \forall k \in \Omega_K^F, t, d, y \tag{5.17}$$

$$\left|f_{ktdy} - B_{kp}(\theta_{ntdy} - \theta_{mtdy})\right| \le (1 - is_{kdyp}^{st2}) M_k^1 \qquad \forall\ k \in \Omega_K^C, t, d, y, p \tag{5.18}$$

$$\left|\theta_{ntdy} - \theta_{mtdy}\right| \le \theta^+ \qquad \forall n,t,d,y \tag{5.19}$$

$$\left|f_{ktdy}\right| \le F_k^+ + f_{ktdy}^{over} \qquad \forall k \in \Omega_K^F, t, d, y \tag{5.20}$$

$$\left|f_{ktdy}\right| \le \sum_p F_{kp}^+ is_{kdyp}^{st2} + f_{ktdy}^{over} \qquad \forall k \in \Omega_K^C, t, d, y \tag{5.21}$$

$$0 \le f_{ktdy}^{over} \le \sum_p is_{kdyp}^{st2} M_k^2 \qquad \forall k \in \Omega_K^C, t, d, y \qquad (5.22)$$

Security Constrained Unit Commitment Constraints:

$$P_g^- u_{gtdy} \le p_{gtdy} \le P_g^+ u_{gtdy} \qquad \forall g \in \Omega_G, t, d, y \qquad (5.23)$$

$$\sum_{q=t-UT_g+1}^{t} s_{gqdy} \le u_{gtdy} \qquad \forall g \in \Omega_G, t \ge UT_g, d, y \qquad (5.24)$$

$$\sum_{q=T+t-UT_g+1}^{T} s_{gqdy} + \sum_{q=1}^{t} s_{gqdy} \le u_{gtdy} \qquad \forall g \in \Omega_G, t \le UT_g - 1, d, y \qquad (5.25)$$

$$\sum_{q=t-DT_g+1}^{t} w_{gqdy} \le 1 - u_{gtdy} \qquad \forall g \in \Omega_G, t \ge DT_g, d, y \qquad (5.26)$$

$$\sum_{q=T+t-DT_g+1}^{T} w_{gqdy} + \sum_{q=1}^{t} w_{gqdy} \le 1 - u_{gtdy}$$

$$\forall g \in \Omega_G, t \le DT_g - 1, d, y \qquad (5.27)$$

$$p_{gtdy} - p_{g,t-1,dy} \le R_g^{HR} u_{g,t-1,dy} + R_g^{SU} s_{gtdy} \qquad \forall g \in \Omega_G, t \ge 2, d, y \qquad (5.28)$$

$$p_{g,1,dy} - p_{g,T,dy} \le R_g^{HR} u_{g,T,dy} + R_g^{SU} s_{g,1,dy} \qquad \forall k \in \Omega_K^C, t, d, y \qquad (5.29)$$

$$p_{g,t-1,dy} - p_{gtdy} \le R_g^{HR} u_{gtdy} + R_g^{SD} w_{gtdy} \qquad \forall g \in \Omega_G, t \ge 2, d, y \qquad (5.30)$$

$$p_{g,T,dy} - p_{g,1,dy} \le R_g^{HR} u_{g,1,dy} + R_g^{SD} w_{g,1,dy} \qquad \forall g \in \Omega_G, d, y \qquad (5.31)$$

$$r_{gtdy}^{sp} \le P_g^+ u_{gtdy} - p_{gtdy} \qquad \forall g \in \Omega_G, t, d, y \qquad (5.32)$$

$$r_{gtdy}^{sp} \le R_g^{10} u_{gtdy} \qquad \forall g \in \Omega_G, t, d, y \qquad (5.33)$$

$$0.07 \sum_{\gamma \in \Omega_G} \gamma \in \Omega_G + 0.1 \sum_{\gamma \in \Omega_G^W} \gamma \in \Omega_G^W + 0.05 \sum_{\gamma \in \Omega_G^H} p_{\gamma tdy} \le \sum_{\gamma \in \Omega_G} r_{\gamma tdy}^{sp}$$

$$\forall t, d, y \qquad (5.34)$$

$$s_{g,1,dy} - w_{g,1,dy} \le u_{g,1,dy} - u_{g,T,dy} \qquad \forall g \in \Omega_G, d, y \qquad (5.35)$$

$$s_{gtdy} - w_{gtdy} \le u_{gtdy} - u_{g,t-1,dy} \qquad \forall g \in \Omega_G, t \ge 2, d, y \qquad (5.36)$$

$$u_{gtdy} \in \{0,1\} \qquad \forall g \in \Omega_G, t, d, y \qquad (5.37)$$

$$0 \le s_{gtdy} \le 1 \qquad \forall g \in \Omega_G, t, d, y \qquad (5.38)$$

$$0 \leq w_{gtdy} \leq 1 \qquad \forall g \in \Omega_G, t, d, y \qquad (5.39)$$

Investment constraints:

$$i_{kp} = \begin{cases} 1: If\ the\ investemnt\ is\ decided \\ 0: Otherwise \end{cases} \qquad \forall k \in \Omega_C, p \qquad (5.40)$$

$$\sum_p i_{kp} \leq 1 \qquad \forall k \in \Omega_C \qquad (5.41)$$

$$1 \leq \sum_k \sum_p i_{kp} \leq N^c \qquad (5.42)$$

Nonanticipativity constraints:

$$i_{kp} = is_{kdyp}^{st2} \qquad \forall k \in \Omega_K^C, d, y, p \qquad (5.43)$$

Other constraints:

$$H(x) \leq 0. \qquad (5.44)$$

The objective function in (5.12) minimizes the net present value of total planning costs throughout the planning horizon. Typical generator costs include fuel costs, start up and shut down costs, and no load costs captured in (5.13) with degradation costs. The estimated salvage value of an asset at the end of the planning horizon (5.15) is used along with the capital cost (5.14).

Network constraints include node balance (5.16), power flows (5.17)- (5.18), and transmission capacity limits (5.20)-(5.21). The big-M (multiplier) reformulation is used to capture the newly included lines in the DC power flow model (5.18). The big-M reformulation is applied to avoid nonlinearities as well as to ensure that only one of those constraints will be binding at each time according to the line investment status; while the use of this big-M reformulation is common for disjunctive constraints, there are computational setbacks due to this mathematical reformulation. Theoretically, the value of

big-M needs to be large enough such that only one set of the disjunctive constraints are active for a particular solution. If the value is too large, the likely result is a substantially increased solution time as the value of the big-M multiplier significantly influence the relaxation of the MIP problem, which results in the branch-and-bound algorithm being required to search many more nodes in the branch-and-bound tree. If the big-M value is too small, the solution time is generally less, but then the resulting solution may not be the true optimal solution. In this research, 120 % of maximum possible values are chosen for the big-M values. The bus voltage angle difference constraint (5.19) proxies the angle stability. It is of note that this constraint would be redundant in the DCOPF model since one can implicitly put angle difference constraint in the power flow constraint properly [90]. The chosen maximum bus angle values are 0.6 radians. The transmission capacity limits are relaxed by allowing the line's flow to exceed the steady state thermal rating (5.20)-(5.21). The positive value of f_{ktdy}^{over} will be utilized to determine the associated cost in the degradation model. Equation (5.22) ensures that the overflow is only allowed when at least one line is invested in the candidate paths.

The chosen SCUC formulation reflects that of [90]. The minimum and maximum operating limits are modeled in (5.23). A binary variable, u_{gt}, represents the generator's commitment state. The variable has a value of one only when the unit is on; otherwise, it has a value of zero. The startup variable, s_{gt}, is equal to one only when the unit is turned on in period *t*. Similarly, the shutdown variable, w_{gt}, equals one only when the unit is shut down in period *t*. The minimum up and down time constraints, (5.24)-(5.27), employ facet defining valid inequalities, which was introduced by Rajan et al. [91] and further analyzed

by Hedman et al. [92] as the use of valid inequalities and facets of the minimum up and down time constraints within the generation unit commitment problem. The ramp rate constraints, (5.28)-(5.31), represent the limited flexibility of generators to ramp up or ramp down based on their commitment status. The spinning reserves, as proxies to enforce the *N*-1 requirement, are restricted by ramping ability of generators in (5.32)-(5.34). The spinning reserve requirement is assumed to be at least sum of 7 % of conventional generation output, 10 % of wind power output, and 5 % of hydro-generation output. These criteria reflects the CAISO's reserve rules, except for the wind power component [93]. Lastly, [64] shows that integrality constraints of the startup and shutdown variables could be relaxed by including constraints (5.35) and (5.36). Therefore, only commitment state variables, u_{gt}, are modeled as binary variables (5.37), while s_{gt} and w_{gt} variables are modeled as continuous variables (5.38) and (5.39).

The model treats the investment decisions as integer variables (5.40). Equation (5.41) ensures that the model choose only one of the investment decisions on the conductor size for each candidate path. The total number of investments is restricted by (5.42).

This model has a two-stage structure. The first stage solves the investment problem. The investment solutions influence the second stage, the production cost model, through the nonanticipativity constraints (5.43). That is, the investment decision, i_{kp}, made in the first stage should be consistently related with the investment status variable in the second stage, is_{kdyp}^{st2}. The remaining constraints (5.44) include piecewise linearized losses and temperature approximation, decomposition routine to ensure a valid approximation, and loss of tensile strength approximation.

5.2.2.1. Piecewise Linearized Losses and Temperatures Approximation

The model includes the piecewise linearized real power losses within the DCOPF formulation. Moreover, the model approximates the line temperatures to capture the elevated temperature operation that will result in annealing. Two slack variables in (5.45) represent the bus angle difference across a line *k*. The slack variables are applied to capture real power losses and line temperatures in (5.46)-(5.52) and (5.53)-(5.60), respectively. The big-M reformulation is utilized to capture the line conductance and the temperature slope properly for the candidate lines in (5.49)-(5.50) and (5.54). Constraints (5.51)-(5.52) ensure that line losses are captured only if an investment is made for each candidate path. The temperature slopes can be obtained from the IEEE standard temperature model in (4.1). The overloading of each line, h^{+}_{ktdy}, is restricted in the area between the steady state thermal limit and the presumed maximum overloading temperature in (5.57)-(5.60). The length of bus angle difference segments is limited by (5.61) and (5.62).

$$\left(\theta_{ntdy} - \theta_{mtdy}\right) - \left(\sum_{\forall i} \delta^{+}_{ktdyi} - \sum_{\forall i} \delta^{-}_{ktdyi}\right) = 0 \qquad \forall k, t, d, y \qquad (5.45)$$

$$l_{ntdy} - \sum_{\forall k(n,;)} l^{-}_{ktdy} - \sum_{\forall k(n,;)} l^{+}_{ktdy} = 0 \qquad \forall n, t, d, y \qquad (5.46)$$

$$l^{-}_{ktdy} - 2G_k\left(\sum_{\forall i} S^{L}_{i} \delta^{-}_{ktdyi}\right) = 0 \qquad \forall k \in \Omega^{F}_{K}, t, d, y \qquad (5.47)$$

$$l^{+}_{ktdy} - 2G_k\left(\sum_{\forall i} S^{L}_{i} \delta^{+}_{ktdyi}\right) = 0 \qquad \forall k \in \Omega^{F}_{K}, t, d, y \qquad (5.48)$$

$$\left|l^{-}_{ktdy} - 2G_{kp}\left(\sum_{\forall i} S^{L}_{i} \delta^{-}_{ktdyi}\right)\right| \leq \left(1 - xs^{st2}_{kdyp}\right) M^{3}_{k} \qquad \forall k \in \Omega^{C}_{K}, t, d, y, p \qquad (5.49)$$

$$\left|l^{+}_{ktdy} - 2G_{kp}\left(\sum_{\forall i} S^{L}_{i} \delta^{+}_{ktdyi}\right)\right| \leq \left(1 - xs^{st2}_{kdyp}\right) M^{3}_{k} \qquad \forall k \in \Omega^{C}_{K}, t, d, y, p \qquad (5.50)$$

$$0 \leq l^{-}_{ktdy} \leq \sum_{p} xs^{st2}_{kdyp} M^{3}_{k} \qquad \forall k \in \Omega^{C}_{K}, t, d, y \qquad (5.51)$$

$$0 \leq l^{+}_{ktdy} \leq \sum_{p} xs^{st2}_{kdyp} M^{3}_{k} \qquad \forall k \in \Omega^{C}_{K_C}, t, d, y \qquad (5.52)$$

$$h_{ktdy} - \sum_{\forall i} B_k S_i^T \delta_{ktdyi}^{+} - \sum_{\forall i} B_k S_i^T \delta_{ktdyi}^{-} = 0 \qquad \forall k \in \Omega_K^F, t, d, y \qquad (5.53)$$

$$\left|h_{ktdy} - \sum_{\forall i} B_{kp} S_{ip}^T \delta_{ktdyi}^{+} - \sum_{\forall i} B_{kp} S_{ip}^T \delta_{ktdyi}^{-}\right| \leq \left(1 - xs_{kdyp}^{st2}\right) M_k^4$$

$$\forall k \in \Omega_K^C, t, d, y, p \qquad (5.54)$$

$$h_{ktdy} - H_k^{+} = h_{ktdy}^{+} - h_{ktdy}^{-} \qquad \forall k \in \Omega_K^F, t, d, y \qquad (5.55)$$

$$h_{ktdy} - \sum_p H_{kp}^{+} x_{kp} = h_{ktdy}^{+} - h_{ktdy}^{-} \qquad \forall k \in \Omega_K^C, t, d, y \qquad (5.56)$$

$$0 \leq h_{ktdy}^{+} \leq T_k^{+} \qquad \forall k \in \Omega_K^F, t, d, y \qquad (5.57)$$

$$0 \leq h_{ktdy}^{+} \leq \sum_p T_{kp}^{+} xs_{kdyp}^{st2} \qquad \forall k \in \Omega_K^C, t, d, y \qquad (5.58)$$

$$0 \leq h_{ktdy}^{-} \leq H_k^{+} - H_\infty \qquad \forall k \in \Omega_K^F, t, d, y \qquad (5.59)$$

$$0 \leq h_{ktdy}^{-} \leq \sum_p \left(H_{kp}^{+} - H_\infty\right) xs_{kdyp}^{st2} \qquad \forall k \in \Omega_K^C, t, d, y \qquad (5.60)$$

$$0 \leq \delta_{ktdyi}^{+} \leq \overline{\delta_i^{+}} \qquad \forall k, i, t, d, y \qquad (5.61)$$

$$0 \leq \delta_{ktdyi}^{-} \leq \overline{\delta_i^{+}} \qquad \forall k, i, t, d, y \qquad (5.62)$$

5.2.2.2. Correction Routine for Piecewise Linear Approximations

The model uses a piecewise linear approximation of a nonconvex constraint. However, in order to produce a valid solution, the model should meet the two conditions: 1) the exclusivity and 2) the adjacency conditions. Reference [4] discusses a similar piecewise linear formulation for loss approximation and describes that, if these conditions are not satisfied, losses can be inaccurately high; the work shows that this breakdown can happen when there are negative LMPs. By introducing binary variables that represent the different blocks of the piecewise linear reformulation of this nonconvex constraint, it is then possible to guarantee that these two conditions are satisfied. In this dissertation, the model employs the correction routine where binary variables that represent the different segments of the

piecewise linear reformulation are added, but only when those conditions are not met (5.63)-(5.76). The correction algorithm reflects that of [4].

$$z^{+}_{ktdy,i+1}\overline{\delta^{+}_{i}} \le \delta^{+}_{ktdyi} \qquad \forall k \in \{\Omega_K, \Omega^{-}_K\}, i, t, d, y \qquad (5.63)$$

$$z^{+}_{ktdy,i+1}\overline{\delta^{+}_{i}} \le \delta^{-}_{ktdyi} \qquad \forall k \in \{\Omega_K, \Omega^{-}_K\}, i, t, d, y \qquad (5.64)$$

$$z^{+}_{ktdy1} + z^{-}_{ktdy1} \le 1 \qquad \forall k \in \{\Omega_K, \Omega^{-}_K\}, i, t, d, y \qquad (5.65)$$

$$z^{+}_{ktdyi}, z^{-}_{ktdyi} \in \{0,1\} \qquad \forall k \in \{\Omega_K, \Omega^{-}_K\}, i, t, d, y \qquad (5.66)$$

$$\delta^{+}_{ktdyi} \le z^{k+}_{itdy}\overline{\delta^{+}_{i}} \qquad \forall k \in \{\Omega_K, \Omega^{-}_K\}, i, t, d, y \qquad (5.67)$$

$$\delta^{+}_{ktdyi} \le z^{k+}_{itdy}\overline{\delta^{+}_{i}} \qquad \forall k \in \{\Omega_K, \Omega^{-}_K\}, i, t, d, y \qquad (5.68)$$

$$z^{k+}_{i+1,ptdy}\overline{\delta^{+}_{i}} \le \delta^{+}_{kptdyi} \qquad \forall k \in \{\Omega^{C}_K, \Omega^{-}_K\}, i, p, t, d, y \qquad (5.69)$$

$$z^{k+}_{i+1,ptdy}\overline{\delta^{+}_{i}} \le \delta^{-}_{kptdyi} \qquad \forall k \in \{\Omega^{C}_K, \Omega^{-}_K\}, i, p, t, d, y \qquad (5.70)$$

$$z^{k+}_{1,ptdy} + z^{k-}_{1,ptdy} \le 1 \qquad \forall k \in \{\Omega^{C}_K, \Omega^{-}_K\}, i, p, t, d, y \qquad (5.71)$$

$$z^{k+}_{iptdy}, z^{k-}_{iptdy} \in \{0,1\} \qquad \forall k \in \{\Omega^{C}_K, \Omega^{-}_K\}, i, p, t, d, y \qquad (5.72)$$

$$\delta^{+}_{kptdyi} \le z^{k+}_{iptdy}\overline{\delta^{+}_{i}} \qquad \forall k \in \{\Omega^{C}_K, \Omega^{-}_K\}, i, p, t, d, y \qquad (5.73)$$

$$\delta^{+}_{kptdyi} \le z^{k+}_{iptdy}\overline{\delta^{+}_{i}} \qquad \forall k \in \{\Omega^{C}_K, \Omega^{-}_K\}, i, p, t, d, y \qquad (5.74)$$

$$\left|\delta^{+}_{ktdyi} - \delta^{+}_{kptdyi}\right| \le \left(1 - xs^{st2}_{kdyp}\right)M^{5}_{k} \qquad \forall k \in \{\Omega^{C}_K, \Omega^{-}_K\}, i, p, t, d, y \qquad (5.75)$$

$$\left|\delta^{-}_{ktdyi} - \delta^{-}_{kptdyi}\right| \le \left(1 - xs^{st2}_{kdyp}\right)M^{5}_{k} \qquad \forall k \in \{\Omega^{C}_K, \Omega^{-}_K\}, i, p, t, d, y \qquad (5.76)$$

5.2.2.3. Loss of Tensile Strength Prediction

The proposed TEP model employs the degradation decomposition model to capture the degradation effect and associated cost. The model assumes that the temperature effect term is proportional to the operating temperature, but only when such temperature is not above

the maximum temperature that incurs a permanent loss of tensile strength. In addition, only the specific number of continous overheating operations are captured to avoid computational burden. With these assumptions in hand, the IEEE standard degradation model in (4.3) is used to obtain the value of the temperature effect term and the time effect term for each conductor type. The model also requires a tuning process to relate the approximated degradation model with the IEEE standard degradation model to ensure the consistency of the degradation result.

The positive temperature overloading segments, h^{+}_{ktdy}, in (5.55) and (5.56) are utilized to approximate the loss of tensile strength in (5.77)-(5.80). The ratio of these positive temperature segments and the maximum allowable operating temperature is multiplied by the loss of strength terms at each time. Note that the time effect term is only applied when there is a continuous overheating operation. An optimization technique, which is presented in [94], is applied in (5.81) and (5.82) to obtain the degradation costs while avoiding a nonlinear term in the objective function. That is, the degradation cost, c_{ktdyp}, has a positive value only when the investment decision is made (5.81); otherwise, it has a value of zero (5.82),

$$d_{ktdy} = \mu\left(\frac{LS_k^{Temp}}{H^{tr}-H_k^{+}} h^{+}_{ktdy} + \frac{LS_k^{Time}}{H^{tr}-H_k^{+}} h^{+}_{k,t-1,dy}\right) \qquad \forall k \in \Omega_K^F, t \geq 2, d, y \qquad (5.77)$$

$$d_{ktdyp} = \mu_p\left(\frac{LS_{kp}^{Temp}}{H_p^{tr}-H_p^{+}} h^{+}_{ktdy} + \frac{LS_{kp}^{Time}}{H_p^{tr}-H_p^{+}} h^{+}_{k,t-1,dy}\right) \qquad \forall k \in \Omega_K^C, t \geq 2, d, y, p \qquad (5.78)$$

$$d_{ktdy} = \mu\left(\frac{LS_k^{Temp}}{H^{tr}-H_k^{+}} h^{+}_{k,1,dy} + \frac{LS_k^{Time}}{H^{tr}-H_k^{+}} h^{+}_{k,T,dy}\right) \qquad \forall k \in \Omega_K^F, d, y \qquad (5.79)$$

$$d_{ktdyp} = \mu_p \left(\frac{LS_{kp}^{Temp}}{H_p^{tr} - H_p^{+}} h_{k,1,dy}^{+} + \frac{LS_{kp}^{Time}}{H_p^{tr} - H_p^{+}} h_{k,T,dy}^{+} \right) \qquad \forall k \in \Omega_K^C, d, y, p \qquad (5.80)$$

$$c_{ktdyp} \geq C_p^{ED} d_{ktdyp} - C_p^{ED^2} (1 - xs_{kdyp}^{st2}) \qquad \forall k \in \Omega_K^C, t, d, y, p \qquad (5.81)$$

$$c_{ktdyp} \geq 0. \qquad \forall k \in \Omega_K^C, t, d, y, p \qquad (5.82)$$

5.2.3. Decomposition Approach

A Lagrange decomposition algorithm is employed to improve the computational efficiency of this complex combinatorial problem. The proposed TEP formulation is well structured for the use of LR since the connection between the investment decision and the system operating condition is only held by the nonanticipativity constraints (4.33). Therefore, by dualizing the nonanticipativity constraints, one can decompose the model into the investment subproblem and the production cost subproblem. Moreover, the production cost subproblem can be decomposed again by each typical day-type. This thesis adopted the LR algorithm from [70]. Figure 5.3 shows an overview of LR algorithm.

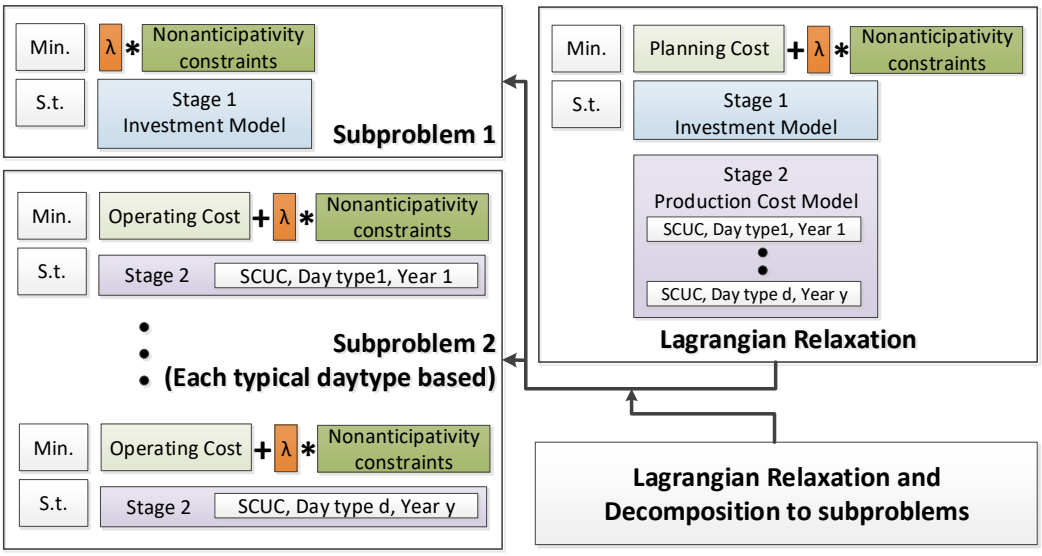

Figure 5.3 Overview of Lagrange Relaxation Algorithm.

First, the Lagrangian can be obtained by dualizing the coupling constraints (5.43) as follows,

$$\mathcal{L} = \sum_y (OC(p,v,w,u,d,c) + IC(i) - SV(i)) + \sum_{ydkp} \left(\pi_{kdyp} \left(i_{kp} - is^{st2}_{kdyp} \right) \right) \tag{5.83}$$

The Lagrangian can be decomposed into an investment subproblem, SP1, and the production cost subproblems, SP2, as follows,

SP1 $Minimize: \sum_y (IC(\boldsymbol{i}) - SV(\boldsymbol{i})) + \sum_{ydkp} \pi_{kdyp} i_{kp}$

Subject to (5.40)-(5.44) (5.84)

SP2 $Minimize: \sum_y OC(p,v,w,u,d,c) - \sum_{ydkp} \pi_{kdyp} is^{st2}_{kdyp}$

Subject to (5.16)-(5.39), (5.45)-(5.82) (5.85)

The subproblems are solved in a parallel environment at each iteration; then the upper and lower bound of the objective function can be obtained based on the solutions from the investment subproblem and production cost subproblem, respectively. Note that the investment solutions from the production cost subproblems are only penalized by the dual variables; therefore, the decomposition algorithm tries to reduce a gap between the upper and lower bound by updating the dual variables at each iteration. The dual variables are updated based on investment status solution of (SP1) and (SP2) at each iteration j as follows,

$$\pi^{j+1}_{kdyp} = \pi^{j+1}_{kdyp} + \lambda_j \left(i^j_{kp} - is^{st2,j}_{kdyp} \right). \qquad \forall k,d,y,p \tag{5.86}$$

The method to choose the step size, λ_j, at each iteration is adopted based on the one presented in [68] and is given as follows,

$$\lambda_j = \frac{\rho\left(UB^j - LB^j\right)}{\sum_{ydkp}\left(\left(i_{kp}^j - is_{kdyp}^{st2,j}\right)^2\right)} \tag{5.87}$$

where UB^j and LB^j represents the upper and lower bounds at iteration j, respectively. Note that the investment solution of (SP1) is used for generating a feasible solution, the upper bound, to the original problem. The algorithm is terminated once the gap between the upper and lower bound reached a presumed termination criterion, which is 0.1 % in this work. The factor ρ is used to tune the step size and can be any number; however, from observation, a higher step size makes it difficult to find a solution with a small termination criterion. Figure 5.4 shows an overview of the decomposition procedure applied in this research.

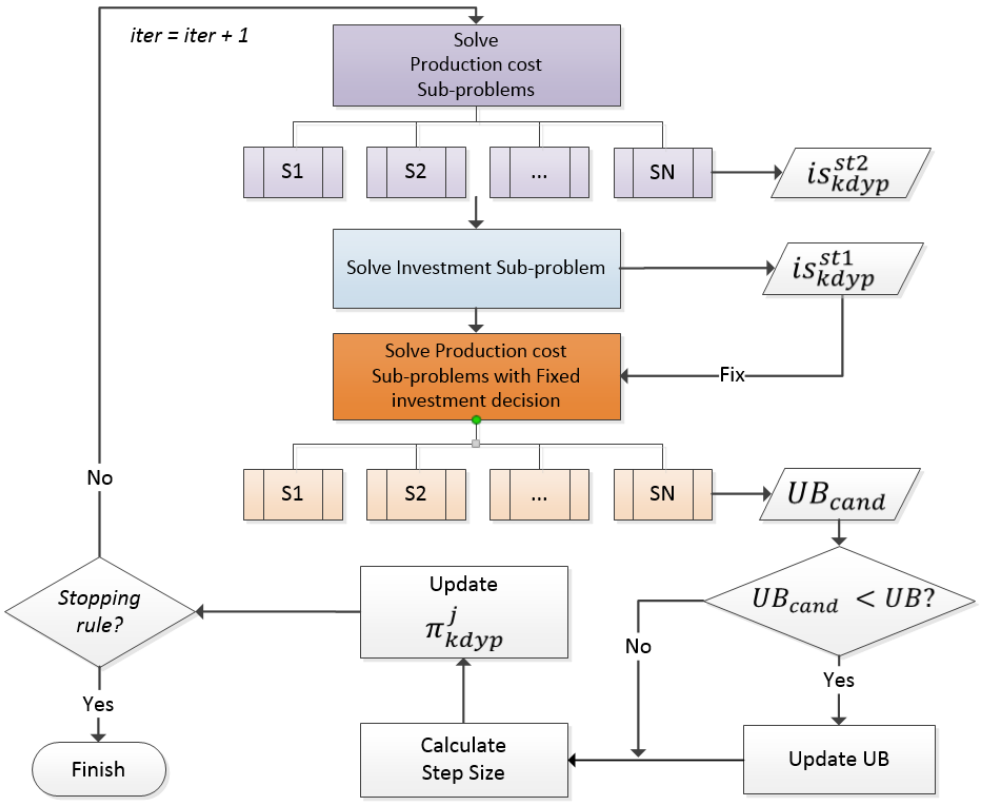

Figure 5.4 Flowchart of Lagrange Relaxation Process.

5.2.4. Renewable Modeling

In this work, wind forecast data was obtained from [95] and classified into each typical day type. The work employed a scenario reduction technique to tackle computational difficulty. A backward reduction method, which is presented in [96], was used to select 100 scenarios for each day type. The backward reduction technique iteratively deletes the scenarios that have the minimum distance of the scenario pairs. The probability of deleted scenarios is reallocated to the remaining scenarios.

5.2.5. Numerical Analysis Design

The proposed TEP formulation provides an optimal path and size of a conductor simultaneously within candidates. However, the case study assumes that the number of candidate paths is limited by geological or political obstacles; therefore, the numerical analysis includes only one candidate path. Thus, the case study can solely focus on the impact of utilizing TCR combined with the degradation model on the optimal selection of conductor size.

The simulation is performed on the IEEE 24-bus Reliability Test System (RTS), which is publicly available from [97]. Hourly loads presented in [98] were aggregated into six typical days representing a typical weekday and weekend day for each of three seasons, as shown in Table 5.1 and Table 5.2, respectively. The test system includes startup costs and no-load costs; shutdown costs are assumed to be zero. An average production cost is obtained from the heat rate data provided in [97] and fuel cost provided in [99]-[100], as shown in Table 5.3 and Table 5.4, respectively. General generator operation data are adopted from [98].

Table 5.1 Typical Day Types

Day Type	Season	Day	Number of Days
1	Winter	Week	85
2	Winter	Weekend	34
3	Summer	Week	65
4	Summer	Weekend	26
5	Spring/Fall	Week	110
6	Spring/Fall	Weekend	44

Table 5.2 Hourly Load Percent Levels for each Day Type [98]

Time		1	2	3	4	5	6	7	8	9	10	11	12
Day Type	1	67	63	60	59	59	60	74	86	95	96	96	95
	2	78	72	68	66	64	65	66	70	80	88	90	91
	3	64	60	58	56	56	58	64	76	87	95	99	100
	4	74	70	66	65	64	62	62	66	81	86	91	93
	5	63	62	60	58	59	65	72	85	95	99	100	99
	6	75	73	69	66	65	65	68	74	83	89	92	94
Time		13	14	15	16	17	18	19	20	21	22	23	24
Day Type	1	95	95	93	94	99	100	100	96	91	83	73	63
	2	90	88	87	87	91	100	99	97	94	92	87	81
	3	99	100	100	97	96	96	93	92	92	93	87	72
	4	93	92	91	91	92	94	95	95	100	93	88	80
	5	93	92	90	88	90	92	96	98	96	90	80	70
	6	91	90	90	86	85	88	92	100	97	95	90	85

Table 5.3 Generator Data (IEEE 24-bus RTS) [97]

Gen Group	Size (MW)	Type	Fuel Costs ($/MWh)	Startup Costs ($)	No-load Costs ($)
U12	12	Oil/Steam	219.38	1322.65	168.29
U20	20	Oil/CT	280.98	130.74	1962.63
U50	50	Hydro	N/A	N/A	N/A
U76	76	Coal/Steam	26.09	1409.05	173.50
U100	100	Oil/Steam	174.42	10963.55	1935.75
U155	155	Coal/Steam	20.61	2261.82	336.90
U197	197	Oil/Steam	174.10	15162.04	2701.52
U350	350	Coal/Steam	21.33	10676.86	480.92
U400	400	Nuclear	8.66	3806.37	341.11

Table 5.4 Fuel Costs (IEEE 24-bus RTS) [99]-[100]

Fuel Type	#2 Oil	#6 Oil	Coal	Nuclear
Costs [$/MBtu]	23.08	19.33	2.35	0.95

The weather conditions that affect the conductor temperature are assumed to be fixed during the whole planning horizon as listed in Table 5.5. Note that the conductor thermal dynamics analysis under various weather conditions or considering stochastic characteristic of weather conditions are not conducted in this study. The wind data, 280 MW generation capacity and 43 % net capacity factor, sampled from [95] was applied to the scenario reduction algorithm presented in [96]. The chosen wind farm capacity is about 10 % of the peak load. The distance between the wind farm and the connecting point is assumed to be 100 miles. The study also assumes that the wind farm will be located at node 18. The chosen four types of ACSR conductors include Sparate, Raven, Quail, and Pigeon conductors. Table 5.6 presents electrical characteristics [101] and capital cost of these conductors [102]-[103]. It is assumed that reconductoring of the line requires only labor and conductor cost; the end-of-service cost of the line is assumed as in Table 5.6. The load growth scenarios for 15-year planning horizon, 3-years per each stage, were created at a rate of 0.9 % each year [104]. The discount rate is assumed to be 3.04 % [105]; fuel costs and other fixed costs are assumed to be fixed.

Table 5.5 Weather Conditions [30]

Ambient Temperature	40 °C	Latitude	30°
Wind Speed	2 ft/s	Sun Time	11:00 am
Wind Direction	90°	Emissivity	0.5
Atmosphere	Clear	Solar absorptivity	0.5
Elevation	328 ft		

Table 5.6 Conductor Data

	Sparate	Raven	Quail	Pigeon
R (Ohm/mile)	1.04	0.85	0.64	0.56
X (Ohm/mile)	0.60	0.59	0.57	0.55
Thermal Capacity (MW)	184	242	276	315
Capital Cost (M$/mile)	0.838	0.846	0.854	0.863
End-of-service Cost (M$/mile)	0.283	0.285	0.286	0.288

Testing is performed using CPLEX 12.6 and parallelized using the Message Passing Interface on an Intel Xeon 3.60 GHz CPU with 48 GB memory. Production cost subproblems are terminated upon reaching an optimality gap of 0.01 %. Also, the decomposition algorithm is terminated after 50 iterations or upon reaching an optimality gap of 1 %.

5.2.6. Test Case: IEEE 24-Bus Reliability Test System

The 100 scenarios are selected from the scenario reduction algorithm. Table 5.7 presents the planning costs ($M) for each conductor type when TCR is not allowed; only the Quail conductor gives a cost saving of 0.06 %. However, in Table 5.8, the result shows that the Raven conductor can provide a better cost saving than the Quail conductor when TCR is allowed with the degradation model. The overall deterioration of the Raven conductor over 15 years is 3.21 %, which is still below the presumed end-of-service criterion. The cost saving of the Sparate conductor is improved in Table 5.8 with 29.4 % of degradation, which is not practical. Table 5.9 shows the temperature and accumulated degradation results for each conductor type. It is of note that difference of capital cost

between each conductor type is relatively small; majority cost savings are coming from the reduced production cost.

Table 5.7 Planning Results (without TCR, $M)

	Sparate	Raven	Quail	Pigeon
Planning Cost	11,211	10,996	10,981	10,987
Investment Cost	49.9	50.4	50.9	51.4
Production Cost	11,161	10,946	10,930	10,936
Degradation Cost	-	-	-	-
Loss of strength (%)	-	-	-	-
Cost Saving (%)	-2.04	-0.08	0.06	-

Table 5.8 Planning Results (with TCR, $M)

	Sparate	Raven	Quail	Pigeon
Planning Cost	11,016	10,974	10,981	10,987
Investment Cost	49.9	50.4	50.9	51.4
Production Cost	10,896	10,916	10,930	10,936
Degradation Cost	69.77	7.58	0.03	-
Loss of strength (%)	29.40	3.21	0.01	-
Cost Saving (%)	-0.26	0.12	0.06	-

Table 5.9 Temperature and Degradation Results (with TCR, $M)

	Sparate	Raven	Quail	Pigeon
Average Overflow (MW)	14.83	1.71	0.01	-
Min Temp. (°C)	40.18	40.14	40.13	40.12
Average Temp. (°C)	65.63	56.68	53.62	51.15
Max Temp. (°C)	124.88	87.48	75.69	68.60
Loss of strength (%)	29.40	3.21	0.01	-

Figure 5.5 shows the line overflow information along with the line temperature and degradation for the Raven conductor on stage 1 in day type 1. Note that the line thermal rating is 242 MW and 75 °C. The result shows that the proposed model can capture the

degradation effects properly while considering the line temperature and continuous operations at the elevated temperatures.

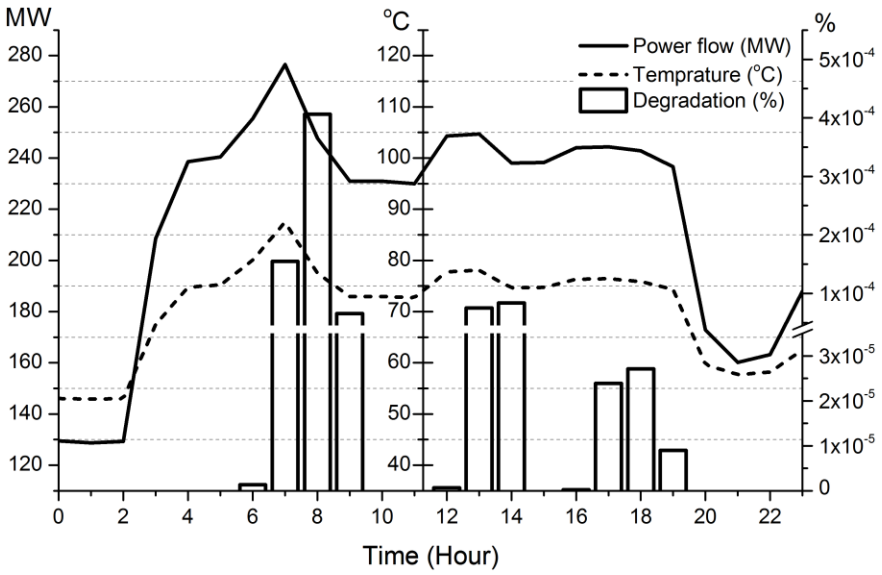

Figure 5.5 Line Power Flow, Temperature, and Degradation Result
(Stage 1/Day type 1, Raven conductor).

Figure 5.6 presents the duration curve of the wind farm output, which is transported through the transmission line when TCR is not applied. All the outputs above the thermal rating of each conductor type are curtailed. However, when TCR is allowed, as shown in Figure 5.7, more wind farm output can be utilized by allowing flexible line operation. Line overflows occurs only when the benefit of the additional line flows exceed the degradation costs, which is captured by the degradation model. The wind farm output curtailments still exist in Figure 5.7 except the Pigeon conductor; nevertheless, the results show that the Quail and Raven conductors can provide cost savings.

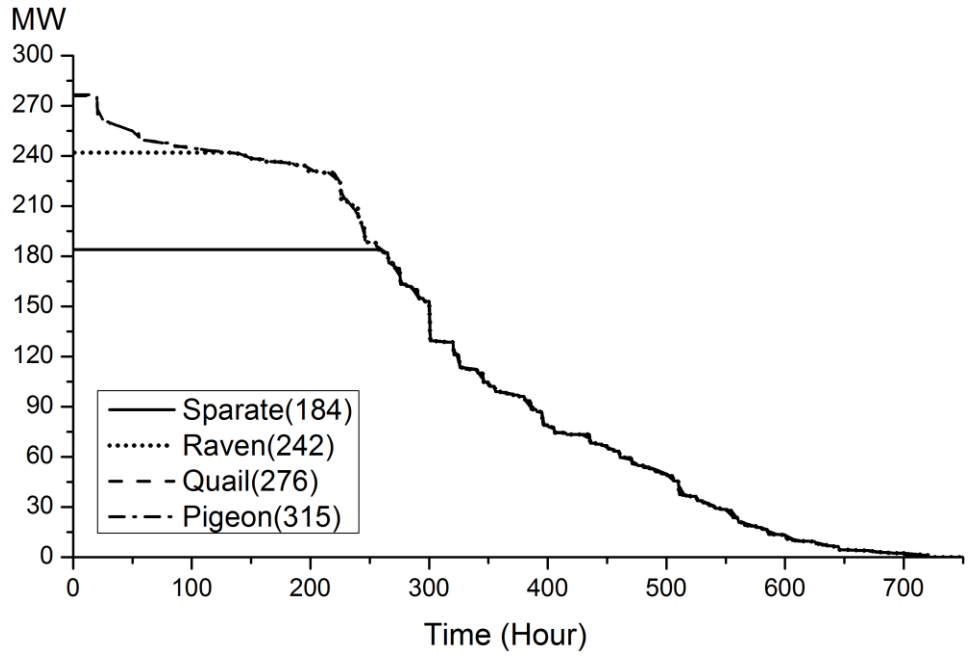

Figure 5.6 Wind Farm Output Duration Curve (without TCR).

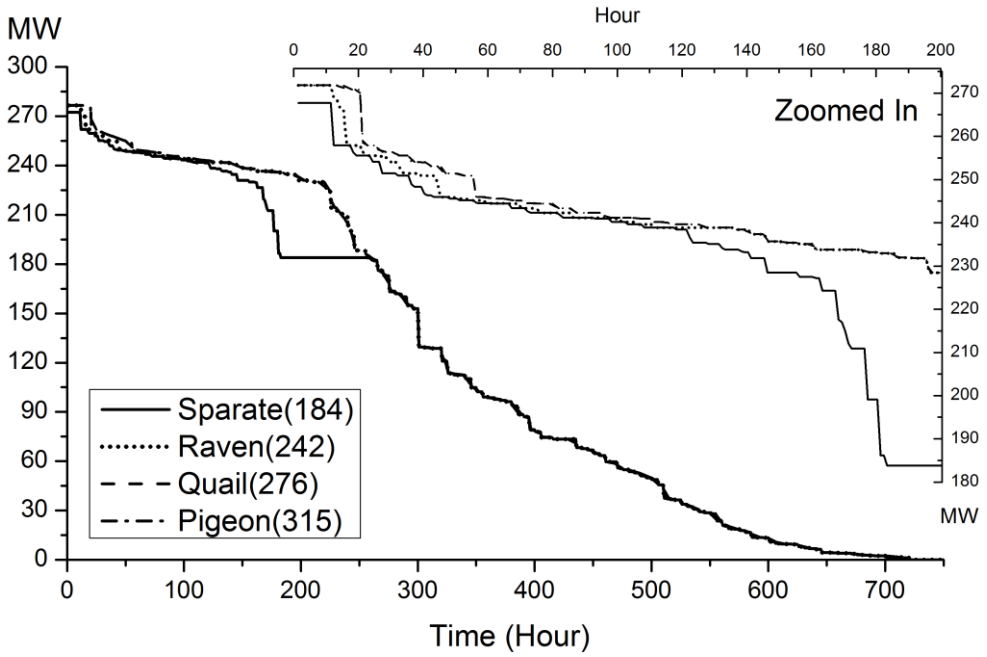

Figure 5.7 Wind Farm Output Duration Curve (with TCR).

This study also performed a sensitivity study with the 100 scenarios to investigate the trend and the main factors of the results Figure 5.8 shows the cost savings results from all the scenarios for Raven conductors, which are represented with a black rhombus symbol, and Quail conductors, which are shown with a white circle symbol. Both conductors provide cost savings in most of the scenarios, except only one case for the Raven conductor; however, the Raven conductor gives higher cost savings in both average and maximum values.

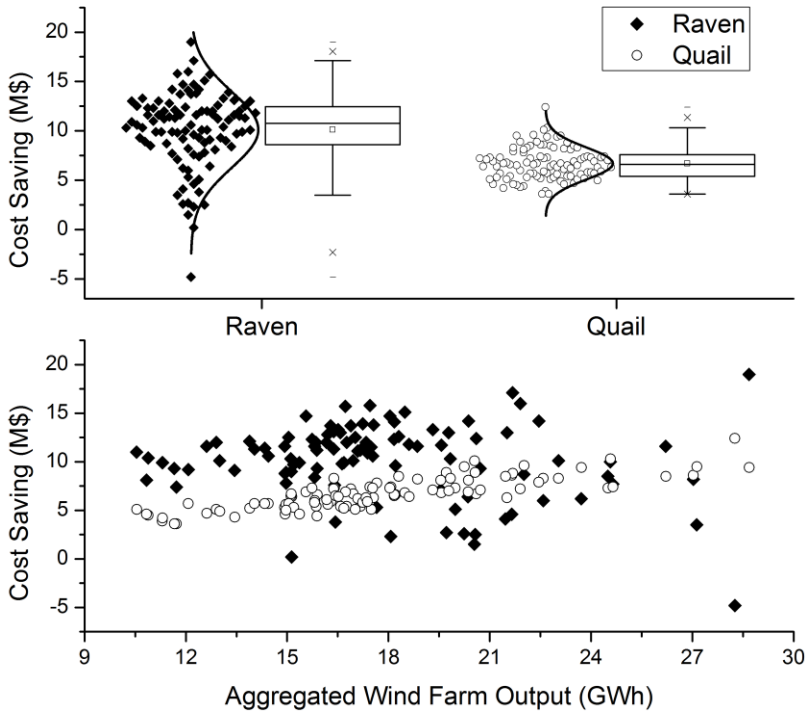

Figure 5.8 Cost Savings Results of Sensitivity Studies
(Raven and Quail Conductor, TCR, 100 Scenarios).

Moreover, the sensitivity studies are conducted based on the different net capacity factors of the wind farm and the line lengths. Both parameters are varied between 50 % and 150 % exogenously. The result, as shown in Figure 5.9, shows that better cost savings

are possible with either higher net capacity of the wind farm or longer line lengths; however, the Raven conductor has higher marginal benefits in both cases. Also, the gap between the Raven and Quail conductors increases as both factors increase.

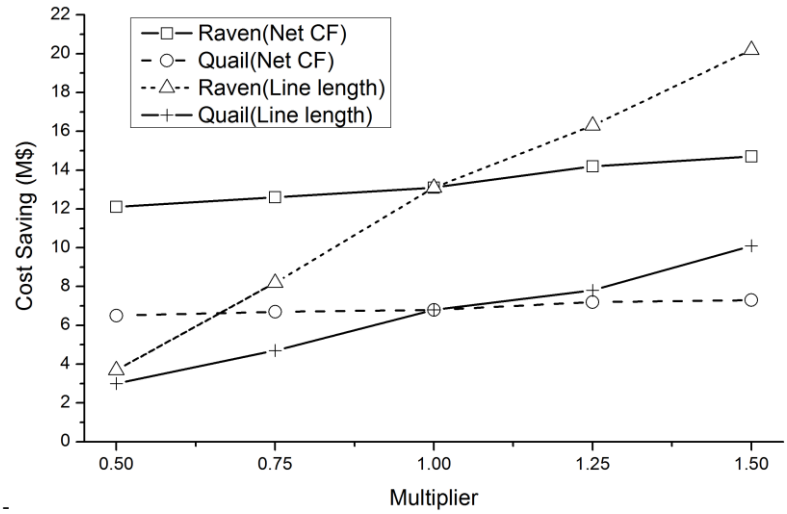

Figure 5.9 Sensitivity Results of the Wind Farm Net Capacity Factor and the Line Length.

5.2.7. Conclusions

In this chapter, this dissertation proposes a static TEP model joint with the degradation model, being able to provide an alternative way to choose optimal conductor size and path for the large wind farm integration. The model is formulated as a MIP problem with the lossy DCOPF coordinated with the SCUC. The TEP model incorporates the degradation decomposition model to approximate the degradation cost associated with the operation of overhead conductors at elevated temperature.

Testing on the IEEE 24-bus RTS shows that employing TCR with the proposed degradation decomposition model helps to achieve a total planning cost saving by choosing a proper conductor type. The results, however, present relatively small amount of cost

savings in percentage. Nevertheless, the proposed model shows the opportunities to save the total planning costs by practicing TCR practices with a proper determination of the penalty price within a TEP model.

5.3. Transmission Expansion Planning Model with Preserved Rights-of-Way

The means for transporting more power through an existing transmission corridor have been given considerable attention in recent studies. Reconductoring a path with a conductor that has a higher thermal capacity, such as an HTLS conductor, is one possible option with minimal structural modification and out-of-service time. Parallel line additions or HTLS parallel line additions are other options that can increase transfer capabilities and reduce operating costs. TCR is another option, which is an operational based method that allows the line flow to exceed the steady-state line rating for a certain penalty price. In this work, the above options are captured to create the proposed TEP model. Numerical simulations conducted on the IEEE-24 and IEEE-118 bus system indicate the effectiveness of the proposed approach to increase system capacity while preserving existing ROW.

5.3.1. Background and Motivation

Political obstacles and environmental issues often impede construction of a new line, especially when a new ROW is required. As a result, various means of transporting more power through existing transmission corridors have given considerable attention. This research proposes a long-term dynamic TEP model that includes the following options to increase transmission capacity while preserving existing ROW: (i) HTLS reconductoring, (ii) parallel line additions, (iii) parallel HTLS line installation (installing two HTLS lines

in parallel), and (iv) TCR options. The TEP model is formulated as an MIP problem that contains a lossy DCOPF and SCUC formulation. The degradation decomposition model is used to capture the impacts of operating conductors at elevated temperatures.

5.3.2. Mathematical Formulation

This section presents the proposed TEP model formulation. The main structure of the model is similar to the one introduced in Chapter 5.2.

$$Minimize: \sum_y (OC(p,v,w,u,d,c) + IC(i) - SV(i)) \tag{5.88}$$

$Subject\ to:$

Objective function:

$$OC(p,v,w,u,d,c): \kappa_y \sum_d N_d \{\sum_t (\sum_g (C_g^{op} p_{gtdy} + C_g^{SU} s_{gtdy} + C_g^{SD} w_{gtdy} + C_g^{NS} u_{gtdy}) + \sum_{k\in\{\Omega_K\}} (c_{ktdy} + c_{ktdyp})\} \tag{5.89}$$

$$IC(i): \kappa_y \sum_{k\in\{\Omega_K\}} \sum_p (L_k i_{kpy} I_p) \tag{5.90}$$

$$SV(i): \kappa_Y \sum_{k\in\{\Omega_K\}} \sum_p (\tau_y L_k i_{kpy} I_p) \tag{5.91}$$

Network constraints:

$$\sum_{\forall \Omega_K^{n-}} f_{ktdy} - \sum_{\forall \Omega_K^{n+}} f_{ktdy} + \sum_{\forall \Omega_G^n}^{g\in\Omega_G} p_{gtdy} - l_{ntdy} = D_{ntdy} \qquad \forall n,t,d,y \tag{5.92}$$

$$\left|f_{ktdy} - B_k(\theta_{ntdy} - \theta_{mtdy})\right| \le \left(\sum_p is_{kdyp}^{st2}\right) M_k^1 \qquad \forall k \in \Omega_K, t, d, y \tag{5.93}$$

$$\left|f_{ktdy} - B_{kp}(\theta_{ntdy} - \theta_{mtdy})\right| \le \left(1 - is_{kdyp}^{st2}\right) M_k^1 \qquad \forall\, k \in \Omega_K, t, d, y, p \tag{5.94}$$

$$-\theta^+ \le \theta_{ntdy} - \theta_{mtdy} \le \theta^+ \qquad \forall n,t,d,y \tag{5.95}$$

$$\left|f_{ktdy}\right| \le \sum_p F_{kp}^+ is_{kdyp}^{st2} + F_{kp}^+ (1 - \sum_p is_{kdyp}^{st2}) + f_{ktdy}^{over} \qquad \forall k \in \Omega_K, t, d, y \tag{5.96}$$

Generator capacity and ramping constraints:

(5.23)-(5.39)

Piecewise linearized losses and temperatures:

$$\left|l^{-}_{ktdy} - 2G_k\left(\sum_{\forall i} S^L_i \delta^{-}_{ktdyi}\right)\right| \le \sum_p is^{st2}_{kdyp} M^3_k \qquad \forall k \in \Omega_K, t, d, y \qquad (5.97)$$

$$\left|l^{+}_{ktdy} - 2G_k\left(\sum_{\forall i} S^L_i \delta^{+}_{ktdyi}\right)\right| \le \sum_p is^{st2}_{kdyp} M^3_k \qquad \forall k \in \Omega_K, t, d, y \qquad (5.98)$$

$$\left|l^{-}_{ktdy} - 2G_{kp}\left(\sum_{\forall i} S^L_i \delta^{-}_{ktdyi}\right)\right| \le \left(1 - is^{st2}_{kdyp}\right) M^3_k \qquad \forall k \in \Omega_K, t, d, y, p \qquad (5.99)$$

$$\left|l^{+}_{ktdy} - 2G_{kp}\left(\sum_{\forall i} S^L_i \delta^{+}_{ktdyi}\right)\right| \le \left(1 - is^{st2}_{kdyp}\right) M^3_k \qquad \forall k \in \Omega_K, t, d, y, p \qquad (5.100)$$

$$\left|h_{ktdy} - \sum_{\forall i} B_k S^T_i \delta^{+}_{ktdyi} - \sum_{\forall i} B_k S^T_i \delta^{-}_{ktdyi}\right| \le \sum_p is^{st2}_{kdyp} M^4_k$$

$$\forall k \in \Omega_K, t, d, y \qquad (5.101)$$

$$\left|h_{ktdy} - \sum_{\forall i} B_{kp} S^T_i \delta^{+}_{ktdyi} - \sum_{\forall i} B_{kp} S^T_i \delta^{-}_{ktdyi}\right| \le \left(1 - is^{st2}_{kdyp}\right) M^4_k$$

$$\forall k \in \Omega_K, t, d, y, p \qquad (5.102)$$

$$h_{ktdy} - \sum_p H^{+}_{kp} is^{st2}_{kdyp} - H^{+}_k\left(1 - \sum_p is^{st2}_{kdyp}\right) = h^{+}_{ktdy} - h^{-}_{ktdy}$$

$$\forall k \in \Omega_K, t, d, y \qquad (5.103)$$

$$0 \le h^{+}_{ktdy} \le \sum_p T^{+}_{kp} is^{st2}_{kdyp} + T^{+}_k\left(1 - \sum_p is^{st2}_{kdyp}\right) \qquad \forall k \in \Omega_K, t, d, y \qquad (5.104)$$

$$0 \le h^{-}_{ktdy} \le \sum_p \left(H^{+}_{kp} - H_\infty\right) is^{st2}_{kdyp} + \left(H^{+}_k - H_\infty\right)\left(1 - \sum_p is^{st2}_{kdyp}\right)$$

$$\forall k \in \Omega_K, t, d, y \qquad (5.105)$$

(5.45)-(5.46), (5.61)-(5.62)

Loss of tensile strength prediction:

(5.77)-(5.82)

Investment constraints:

$$i_{kpy} = \begin{cases} 1: If\ the\ investemnt\ is\ decided \\ 0: Otherwise \end{cases} \qquad \forall k \in \Omega_K, p, y \qquad (5.106)$$

$$\sum_y \sum_p i_{kpy} \leq 1 \qquad \forall k \in \Omega_K \qquad (5.107)$$

$$is_{kdyp}^{st2} = \sum_{q \leq y} i_{kpy} \qquad \forall k \in \Omega_K, d, y \qquad (5.108)$$

Nonanticipativity constraints:

$$is_{kdyp}^{st1} = is_{kdyp}^{st2} \qquad \forall k \in \Omega_K, d, y, p \qquad (5.109)$$

The objective, (5.88), minimizes total system costs throughout the planning horizon and is evaluated in terms of discounted costs, i.e., the cost function takes into consideration the time value of money. Operating costs include typical generator costs (fuel costs, start up and shut down costs, no load costs of generators) and degradation costs (5.89). The salvage value is considered as a percentage of depreciation of the initial capital cost in (5.91) at the end of the planning horizon.

The node balance constraint (5.92) ensures that the net power injection over all lines connected to node *n* equals the sum of the load, losses, and power withdrawn at that node. The active power flows are determined by the product of the line susceptance associated with the line investment status and the angle different across the buses (5.93) and (5.94). To capture the situation where the new lines are included in the power flow model, disjunctive constraints are required and a reformulation, using big-M (multiplier) values, are used to ensure the required properties. The bus voltage angle difference constraint (5.95) provides a proxy for angle stability.

The transmission thermal constraints are relaxed to add flexibility by allowing the line's flow to exceed the steady-state operating level (5.96). The line thermal ratings are picked up according to their investment status. The cost associated with exceeding the steady-state operation level is determined based on a positive value of f_{ktdy}^{over} by the degradation model.

The chosen SCUC formulation reflects that of Chapter 5.2. Generator capacity constraints are taken from (5.23)-(5.39). The piecewise linearized real power losses are modeled within the DCOPF formulation. The big-M reformulation is applied again to capture the line conductance properly (5.97)-(5.100). Also, the linearized current-temperature equations are applied as in (5.101)-(5.102). The gap between the line temperature and the maximum steady-state temperature is captured in (5.103) with two slack variables. The maximum operating temperature is assumed to be limited in (5.104)-(5.105). Thus, the allowable overloading of each line is limited in the region between the steady-state operating temperature and the emergency line temperature. The loss of tensile strength constraints are taken from (5.77)-(5.82). The investment decisions are treated as integer variables; the decisions can be made annually as in (5.106). Only one of the investment decisions can be made in a whole planning horizon for each line as in (5.107). The investment status variables have a value of one after each investment decision made; otherwise, it has a value of zero (5.108).

The coupling constraints (5.109) are introduced based on the fact that only investment status variables connect the investment decision and the system operating conditions. That is, the investment decision made in the investment model, which is indexed by 'st1', should be consistent with that in the production model, which is indexed by 'st2'.

5.3.3. Numerical Analysis Design

The chosen case study includes a modified version of the IEEE 24-bus RTS and IEEE 118-bus test system [72]. The transmission capacity of the original system is redundant; therefore, system modifications need to be made to carry out further TEP studies. The HTLS reconductoring, parallel line addition, parallel HTLS line installation, and TCR are considered as possible options.

The test systems include startup costs and no-load costs; shutdown costs are assumed to be zero. Also, generator cost information is same as the one presented in Chapter 5.2. It is assumed that the line resistance and reactance after addition of a parallel line decreased by 50 % and 26 %, respectively [106]. Furthermore, the ampacity of HTLS reconductored lines assumed to be increased by a factor of two. Note that the comparison of the different type of HTLS conductors is out of the scope of this research.

The weather condition parameters have adopted the one presented in [30] and assumed to be fixed. The load growth scenarios for a 15-year planning horizon, 3-years per each stage, were assumed as a hypothetical to create a long-term planning problem. As same as Chapter 5.2, it is assumed that the load grows at a rate of 0.9 % each year [104], the discount rate is 3.04 % [105]; fuel costs, as well as other fixed costs, are assumed to be fixed for the simplicity. The model is implemented in the C++ callable library of CPLEX 12.6 and parallelized using the Message Passing Interface. All of the simulations are conducted on Intel Xeon 3.60 GHz CPU with 48 GB memory. Production cost subproblems are terminated upon reaching an optimality gap of 0.01 %. Also, the decomposition algorithm is terminated after 50 iterations or upon reaching an optimality gap of 1 %.

The proposed model is an MILP problem. Two independent factors may influence difficulties in solving the problem. First, the consideration of multiple time periods creates a problem that is very large and difficult to solve since the variables are linked across the periods. Second, the large number of integer variables generate a combinatorial number of different problems, which increases the computational difficulty and slows down the convergence of the Lagrange decomposition algorithm. This work tackles the first factor by introducing a decomposition technique. For the second factor, one possible approach, to improve the computational efficiency, is to reduce the number of integer variables. There are two types of integer variables, unit commitment variables and line investment decision variables. Thus, instead of investigating the option of new lines across all existing corridors, it is preferable (to reduce the computational burden) to determine potential candidate lines before solving the problem.

Different type of criteria could be conducted to choose candidate lines. S. Z. Moghaddam et al. [107] introduced several parameters related to LMP to determine candidate lines and selected the best candidate lines based on an analytical hierarchy process. Since the proposed model preserves the ROW, a simplified method can be applied. First, the congested lines, which impede more efficient generation dispatch, could be classified as candidate lines. Uprating those congested lines could release congestion and improve the efficiency. However, it is important to investigate carefully whether such congestion is due to thermal limits. If the line flow is limited due to stability constraints, increasing line thermal limits cannot resolve the problem. In the DCOPF, bus angle difference limits are proxies for stability limitations. Thus, for simplicity, only specific

lines with thermal limits below the product of line susceptance and the maximum bus angle difference can be considered as a candidate line. Second, lines that have large LMP difference between two connecting buses could be treated as candidate lines. A location with high LMP indicates that cheap energy cannot access this location. Also, the low LMP value shows that excessive cheap energy is available, which is not utilized [108]. Thus, one can conclude that the large LMP difference could lead to low delivery efficiency. Note, however, that looking at the LMP difference is only a heuristic way to identify candidates since LMPs are based on dual variables, which do not directly reflect how the overall cost would change if that large LMP difference between the nodes could be alleviated. Since transmission lines are lumpy assets, indicators that are based on the marginal value to deliver a MW of energy to a particular location (i.e., LMPs) are not always preferred.

The work defines the candidate lines, which are presented in Table 5.10, based on the LMP differences by using MATPOWER. There is a lack of reference to determine a specific value of the LMP gap. Thus, in this work, the LMP difference of all branches is compared first, and the lines that have relatively large LMP gaps are chosen as candidates.

Table 5.10 Predetermined Candidate Lines

Branch Number	From Bus	To Bus
21	12	23
23	14	16
25	15	21
28	16	17

5.3.4. Test Case: IEEE 24-Bus Reliability Test System

The modified IEEE 24-bus RTS has 4,310 MW of generation capacity and 3,110 MW as its peak load. Three generators and two loads, as shown in Table 5.11, are added into the

system, and existing parallel lines have been removed. Note that the modified system is still reliable but may not be efficient. Thus, system expansion will be conducted only if net cost savings from the investment exceeds its capital cost; as a result, this study is aimed primarily at making an economic based investment decision (operational cost savings versus capital investment).

Table 5.11 Modification of IEEE 24-bus RTS

Bus	Type	Capacity (MW)	Bus	Load (MW)
13	Coal/Steam	350	15	160
21	Nuclear	400	16	100
23	Coal/Steam	155		

Two types of conductors have been considered, ACSR and ACCR. The 2 kcmil 1/6 (Sparrow) and 336 kcmil 18/1 (Merlin) Southwire ACSR conductors are used for parallel line addition according to the line rating of the test system. The 300 kcmil 26/7 (Ostrich) and 336 kcmil 26/7 (Linnet) 3M ACCR conductors are used for HTLS reconductoring and parallel HTLS line installation. The electrical characteristic of each conductor is presented in Table 5.12 and Table 5.13, respectively [101]-[102]. Also, The capital cost of HTLS reconductoring, parallel line addition, and parallel HTLS line installation is presented in Table 5.14 [109].

Table 5.12 Conductor Electrical Properties (ACSR)

	Southwire ACSR (Sparrow)	Southwire ACSR (Merlin)	Unit
Resistance (25°C)	0.25	0.05	Ohms/mile
Resistance (75°C)	0.33	0.06	Ohms/mile
Ampacity (Steady state)	184	519	Amps
Ampacity (Emergency)	211	596	Amps

Table 5.13 Conductor Electrical Properties (ACCR)

	3M ACCR (Ostrich)	3M ACCR (Linnet)	Unit
Resistance (at 25°C)	0.3004	0.2568	Ohms/mile
Resistance (at 75°C)	0.3597	0.3144	Ohms/mile
Resistance (at 240°C)	0.5555	0.4855	Ohms/mile
Ampacity (Steady state)	864	944	Amps
Ampacity (Emergency)	926	1012	Amps

Table 5.14 Capital Costs of Investment [$/Mile]

Line Length	138 kV	230 kV	138 kV	230 kV
	Typical ACSR line		HTLS Reconductoring	
> 10	630,200	927,000	794,052	1,168,020
3 ~ 10	756,240	945,300	952,862	1,401,624
< 3	1,112,400	1,390,500	1,191,078	1,752,030
Line Length	Parallel Line Addition		HTLS Parallel Line Addition	
> 10	1,009,600	1,484,00	3,634,560	5,342,400
3 ~ 10	1,211,520	1,780,800	4,361,472	6,410,880
< 3	1,514,400	2,226,000	5,451,840	8,013,600

Four cases have been considered in addition to a base case. Only a total production cost is examined in the base case without transmission expansion. In case A, all alternatives are considered in a model. In case B, only the HTLS reconductoring is applied. In case C, only the addition of a parallel line is considered. In case D, the parallel HTLS line installation is chosen as an option. Thus, one can analyze the economic benefits of each alternative as well as the combination of alternatives. In all cases, the expansion strategies are obtained with and without the degradation model to point out the impact of modeling the degradation. Also, the lossy DCOPF and lossless DCOPF models are compared in all cases.

Table 5.15 presents the investment decisions along with the resulting planning costs ($M) when losses and degradations are ignored. The HTLS reconductoring gives better

cost savings than other options since it provides higher thermal capacity with the lowest investment cost. Also, the results of case A and case B are identical. That is, there are no additional benefits by taking any combination of alternatives. However, in Table 5.16 and Table 5.17, the results show that the addition of a parallel line is favored in comparison to the HTLS reconductoring option when losses are considered. Note that the cost savings in Table 5.17 are less than other case studies. The reason is that the TCR allows more flexible system operation; thus, the total planning cost of the base case is reduced. Therefore, even the total planning cost of each case is below the costs when the degradation effects are ignored, the percentages of the cost savings are relatively small. Table 5.18 presents the accumulated degradation effect for the lines that TCR is activated, line 21 and 25. Figure 5.10 and Figure 5.11 shows the line overflow history along with the line temperature of line 25 at stage 1 in day type 2 and at stage 5 in day type 2, respectively. Stage 5 has fewer line overloads as compared to stage 2 due to added lines. Note that the line thermal limit is 500 MW and 75 °C.

Table 5.15 Planning Results (without Losses and TCR, RTS-24)

	Base	Case A	Case B	Case C	Case D
HTLS Reconductored	-	25(1) 28(1)	25(1) 28(1)	-	-
Parallel Line Added	-	-	-	25(3) 28(1)	-
HTLS Parallel Line Added	-	-	-	-	28(1)
Planning Cost ($M)	2,123	2,028	2,028	2,030	2,072
Production Cost ($M)	2,123	2,008	2,008	2,009	2,030
Investment Cost ($M)	-	27	27	21	43
Cost Saving [%]	-	4.5	4.5	4.4	2.4

Table 5.16 Planning Results (without Losses, with TCR, RTS-24)

	Base	Case A	Case B	Case C	Case D
HTLS Reconductored	-	-	25(1) 28(1)	-	-
Parallel Line Added	-	23(1) 25(1) 28(1)	-	23(1) 25(1) 28(1)	-
HTLS Parallel Line Added	-	-	-	-	28(1)
Planning Cost ($M)	2,465	2,338	2,374	2,338	2,402
Production Cost ($M)	2,465	2,286	2,347	2,286	2,359
Investment Cost ($M)	-	52	27	52	43
Cost Saving [%]	-	5.2	3.7	5.2	2.6

Table 5.17 Planning Results (with Losses and TCR, RTS-24)

	Base	Case A	Case B	Case C	Case D
HTLS Reconductored	-	-	25(1) 28(1)	-	-
Parallel Line Added	-	23(1) 28(1)	-	23(1) 28(1)	-
HTLS Parallel Line Added	-	-	-	-	28(1)
Planning Cost ($M)	2,378	2,333	2,366	2,333	2,369
Production Cost ($M)	2,374	2,308	2,327	2,308	2,317
Investment Cost ($M)	-	24	27	24	43
Degradation Cost ($M)	4.0	0.7	0.3	0.7	1.0
Cost Saving [%]	-	1.9	0.5	1.9	0.4

Table 5.18 Degradation Information (Case A, with Losses and TCR)

Line No.	Average Overflow (MW)	Average Temp. (°C)	Max/Min Temp. (°C)	Loss of Strength (%)
21	0.3	71.4	78.7/56.8	0.02
25	5.7	77.0	80.8/66.6	0.21

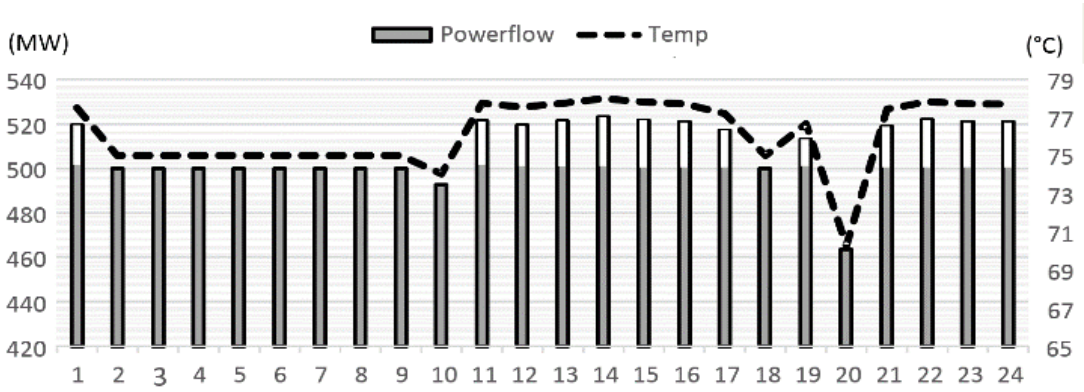

Figure 5.10 Line Power Flow and Temperature (Line 25, Stage 1/Day type 2, Case A, Losses and Degradations are Considered).

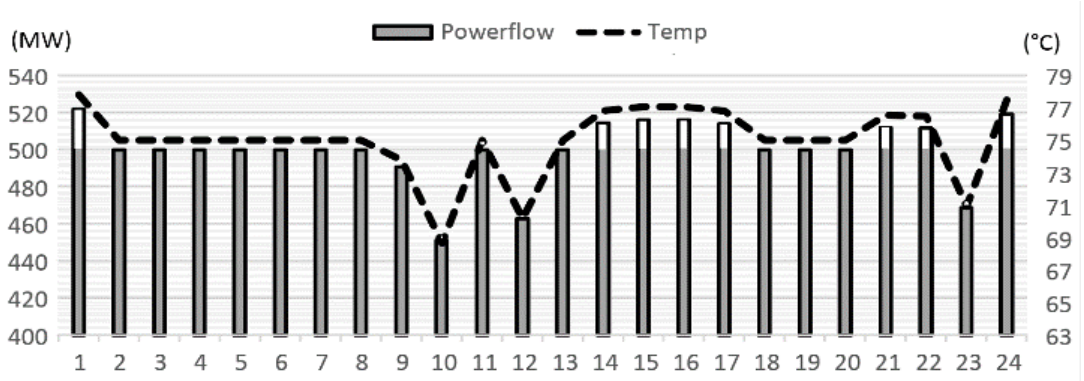

Figure 5.11 Line Power Flow and Temperature (Line 25, Stage 5/Day type 2, Case A, Losses and Degradations are Considered).

5.3.5. Test Case: IEEE 118-Bus Test System

The modified IEEE 118-bus test system has 7,179 MW of generation capacity and 5,219 MW of total peak load; Table 5.19 shows the added generators and load. Presumed candidate lines are presented in Table 5.20. Two types of conductors have been applied, ACSR (Raven and Partridge) and ACCR (Ostrich), based on the original line ratings. Table 5.21 shows the electrical properties of the Raven and Partridge conductor. Note that the ACCR (Ostrich) conductor is almost two times heavier than the ACSR (Raven) conductor.

Thus, it is assumed that additional tower upgrades are needed to reconductor the ACSR (Raven) conductor to the ACCR (Ostrich) conductor.

Table 5.19 Modification of IEEE 118-bus Test System

Bus	Type	Capacity (MW)	Bus	Load (MW)
10, 80	Coal/Steam	350	15	700
25	Coal/Steam	465		
26	Coal/Steam	155		

Table 5.20 Predetermined Candidate Lines

Branch Number	From Bus	To Bus	Branch Number	From Bus	To Bus
13	8	9	42	26	30
15	9	10	111	65	68
25	15	17	130	77	82

Table 5.21 Conductor Electrical Characteristics

	Southwire ACSR (Raven)	Southwire ACSR (Partridge)	Unit
Resistance (at 25°C)	0.839	0.332	Ohms/mile
Resistance (at 75°C)	1.145	0.411	Ohms/mile
Ampacity (Steady state)	242	475	Amps
Ampacity (Emergency)	306	595	Amps

All investment alternatives are considered together in a model with and without taking into account degradation effect and losses. Table 5.22 presents the investment decisions along with the resulting planning costs ($M). The HTLS reconductoring is still favored when losses are not considered; a parallel line is added to the line 111 since this line needs an additional tower upgrade as mentioned above. The addition of a parallel line is still most favored when losses are considered. Lastly, allowing TCR provides production cost savings, but the investment decisions are not changed in this numerical analysis.

Table 5.22 Planning Results (with Losses and TCR, IEEE 118-bus Test System)

	Base	Case E	Case F
Losses	N/A	Applied	Applied
Degradation (TCR)	N/A	N/A	Applied
HTLS Reconductored	13(1), 15(1) 25(1), 42(1)	-	-
Parallel Line Added	111(1)	13(1), 15(1) 25(1), 42(1) 111(1), 130(1)	13(1), 15(1) 25(1), 42(1) 111(1), 130(1)
HTLS Parallel Line Added	-	-	-
Planning Cost ($M)	3,667	4,990	4,973
Production Cost ($M)	3,657	4,974	4,957
Investment Cost ($M)	9	16	16
Degradation Cost ($M)	-	-	0.1

5.3.6. Conclusions

The work proposes a TEP model that considers various alternatives to increase transmission capacity without needing new ROW. The HTLS reconductoring, parallel line addition (with a traditional conductor), parallel HTLS line installation, and thermal constraint relaxation options are modeled in the case studies. The model is formulated as an MIP problem with a lossy DCOPF based SCUC. A parallelization algorithm, along with the use of Lagrange relaxation, is developed to improve the computational performance of this complex combinatorial problem.

This study presents the importance of acknowledging TCR practices within a TEP model. The numerical results show that the HTLS reconductoring is usually preferred when real power losses are ignored. Also, the results show that an HTLS conductor is a valuable economic option when existing ROW cannot accommodate a parallel line and, thus, reconductoring with an HTLS conductor is the preferred option. On the other hand, the

parallel line addition option (with traditional conductors) was generally favored when taking into consideration losses. The results, therefore, demonstrate that when it is possible to add a parallel line in the same ROW, this seems to be a preferred option. However, when such options are not available, reconductoring a line with HTLS (replacing an older conductor with an HTLS conductor) seems to be a preferred way to increase the transfer capability within a network without having to acquire additional ROW. However, there is no guarantee that the addition of a parallel line always dominates other options. As expected, overloading condition and the relative cost of each investment option, is shown to be key factors that may affect optimal solutions for a long-term transmission expansion.

CHAPTER 6. OFFLINE PENALTY PRICE DETERMINATION FOR THERMAL CONSTRAINT RELXATIONS

System operators manage market models, which respect complex operating requirements and strict physical restrictions of resources, to clear electric energy markets while ensuring a reliable operation of power systems. Moreover, system operators use CRs, which allow certain constraints to be relaxed for penalty prices, to cope with model infeasibility, obtain possible gains in market surplus, and cap shadow prices. This chapter presents an offline based penalty price determination process for TCR to improve existing industry practices that do not consider the true cost of relaxations. This work introduces a systematic methodology to capture the cost of relaxations considering probabilistic weather conditions and associated conductor degradation risk. The numerical analysis investigates the impact of the proposed method on an electric energy market; the results show that exercising TCR with a proper selection of penalty prices can provide net benefits to market participants.

6.1. Background and Motivation

System operators must manage generation scheduling while considering complex operational requirements and strict physical restrictions, to ensure a reliable supply of electric energy. To do this, system operators solve various market models, which are typically optimization problems. However, even with an advanced software and algorithmic performance, accurate modeling of every single physical characteristic into an optimization model is not possible nor practical; therefore, market models to date

approximate many system conditions. Most common approximations include a linearized direct current power flow, linear ramping constraints, and proxy reserve requirements. Approximated system conditions inherent in market models require additional adjustment processes, including reliability unit commitment and OMCs [110]-[111].

Moreover, system operators employ CR practices, which allow certain constraints to be relaxed for penalty prices, in their market model. That is, instead of strictly adhering to all the approximated system conditions, market operators treat certain constraints as soft constraints by adding slack variables into the constraints and penalty term into the objective function. Although system operators employ CR practices on a much broad basis, this research only focuses on TCR practices that allow a line flow to exceed its thermal rating, based on a predefined penalty price.

Due to the influence that penalty prices have on generation scheduling and market settlement, it is important to ensure that system operators choose penalty prices such that economic (price) signals avert market inefficiencies. The research motivation emerged from the fact that existing industry practices for determining penalty prices are neither transparent nor systematic; rather, the existing process relies on operators' judgment and stakeholders' agreements. For example, in [38], the market monitoring report states that the PJM has been using CR practices; however, public information regarding a detailed description of the procedure is limited. Moreover, in the MISO system, TCRs occur frequently within their market models. While they often correct for many of these relaxations out of the market, there are frequent real-time (actual), short-term TCRs that occur. MISO operators often try to avoid this from happening by manually de-rating the

line's capacity. That is, the real-time SCED tool will have an artificial rating chosen by the operator [112].

In Chapter 5, this dissertation presents a linearized conductor degradation model that could be incorporated into market optimization models as a set of constraints. However, such an approach lacks scalability and requires an overhaul of existing market model. Instead, this work aims to propose a risk-based method to determine penalty prices on an offline basis. The proposed method determines penalty prices for a set look-ahead period while considering the conductor degradation risks. The contribution of this work includes:

(1) An offline-based systematic method for determining penalty prices for TCR. The proposed model captures the cost of violating transmission thermal limits based on the conductor degradation risk.

(2) A conductor degradation risk quantification while considering probabilistic weather conditions in the penalty price determination process.

(3) An effective way to enhance the overall efficiency and transparency of market operations through an advanced approach that determines penalty prices based on the risk, which indicates the expectation of the consequence associated with thermal constraint relaxations.

This chapter presents the risk-based penalty price determination model along with the market models including SCUC and SCED in Section 6.2. Section 6.3 provides the numerical results. Lastly, Section 6.4 gives a conclusion.

6.2. Risk-based Penalty Price Determination Model

This section introduces the proposed procedure to determine penalty prices for TCR based on conductor degradation risks. The model mimics penalty price determination procedures that are used by ISOs. The proposed model sets penalty prices for a given period (e.g., one year in this work) while anticipating system operating conditions by solving look-ahead market models. The posted penalty prices shall be used for the following operating periods until the predetermined adjustment period is reached. Also, system operators can review and override penalty prices if needed; for example, when an abnormal deviation of system operation condition occurs.

The proposed model sets penalty prices such that the total collected relaxation cost, which is collected by exercised TCR and associated penalty prices, is as close as possible to the total expected conductor degradation cost. Figure 6.1 presents the flowchart of the proposed model. First, the penalty price determination model solves the market models, the day-ahead SCUC and real-time SCED model, for a planning period to obtain initial line flow information. This study assumes that system operators allow TCR in the real-time SCED, but not in the day-ahead SCUC. This assumption is based on the fact that CRs occurring in a day-ahead SCUC are typically corrected in an OMC phase, as investigated in [112]. Second, given the line flow information, the risk-based conductor degradation model computes the expected conductor degradation effect by multiplying the probability of the temperature and its related degradation effect. The proposed model obtains the expected degradation cost as in (6.5) and the total collected relaxation cost from the activated TCR and associated penalty prices. This model sets penalty prices such that the

total collected relaxation cost is as close as possible to the total expected conductor degradation cost. To do this, the proposed model updates penalty prices, as in (6.6), until the process meets a termination criterion. Lastly, this research assumes that a tariff with the determined penalty prices shall be posted; therefore, the penalty prices can affect the market clearing prices.

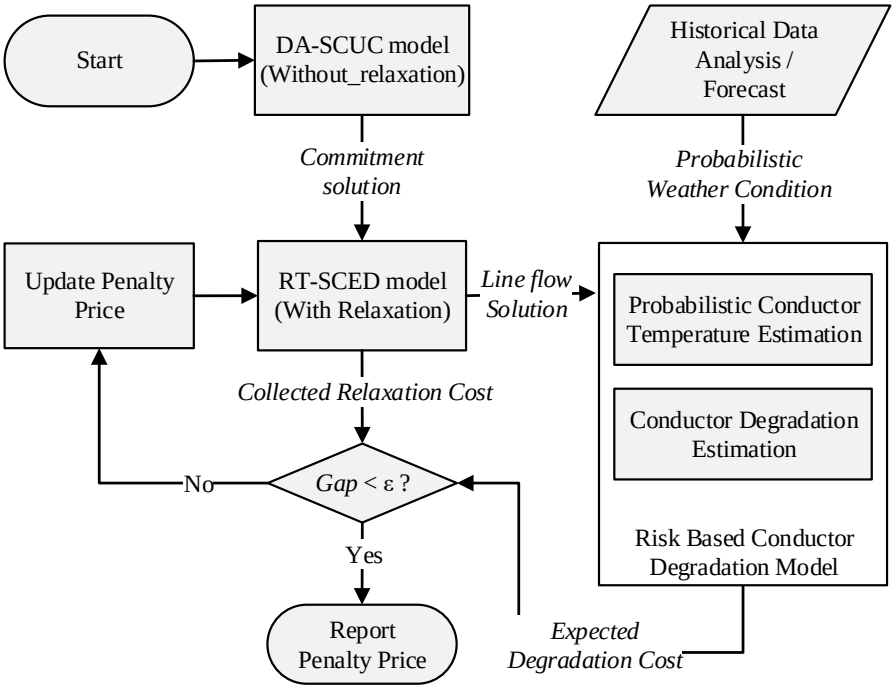

Figure 6.1 Flowchart of the Risk-Based Penalty Price Determination Model.

6.2.1. Risk-based Conductor Degradation Effect Prediction

In this work, conductor degradation risk is quantified based on the expected degradation effect due to TCR while considering probabilistic ambient weather conditions. When market models merely determine generation dispatch set point and line flows, the joule heating shall be the only one variable in the conductor thermal dynamics model, which is introduced in Chapter 4. If a deterministic ambient weather condition is assumed,

conductor temperatures shall be constant for fixed line flows; however, slightly different ambient weather condition can cause a high variation of conductor temperatures even with fixed line flows. Therefore, it is necessary to consider probabilistic weather conditions when analyzing conductor temperatures and associated degradation effects. This research considers probabilistic weather conditions when analyzing conductor temperature and associated degradation effect to capture the erratic changes in weather conditions effectively. The risk quantifying method is based on the one presented in [113]. This research considers two probabilistic weather conditions: ambient temperature and wind speed. The erratic behavior of air temperature and wind speed are modeled as a Normal and Weibull distribution, respectively in (6.1)-(6.2). The joint distribution of weather condition, φ, is represented as the product of each distribution factor as in (6.3); this work ignores the correlation between two weather conditions for the sake of simplicity,

$$Pr(T_a|\mu,\sigma) = \frac{1}{\sqrt{2\pi\sigma^2}} e^{-(T_a-\upsilon)^2/2\sigma^2} \tag{6.1}$$

$$Pr(W_s|\gamma,\beta) = \frac{\gamma}{\beta} {W_s}^{\gamma-1} e^{-{W_s}^{\gamma}/\beta} \tag{6.2}$$

$$Pr(\varphi) = Pr(T_a)\, Pr(W_s). \tag{6.3}$$

Here υ, σ, γ, and β are the scale and shape parameters. Also, T_a is the air temperature in °C and W_s is the wind speed in ft/s. Note that a better estimation of the probability distribution of the weather condition shall obviously provide better information to the penalty price determination process. Note that the proposed methodology, which evaluates the conductor degradation risk and determines penalty prices, can accommodate any form of probability functions without significant modifications. The conductor degradation risk can be

expressed based on the joint distribution of ambient weather condition and system operating conditions as follows,

$$Risk(X_k) = \sum_{\varphi \in \Upsilon} E\big(Deg(Y(\varphi)|X_k)\big)$$
$$= \sum_{\varphi \in \Upsilon} \{Pr(Y(\varphi)|X_k) \cdot Deg(Y(\varphi)|X_k)\} \qquad \forall k \qquad (6.4)$$

where $E\big(Deg(Y(\varphi)|X_k)\big)$ is the expected conductor degradation effect from the system operating condition X_k and the associated conductor temperature states $Y(\varphi)$ within the weather condition $\varphi \in \{\varphi_1, .., \varphi_n\}$ for each line k.

Lastly, the expected conductor degradation cost can be calculated as in (6.5) by assuming that a conductor should be replaced when it reaches a specific loss of tensile strength level; this work adopts a 10 % criterion [89]. The reconductoring cost, C_k^{ED}, includes conductor material, accessories, and labor costs while assuming continuous use of existing transmission tower. Although an out-of-service cost during a reconductoring period would also affect the overall reconductoring cost, this work does not consider such a cost to avoid a two-stage decision-making process.

$$Cost(X_k) = Risk(X_k) \cdot C_k^{ED} \qquad \forall k \qquad (6.5)$$

6.2.2. Penalty Price Determination

The goal of the proposed model is to set penalty prices such that total system-wide gap between collected relaxation costs and expected degradation costs can be as close as possible. The relaxation costs are obtained from the activated TCR and associated penalty prices. The expected conductor degradation costs are obtained from the risk-based conductor degradation model with line flow information and probabilistic weather

condition. By comparing both cost factors, the proposed model updates penalty prices, as in (6.6), so that the total system-wide gap decreases at each iteration j. The penalty price updating algorithm is based on an approximated subgradient method. The step size, λ, is updated as in (6.7) and the factor ρ is used to tune the step size.

$$P_k^{j+1} = P_k^j + \lambda_j\left(Expect_k^j - Collect_k^j\right) \qquad \forall k \qquad (6.6)$$

$$\lambda_j = \frac{\rho\left\|\sum_k Expect_k^j - \sum_k Collect_k^j\right\|}{\sum_k\left(\left(Expect_k^j - Collect_k^j\right)^2\right)} \qquad \forall k \qquad (6.7)$$

Here, $Expect_k^j$ and $Collect_k^j$ represents the expected degradation cost and the collected relaxation cost, respectively, for each line k at iteration j. The model has two termination criteria: (1) the maximum cost gap and (2) the maximum number of iterations.

The proposed model determines penalty prices while considering anticipated system operating conditions and estimated line overflows over a presumed period. Thus, it is important to set a proper look-ahead planning period. In this work, one year of operation has been chosen for the planning period.

6.2.3. Market Model Formulation

The proposed penalty price determination model solves market models to anticipate system operating condition. It is assumed that ISOs purchase energy on behalf of customers; therefore, a single side auction market is considered. However, the proposed penalty price determination model can adopt any form of market auction models. First, the model obtains generator commitment schedules from the SCUC model, which is represented by (6.8)-(6.33).

$$Minimize: \sum_{gti} C_{gi}^{op} p_{git} + \sum_{gt}\left(C_{gt}^{SP} r_{gt}^{sp} + C_{gt}^{NS} r_{gt}^{ns}\right) + \sum_{gt}(C_{g}^{NL} u_{gt} + C_{g}^{SU} v_{gt} + C_{g}^{SD} w_{gt}) \quad (6.8)$$

Subject to

$$-p_{nt}^{inj} + \sum_{\forall \Omega_G^n} p_{gt}^{total} = D_{nt} \qquad \forall n,t \qquad (6.9)$$

$$\sum_n p_{nt}^{inj} = 0 \qquad \forall t \qquad (6.10)$$

$$\sum_n p_{nt}^{inj} PTDF_{nk}^{REF} \le F_k^+ \qquad \forall k,t \qquad (6.11)$$

$$-\sum_n p_{nt}^{inj} PTDF_{nk}^{REF} \le F_k^+ \qquad \forall k,t \qquad (6.12)$$

$$0 \le p_{git} \le u_{gt} P_{gi}^+ \qquad \forall g,i,t \qquad (6.13)$$

$$p_{gt}^{total} = \sum_i p_{git} \qquad \forall g,t \qquad (6.14)$$

$$p_{gt}^{total} + r_{gt}^{sp} \le P_g^+ u_{gt} \qquad \forall g,t \qquad (6.15)$$

$$P_{gt}^- u_{gt} + r_{gt}^{sp} \le p_{gt}^{total} \qquad \forall g,t \qquad (6.16)$$

$$0 \le r_{gt}^{sp} \le P_g^+ u_{gt} - p_{gt}^{total} \qquad \forall g,t \qquad (6.17)$$

$$r_{gt}^{sp} \le R_g^{10} u_{gt} \qquad \forall g,t \qquad (6.18)$$

$$0 \le r_{gt}^{ns} \le R_g^{10}(1 - u_{gt}) \qquad \forall g,t \qquad (6.19)$$

$$p_{gt}^{total} + r_{gt}^{sp} \le r_t^{req} \qquad \forall g,t \qquad (6.20)$$

$$0.07 \sum_{\gamma \in \Omega_G^C} p_{\gamma t}^{total} + 0.05 \sum_{\gamma \in \Omega_G^H} p_{\gamma t}^{total} \le r_t^{req} \qquad \forall t \qquad (6.21)$$

$$0.5 r_t^{req} \le \sum_g r_{gt}^{sp} \qquad \forall t \qquad (6.22)$$

$$r_t^{req} \le \sum_g (r_{gt}^{sp} + r_{gt}^{ns}) \qquad \forall t \qquad (6.23)$$

$$p_{gt}^{total} - p_{g,t-1}^{total} \le R_g^{HR} u_{g,t-1} + R_g^{SU} v_{gt} \qquad \forall g,t \qquad (6.24)$$

$$p_{g,t-1}^{total} - p_{gt}^{total} \leq R_g^{HR} u_{gt} + R_g^{SD} w_{gt} \qquad \forall g, t \qquad (6.25)$$

$$v_{gt} - w_{gt} = u_{gt} - u_{g,t-1} \qquad \forall g, t \qquad (6.26)$$

$$\sum_{q=t-UT_g+1}^{t} v_{gq} \leq u_{gt} \qquad \forall g, t \geq UT_g \qquad (6.27)$$

$$\sum_{q=T+t-UT_g+1}^{T} v_{gq} + \sum_{q=1}^{t} v_{gq} \leq u_{gt} \qquad \forall g, t \leq UT_g - 1 \qquad (6.28)$$

$$\sum_{q=t-DT_g+1}^{t} w_{gq} \leq 1 - u_{gt} \qquad \forall g, t \geq DT_g \qquad (6.29)$$

$$\sum_{q=T+t-DT_g+1}^{T} w_{gq} + \sum_{q=1}^{t} w_{gq} \leq 1 - u_{gt} \qquad \forall g, t \leq DT_g - 1 \qquad (6.30)$$

$$u_{gtdy} \in \{0,1\} \qquad \forall g, t \qquad (6.31)$$

$$0 \leq v_{gtdy} \leq 1 \qquad \forall g, t \qquad (6.32)$$

$$0 \leq w_{gtdy} \leq 1. \qquad \forall g, t \qquad (6.33)$$

The objective (6.8) minimizes total costs of acquiring energy, spinning, and non-spinning reserves. The costs of spinning and non-spinning reserves are assumed to be 25 % and 15 % of the final generator cost segment, respectively. The network constraints model the energy balance requirements at every node in (6.9)-(6.10) and the transmission line limits along with power flows, which are approximated using PTDFs, in (6.11)-(6-12). The generator operating requirements include the relation of the generation production segments to the total production (6.13)-(6.14) and the maximum and minimum generation capacity limits (6.15.)-(6.16). The spinning and non-spinning reserves are restricted by the ramping ability of generators in (6.17)-(6.19). A proxy *N*-1 requirement is enforced in (6.20). Also, it is assumed that the total operating reserve requirement is restricted such that it must exceed the sum of 7 % of conventional generation and 5 % of hydro-generation (6.21). Also, the model requires that 50 % of the total operating reserve requirement should

be fulfilled by the spinning reserves in (6.22) and the amount of spinning and non-spinning reserve acquired must be greater than or equal to the total reserve requirement in (6.23). The hourly ramping restrictions are represented in (6.24)-(6.25). The integrality constraints of the startup and shutdown variables are relaxed by including constraints (6.26)-(6.33) and employing facet defining valid inequalities for the minimum up and down time constraints, (6.27)-(6.30).

The SCED model is presented in (6.34)-(6.45). The SCED model employs TCR by including the slack variables in (6.35)-(6.36) and penalize them in the objective function (6.34). The predetermined generator commitment schedules are used as input data.

$$Minimize: \ \sum_{gti} C_{gi}^{op} p_{git} + \sum_{gt}(C_{gt}^{SP} r_{gt}^{sp} + C_{gt}^{NS} r_{gt}^{NS}) + \sum_{kt} P_k s_{kt} \quad (6.34)$$

Subject to

$$\sum_n p_{nt}^{inj} PTDF_{nk}^{REF} - s_{kt} \le F_k^+ \qquad \forall k,t \qquad (6.35)$$

$$-\sum_n p_{nt}^{inj} PTDF_{nk}^{REF} + s_{kt} \le F_k^+ \qquad \forall k,t \qquad (6.36)$$

$$0 \le p_{git} \le U_{gt} P_{gi}^+ \qquad \forall g,i,t \qquad (6.37)$$

$$p_{gt}^{total} + r_{gt}^{sp} \le P_g^+ U_{gt} \qquad \forall g,t \qquad (6.38)$$

$$P_{gt}^{min} U_{gt} + r_{gt}^{sp} \le p_{gt}^{total} \qquad \forall g,t \qquad (6.39)$$

$$0 \le r_{gt}^{sp} \le P_g^+ U_{gt} - p_{gt}^{total} \qquad \forall g,t \qquad (6.40)$$

$$r_{gt}^{sp} \le R_g^{10} U_{gt} \qquad \forall g,t \qquad (6.41)$$

$$0 \le r_{gt}^{ns} \le R_g^{10}(1 - U_{gt}) \qquad \forall g,t \qquad (6.42)$$

$$p_{gt}^{total} - p_{g,t-1}^{total} \le R_g^{HR} U_{g,t-1} + R_g^{SU} V_{gt} \qquad \forall g,t \qquad (6.43)$$

$$p_{g,t-1}^{total} - p_{gt}^{total} \le R_g^{HR} U_{gt} + R_g^{SD} W_{gt} \qquad \forall g,t \qquad (6.44)$$

$$s_{kt} \geq 0 \qquad \forall k, t \qquad (6.45)$$

(6.9)-(6.10), (6.14), (6.20)-(6.23)

6.3. Numerical Results

6.3.1. Analysis Design

The chosen case study includes a modified version of the IEEE Reliability Test System and IEEE 118-bus test system [97]. The transmission capacity of the original system is redundant; therefore, system modifications have been made to carry out further studies. The case study was conducted with the following analysis design and assumptions. First, the SCUC model without TCR was solved for the entire year (8760 hours) with Rate B as line ratings. Second, generator commitment schedules from the SCUC model were fed into the SCED model. It is assumed that, for the SCED model with relaxations, the line ratings are de-rated to Rate A. The purpose of such an analysis setting is to examine the benefits of exercising TCR along with a proposed method to properly select penalty prices that capture the true cost of relaxations. For instance, a line's steady-state rating may be set at Rate B even though there are degradation risks when the line operates above Rate A, at times, when ambient weather conditions are very severe. By enabling TCR, it is possible to set the steady-state rating at Rate A, but allow the line's flow to be relaxed for the penalty prices when it is beneficial. By doing so, exercising TCR can enhance the modeling and utilization of the transmission asset, which increases the social welfare. Lastly, the SCED model without TCR was solved while setting Rate B as line ratings to compare the results.

This work assumes that there is no negative effect on reliability, stability, or no excessive sagging by exercising TCR; therefore, TCR is allowed only for lines that are thermally limited. In reality, taking care of these issues can be achieved by restructuring the SCED model to include a simultaneous feasibility test on reliability and a maximum overload of the line to ensure excessive sagging does not occur; while such modifications can be made, our focus in this research is on the penalty price determination for TCR. Lastly, it is critical to keep in mind that TCRs are assumed to be short lived; the *N*-1 criterion applies to a 30 minutes period [114]. Short-term overloads are allowed to occur today; however, operators then take corrective actions to push the market solution back to a solution without relaxations.

The model is implemented in the Java callable library of CPLEX 12.6. All the simulations are performed on the Intel Xeon 3.60 GHz CPU with 48 GB memory. The risk-based penalty pricing model was terminated upon reaching a gap of 0.5 % or maximum iteration number of 30.

6.3.2. Test Case: IEEE Reliability Test System

A simulation is performed on the modified IEEE RTS. Three lines which connect node 114-116, 214-216, and 314-316, respectively, are de-rated. Three types of ACSR conductors including Raven, Pelican, and Parakeet are selected for the original lines based on their line ratings. Also, the Penguin conductor is used for the de-rated lines. Based on the fact that weather conditions can considerably affect the determination of thermal ratings, this work calculates the conductor thermal ratings using the IEEE standard temperature model in (4.1) instead of using the original conductor ratings from [97]. Rate B is

determined at the line flow that causes a line temperature of 85 °C. Rate A is assumed to be 75 % of Rate B and Rate C is the line flow at 100 °C. Table 6.1 presents the deterministic weather condition parameters from [30] that are used to determine the steady-state line ratings. Table 6.2 presents the electrical characteristics [102] and capital cost of these conductors [103]. Probabilistic weather conditions were obtained according to the five years of historical data for the state of Arizona, US [115]. The mean and standard deviation of air temperature and wind speed are listed in Table 6.3.

Table 6.1 Conductor Information

	Raven	Penguin	Pelican	Parakeet
Structure(Al/St)	6/1	6/1	18/1	24/7
Rate A(MW)	160	247	433	483
Rate B(MW)	214	330	578	645
Rate C(MW)	241	370	667	744
Capital Cost (M$/mile)	0.84	0.87	0.91	0.94
End-of-service Cost (M$/mile)	0.29	0.30	0.32	0.34

Table 6.2 Deterministic Weather Parameters

Wind Speed	2 *ft/s*	Emissivity	0.5
Wind Angle	45 °	Absorptivity	0.5
Ambient Temperature	35 °C	Solar Time	12:00 PM
Elevation	150 *ft*	Atmosphere	Clear
Latitude	38.5 °	Line Direction	North-South

Table 6.3 Statistics of Ambient Weather Conditions

	Mean	Standard Deviation
Air Temperature (°C)	21.4	10.5
Wind Speed (*ft/s)*	6.3	4.5

In the modified test system, three de-rated lines are thermally limited. The proposed model sets penalty prices for these lines such that the estimated relaxation cost, the whole collected penalty cost over the year, is closer to the expected degradation cost insofar as

possible within the forecasted system operating conditions. Table 6.4 presents the determined penalty prices for the lines that are thermally limited and the associated expected degradation effects.

Table 6.4 Determined Penalty Prices and Degradation Effects (IEEE RTS)

Line Number	25	65	104
Conductor Type	Penguin	Penguin	Penguin
Location	114-116	214-216	314-316
Penalty Price ($/MW)	0.66	12.18	8.45
Expected Degradation Effect (%)	0.004	0.091	0.063

The result shows that setting individual penalty prices for each line can provide better price signals since the benefit of practicing TCR depends on the location of the lines and the specific system conditions of each operating period. For instance, the benefit of practicing TCR on line 25 is relatively smaller than the benefits of other two lines. As a result, fewer line relaxations are expected that lead to a lower degradation effect as well as a lower penalty price. The proposed model attempts to find penalty prices such that an appropriate amount of charges can be collected from the overall market, while considering the risk exposures and the potential degradation impacts on transmission lines. Hence, a lower penalty price infers that lower degradation effects are expected, and it is not necessary to set a higher penalty price for that line (for the same relative overload). Even with a lower penalty price, relaxations do not occur very frequently. Figure 6.2 shows the convergence result of the proposed model; the simulation converged after ten iterations.

Figure 6.3 presents a line flow histogram for the three de-rated lines. The results of non-relaxed cases show that even with the same conductor type, congestion frequency has different patterns based on the location of the line. Also, the results indicate that relaxations

do not always occur because the benefits of relaxations are not always greater than penalty prices. Line 25 is less congested in the non-relaxed case, and its thermal rating is not violated as much in the relaxed case even when the penalty price for this line is relatively small.

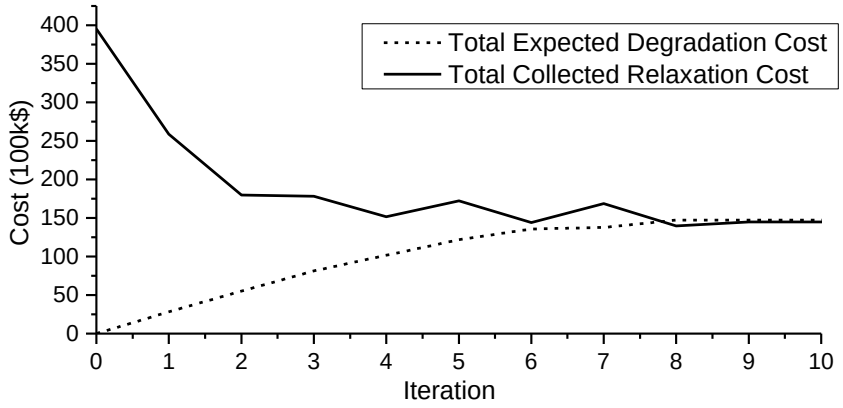

Figure 6.2 Convergence Performance of the Algorithm (IEEE-RTS).

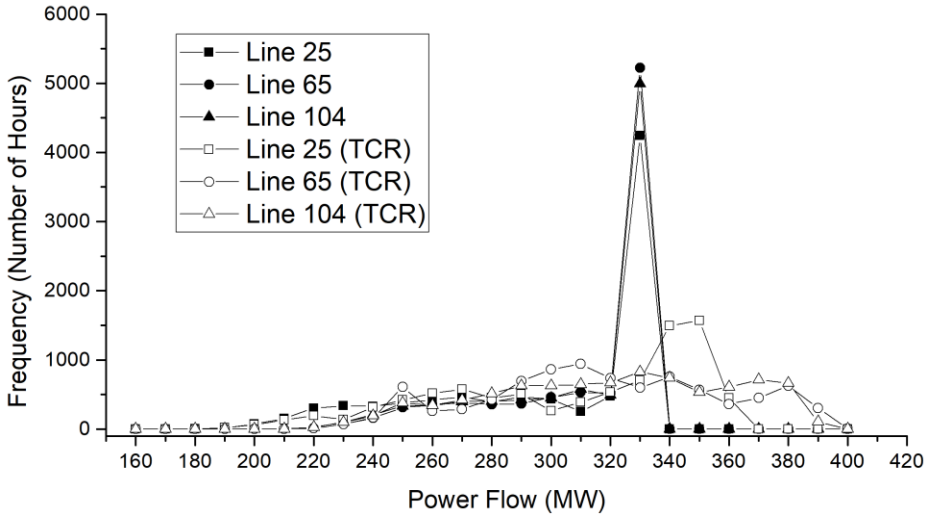

FIGURE 6.3 Line Flow Results for the Congested Lines with and without Relaxation (IEEE-RTS).

When comparing market settlements, as expected, the TCR provides about 1.85 % of total system cost savings compared to the non-relaxed case over the entire year. Although

the total system cost is lower in the relaxed case, there is no guarantee that either LMPs or overall load payment will be lower. Nevertheless, in this case study, average LMPs decreased by 9 % in the relaxed case. Also, other settlements show deviations in the relaxed case compared to the non-relaxed case.

One notable aspect is that generators are receiving higher revenue (and profit) through the entire year while consumers have the lower payment. Instead of having a few peak prices, the TCR made it such that the overall payment to the generators, collectively, increased. For instance, in the non-relaxed case, some cheaper generators are not entirely dispatched due to congestion and, hence, setting prices. However, with TCR, the marginal units (on average) are generators with higher costs. Lastly, the relaxed case shows significantly decreased congestion rent, which is the difference between the amount paid by consumers and generators' revenue. Congestion rent is used to fund the Financial Transfer Rights (FTR) market, where market participants purchase FTRs to hedge against price risks due to congestion. TCR limits FMPs as well as LMP gaps between nodes that are connected by the transmission lines, as presented in Table 6.5. This implies that, by capping FMPs, system operators can manage price volatility risks between specific nodes and congestion rent. Figure 6.4 and Table 6.6 compares all of the settlement factors.

Table 6.5 Market Price Comparison (Mean Value, $/MWh)

Line Number	25	65	104
LMP Gap (Without TCR)	7.4	25.7	21.9
LMP Gap (With TCR)	0.3	7.7	5.4
FMP (Without TCR)	11.3	35.5	31.9
FMP Gap (With TCR)	0.6	11.2	7.8

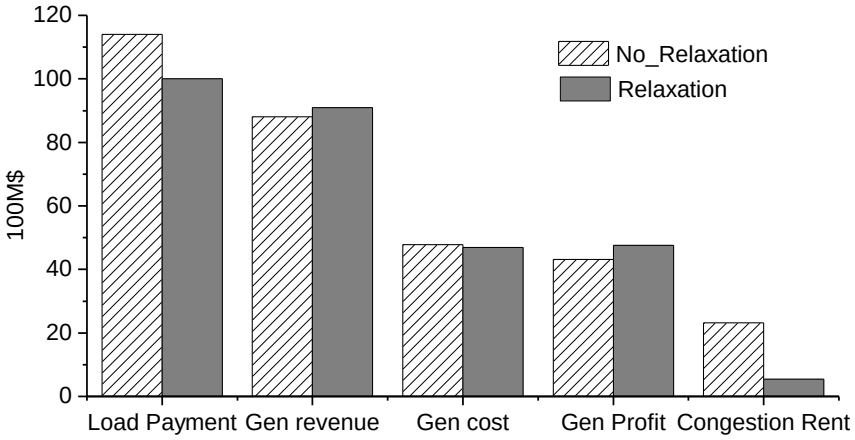

Figure 6.4 Market Settlements Comparison (IEEE-RTS).

Table 6.6 Market Settlements ($M/year)

Model	Total cost	Gen. revenue	Gen. profit	Gen. uplift	Load payment + uplift	Congestion Rent
No Relaxation	478.5	881.4	431.2	28.3	1,142.2	232.4
Relaxation	469.8	909.6	476.0	36.2	1,000.6	54.7
Gap (%)	-1.8	3.2	10.4	27.9	-12.4	-76.5

6.3.3. Test Case: IEEE 118-Bus Test System

Lastly, the numerical analysis includes additional case studies with the modified IEEE 118-bus test system. Three cases have been considered to show the scalability of the proposed model as described in Table 6.7. Line ratings of the de-rated lines and the probabilistic weather conditions are taken from Table 6.2 and Table 6.3, respectively. Table 6.8 presents the determined penalty prices and the associated expected degradation effects for each case. The result shows that the proposed model can set penalty prices for each line while considering the true cost of exercising TCR.

Figure 6.5 shows the convergence result of all cases. The number of iterations tends to increase with the number of lines that are de-rated; however, in all cases, the proposed model finds penalty prices as intended within the maximum number of iteration limit. Figure 6.6 presents the convergence result of case A for each de-rated line. Lastly, Table 6.9 summarizes the total computing times and the number of iterations. The majority of time is used to solve SCUC and SCED models and relatively little time is consumed on temperature and degradation effect calculations.

Table 6.7 Analysis Design of IEEE 118-bus Test System

Line Number	Conductor Type	Location	Case A	Case B	Case C
13	Penguin	8-9	Applied	Applied	Applied
42	Penguin	26-30	Applied	Applied	Applied
49	Raven	17-30	-	Applied	Applied
63	Raven	37-38	Applied	Applied	Applied
80	Raven	49-66	-	Applied	Applied
115	Raven	68-81	-	-	Applied
142	Raven	82-83	-	-	Applied

Table 6.8 Determined Penalty Prices and Corresponding Expected Degradation Effects (IEEE 118-bus Test System)

Line Number	Penalty Price ($/MWh)			Degradation Effect (%)		
	Case A	Case B	Case C	Case A	Case B	Case C
13	40.0	40.1	40.1	0.24	0.24	0.24
42	26.4	26.1	26.3	0.12	0.12	0.12
49	N/A	35.0	34.9	N/A	0.05	0.05
63	30.3	28.6	25.6	0.11	0.10	0.10
80	N/A	35.4	42.8	N/A	0.06	0.09
115	N/A	N/A	35.4	N/A	N/A	0.06
142	N/A	N/A	25.9	N/A	N/A	0.05

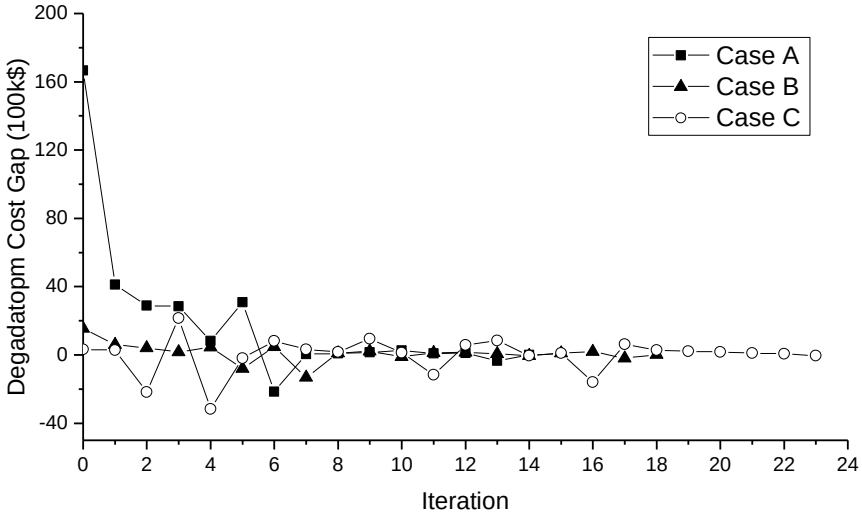

Figure 6.5 Convergence Performance of the Algorithm
(IEEE 118-Bus Test System).

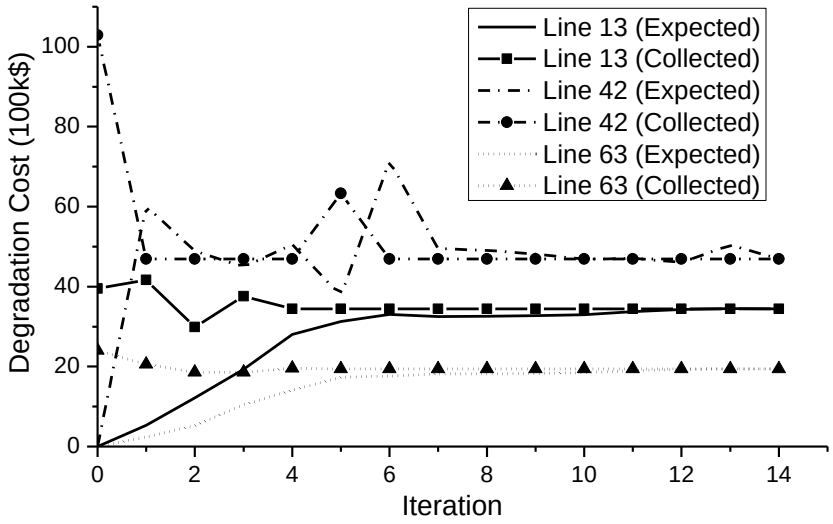

Figure 6.6 Convergence Performance of each Line
(IEEE 118-Bus Test System, Case A).

Table 6.9 Computational Performance

	IEEE RTS	IEEE-118 (Case A)	IEEE-118 (Case B)	IEEE-118 (Case C)
Iteration	10	15	19	24
Time (min)	104	173	227	279

6.4. Conclusions

Power system operators must account for all the complex operating and reliability requirements inherent in the system. Even with the improved algorithmic performances, market models cannot fully capture all the complexities of the power systems. Thus, market models employ various approximated system conditions as a set of constraints. Moreover, market operators employ CR practices, which allow certain constraints to be relaxed for penalty prices, to cope with model infeasibility, to cap shadow prices, and to gain possible gains in market surplus. Since CR practices influence market prices and settlements, the key is to set the penalty prices properly by considering the true cost of violating constraints.

This research focuses on a TCR and proposes a risk-based methodology to determine penalty prices on an offline basis. The proposed model provides a logical way to set penalty prices by capturing the true cost of violating steady-state thermal limits; the model considers the probabilistic line temperatures and quantifies associated line degradation risks. Numerical analysis results show that all market participants can achieve benefits by practicing TCR with a proper selection of the penalty prices.

CHAPTER 7. ONLINE PENALTY PRICE DETERMINATION FOR THERMAL CONSTRAINT RELAXATIONS

In Chapter 6, this dissertation presents an offline risk-based penalty price determination model, which considers probabilistic weather conditions to estimate the degradation risk of a conductor. However, the prior model forecasts the system operating state and weather condition to analyze the risks, which may bring an inaccuracy of the model due to forecasting errors. Moreover, the fixed penalty price scheme used in the prior model does not capture the duration and magnitude of the relaxations. This chapter proposes an online penalty price determination model. The primarily objective of this work is to develop a systematic method to define staircase penalty prices that consider the duration and magnitude of the relaxations concurrently on an online basis.

7.1. Background and Motivation

System operators manage the power systems with diverse market optimization models at different time intervals. However, at times, market models have a hard time to get a solution with available resources in the system while respecting all the requirements. Thus, system operators introduce CR practices, which allow specific constraints could be violated with predetermined penalty prices. Theoretically, putting high enough penalty prices would be sufficient to prevent the infeasible situations. However, CR practices also have an impact on shadow prices (i.e., market clearing prices). That is, CR practices could be used to cap market clearing prices. For example, when a node balance constraint is relaxed, the LMP shall be capped by the penalty price of the node balance constraint relaxation.

Therefore, it is crucial to set the penalty prices properly. This research proposes following criteria as necessary conditions for determining penalty prices for TCR.

(1) Penalty prices should reflect what CR practices could cause to the system.

(2) Penalty prices should be able to capture the magnitude and duration of the relaxations.

(3) Penalty prices should enable the prioritization of constraints so that constraints that are less significant can be relaxed more frequently than other constraints that are more significant, more important to ensure reliable operations.

(4) Penalty prices should avoid market price distortion.

Although the prior work in Chapter 6 successfully provides a systematic method for determining penalty prices based on the conductor degradation risk on an offline basis, the work does not fully meet the criteria above. First, the model forecasts the system operating state and weather condition to analyze the risks, which may bring an inaccuracy of the model due to forecasting errors. Such inaccuracy could cause market price distortions at times. Second, the fixed penalty price scheme used in the model does not capture the duration and the magnitude of the relaxations. Moreover, as presented in Chapter 3, none of the existing industry practices on penalty price determination for TCR considers both the magnitude and duration of the relaxations. Although MISO allows the temporary override of penalty prices by operators during exceptional conditions, MISO does not systematically update the prices to reflect the operating condition. Also, the existing industry practices do not consider the actual impact of transmission thermal limit violations on assets. This work proposes an online penalty price determination model. The primarily

objective of this work is to develop a systematic method to define staircase penalty prices that respect the above criteria. That is, the model considers the duration and magnitude of the relaxations simultaneously on an online basis; moreover, the model captures the trade-off between relaxing transmission thermal limits and its impact on conductor materials.

7.2. Online Penalty Price Determination Model

The main goal of the online penalty price determination model is to provide staircase penalty prices to a real-time SCED model, which typically runs at every 5 minutes. As discussed in Chapter 4, transmission line overflows, which are enabled by TCR, can elevate transmission line temperatures that can cause degradations on conductor materials. This research utilizes the IEEE standard temperature model and the IEEE standard degradation model, which are defined in Chapter 4, to estimate the line temperatures and associated degradation effects. Both IEEE standard models have nonlinear characteristics, which make it hard to incorporate the models into a market optimization model as is. In Chapter 5, the work keeps the nonlinearity of the IEEE standard models and applies an offline based methodology to predict conductor degradation effect and set penalty price accordingly. The main reason for such an offline approach was that the IEEE standard degradation model does not provide meaningful information for a short-term period because the model was developed to predict the degradation effect for long-term operations (e.g., hundreds of operating hours at elevated temperature) based on an ordered series of temperature history. Moreover, the IEEE standard degradation model does not consider line temperatures that are lower than 95 °C. That is, for a line temperature lower than 95 °C, the IEEE standard

degradation model cannot provide a level of degradation effect, and as a result, the associated impact on the penalty price determination shall be zero.

As mentioned, the primary goal of the proposed online penalty price determination model is to set staircase penalty prices. The design of a staircase penalty price scheme can be classified into the three categories: (1) set the number of segments, (2) define the length of segments, and (3) determine penalty prices for each segment. The main contribution of this work is to set penalty prices for each segment while assuming that there is a base staircase penalty price. The proposed model provides a price adder only if there is a positive anticipated marginal degradation effect due to a line temperature above 95 °C. That is, this study acknowledges the already existing penalty price schemes in the industry; moreover, this research envisions the enhancement of the existing practices by providing the price adder, which reflects the impact of the duration and magnitude of the relaxations. This functionality can help system operators to reduce or eliminate the operator's manual intervention to cope with model infeasibility or possible risk on the transmission assets. Note that the research does not try to enhance the functionality of the IEEE standard degradation model; instead, this research utilizes the IEEE standard model while trying to tackle the limitations. Figure 7.1 presents the flowchart of the proposed method.

Although the proposed penalty price determination process is not applied to a market optimization model as a set of constraints, the proposed model can be classified as an online based model since the execution of the model aligns with the real-time operations. Lastly, without loss of generality, it is hard to determine the actual degradation effect of conductors without a detailed physical investigation. A conductor may not suffer from degradations as

expected from the proposed studies. There could be multiple reasons including ambient weather condition differences or, more importantly, actual line flow deviations from the DC-based line flow calculation. Therefore, it would be required to evaluate anticipated degradation effects and actual degradation effect routinely so that a penalty price determination process can keep updated based on archived events as well.

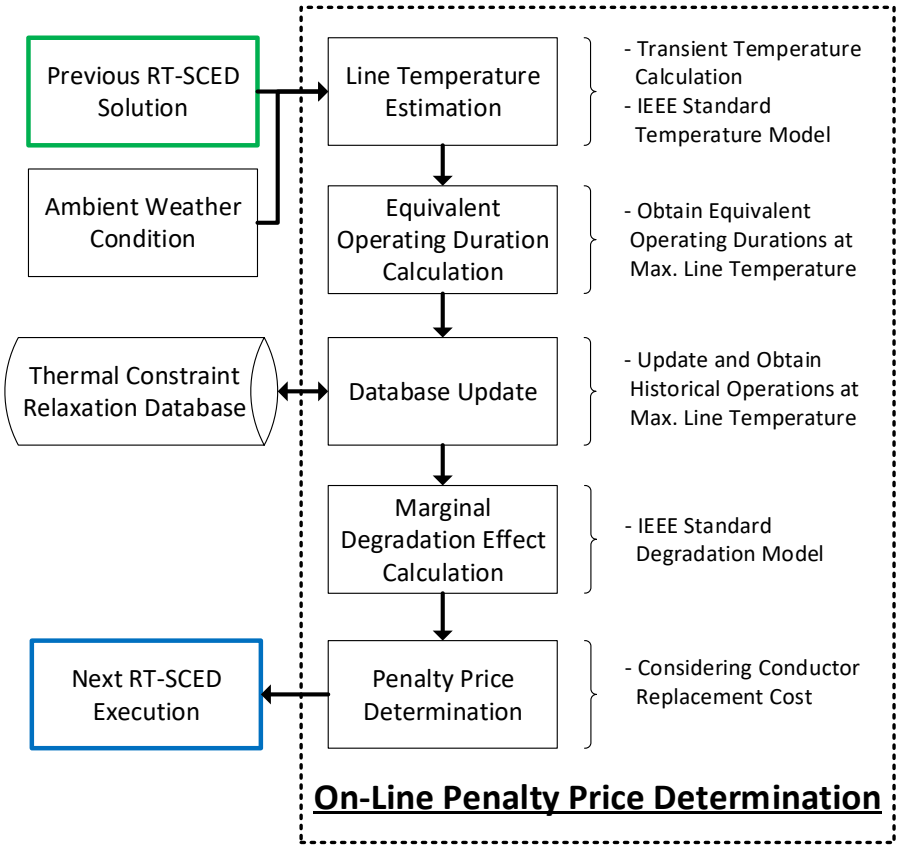

Figure 7.1 Flowchart of the Online Penalty Price Determination Model.

7.2.1. Line Temperature Estimation

An estimation of line temperature is an essential part of the proposed penalty price determination model. The work estimates the temperature by utilizing the IEEE standard temperature model in (4.1). The work considers a transient temperature estimation, which

is presented in Chapter 4, while assuming step changes in power flow. Note that the prior work in Chapter 5 only considers a steady-state temperature estimation. First, the model calculates the initial line temperature from the previous market model execution. After obtaining the initial temperature, the model anticipates the line temperatures at the relaxation points, where the relaxations begin at each staircase segment, considering the step changes in line flows.

7.2.2. Equivalent Operating Duration Calculation

In the previous step, the model obtained the anticipated temperatures at each relaxation point. The next step is to calculate the conductor degradation effects at each relaxation point. The IEEE standard degradation model in (4.3) is a function of line temperature and operating duration. That is, the model requires an ordered series of temperature and operating duration history to calculate the final level of degradation effect [34]. Instead, this research introduces an operating duration conversion method which maps the temperature and operating duration set of each relaxation point to an equivalent operating duration at predetermined maximum line temperature. Therefore, the entire penalty price determination process, after the operating duration conversion, only deals with the single, maximum, temperature along with different operating durations.

The research makes several assumptions at this point. First, the penalty price determination model only considers the degradation effect on aluminum strands. Thus, the 10 % degradation criterion for a whole conductor, which was used so far throughout this dissertation, is translated into the degradation criterion for aluminum strands accordingly. Let

Deg_T^+ and Deg_{al}^+ as the maximum degradation level of a whole conductor and aluminum strands in percentage, respectively. Then the Deg_{al}^+ can be obtained as follows,

$$Deg_{al}^+ = (Deg_T^+ - 100)\frac{STR_T}{STR_{al}} + 109\frac{STR_{st}}{STR_{al}} + 100. \quad (7.1)$$

Second, let T^+ as the predetermined maximum temperature in °C, T_i and D_i as the anticipated temperatures and operating durations, in hours, at relaxation point i, and D_i^{eq} as the equivalent operating duration, in hours, at relaxation point i. Also, let d_i be a diameter of an aluminum strand in inches. Then the D_i^{eq} can be obtained from the following equation,

$$D_i^{eq} = \left(\frac{\alpha(T_i)}{\alpha(T^+)} {D_i}^{\beta(T_i)}\right)^{\beta(T^+)^{-1}} \quad \forall i \quad (7.2)$$

where

$$\alpha(T_i) = -0.24T_i + 134 \quad (7.3)$$

$$\beta(T_i) = -(0.001T_i - 0.095)(10di)^{-1}. \quad (7.4)$$

7.2.3. Transmission Thermal Constraint Relaxation Database Update

The process updates the TCR database with the temperature and operating duration set after the conversion process; therefore, the database only keeps track of operations at the predetermined maximum temperature, T^+. The updated operating history at the maximum temperature will be used as a base to calculate the marginal degradation effect in the next step. Also, the database updating process helps to evaluate anticipated degradation effects from the proposed model and degradation effect from the IEEE standard degradation model.

7.2.4. Marginal Degradation Effect Estimation

At this stage, the model knows the equivalent operation durations at maximum line temperature at each relaxation point. Also, the model knows the accumulated operation history at the maximum temperature. Next step is to calculate the marginal degradation effect at each relaxation point.

First, let h^+as the accumulated operation history at the maximum temperature in hours. Then, the marginal degradation effect, in percentage, at each relaxation point can be calculated from the following equation,

$$deg_i^{al} = Deg_{al}\left(T^+, h^+ + D_i^{eq}\right) - Deg_{al}(T^+, h^+) \qquad \forall i \qquad (7.5)$$

where

$$Deg_{al}(T, D) = 100 - \alpha(T)D^{\beta(T)}. \qquad (7.6)$$

7.2.5. Penalty Price Calculation

The last step is to set penalty prices at each segment of the staircase penalty price scheme. The model translates the anticipated marginal degradation effect at each segment into a conductor degradation cost. Note that an out-of-service cost is an important factor to consider; however, in this work, such cost is not applied for the sake of complexity. Nevertheless, the conductor replacement cost, which may include the out-of-service cost or not, is a scaling factor. Thus, the proposed penalty price determination model can be extended to incorporate other possible costs. Based on the degradation effects at each relaxation point, the proposed model set penalty prices as follows,

$$P_i = \frac{C^{ED}\left(deg_{i+1}^{al} - deg_i^{al}\right)}{\overline{SL_i} \cdot Deg_{al}^{+}} \qquad \forall i \qquad (7.7)$$

where P_i is the penalty price, in \$/MWh, for each staircase segment and $\overline{SL_t}$ is the length of each segment. The model assumes that a marginal effect is constant between each segment; thus, the model has another linearization at this point. Ideally, if the model has an infinite number of segments, this model will provide an exact representation of the degradation effect or cost. Thus, this is a trade-off between the accuracy and tractability of the model.

7.3. Numerical Results

7.3.1. Analysis Design

This section presents the evaluation results of the proposed online penalty price determination model. The case study includes the following design and assumptions. First, the analysis assumes a base staircase penalty price scheme that has three segments as presented in Table 7.1. The chosen base staircase penalty price scheme is a combination of the penalty price design of CAISO [41] and SPP [42]. Second, the study uses a Raven ACSR conductor; Table 7.2 presents the electrical characteristic and capital cost of the conductor [102]. The steady-state thermal ratings of the conductor are taken from Table 6.1. Third, the study considers deterministic weather conditions, as presented in Table 7.3, to estimate the line temperatures. Note that the model can utilize real-time weather condition data if available. Lastly, the study sets the penalty price determination interval as 5 minutes; however, the analysis does not include any market optimization model, such as real-time SCED model. Instead, the analysis assumes hypothetical power flows at each interval and investigates the performance of the penalty price determination model. The proposed model and the

IEEE standard models, which are defined in Chapter 4, are implemented in Java. All of the simulations are conducted on Intel Xeon 3.60 GHz CPU with 48 GB memory.

Table 7.1 Base Staircase Penalty Price Scheme

Segment	1	2	3
Length (MW)	15	30	30
Base Price ($)	500	1000	1500

Table 7.2 Raven ACSR Conductor Data

Structure (Al/St)	6/1
Rate A (MW)	160
Rate B (MW)	214
Rate C (MW)	241
Capital Cost (M$/mile)	0.84
End-of-service Cost (M$/mile)	0.29
Length (mile)	50

Table 7.3 Deterministic Weather Condition

Wind Speed	2 *ft/s*	Solar Time	12:00 PM
Wind Angle	45 °	Atmosphere	Clear
Elevation	150 *ft*	Line Direction	North-South
Latitude	38.5 °	Ambient Temperature (Summer)	35 °C
Emissivity	0.5	Ambient Temperature (Winter)	15 °C
Absorptivity	0.5		

7.3.2. The Impact of the Magnitude of the Relaxations

The analysis assumes three power flow cases, as presented in Table 7.4, to investigate the impact of the magnitude of relaxations on the penalty price determination. The study uses the summer weather condition from Table 7.3 along with the scheduling time at noon. The Case A does not involve relaxations. The Case B and Case C have relaxations with different magnitudes. Table 7.5 and Table 7.6 present the line temperature estimation results and penalty price adder determination results, respectively.

Table 7.4 Case Study Data (Case A-C, Power Flow, MW)

Interval	1	2	3	4
Case A	80	80	120	120
Case B	140	140	170	170
Case C	160	170	190	220

Table 7.5 Temperature Estimation Results (Case A-C, °C)

Interval		1	2	3	4
Case A	Initial	59	59	65	69
	Segment 1	79	79	83	84
	Segment 2	89	89	93	94
	Segment 3	102	102	106	107
Case B	Initial	80	80	88	92
	Segment 1	90	90	94	95
	Segment 2	100	100	104	106
	Segment 3	113	113	118	120
Case C	Initial	90	93	101	117
	Segment 1	94	96	99	107
	Segment 2	105	107	111	118
	Segment 3	119	120	124	132

Table 7.6 Penalty Price Adder Determination Results (Case A-C, $/MWh)

Interval		1	2	3	4
Case A	Segment 1	-	-	-	-
	Segment 2	-	-	-	-
	Segment 3	611	611	939	1,096
Case B	Segment 1	-	-	-	65
	Segment 2	473	473	840	976
	Segment 3	1,161	1,161	1,181	1,191
Case C	Segment 1	-	126	786	1,073
	Segment 2	910	978	987	1,221
	Segment 3	1,186	1,193	1,204	1,439

The results show that the proposed model sets the penalty price adders while capturing the magnitude of the relaxations properly. In Case A, the model only sets the penalty price adders at the last segments. The model anticipates that the line temperatures at the first two segments of Case A shall be lower than 95 °C; as a result, the model sets the price adders to zero. Although the step changes in the line flows between the line flow, 80 MW, and the line flows at the first two segments, 160 MW and 175 MW, are substantial, the size of the transient temperature increases in 5 minutes are relatively less significant. In Case B, the line flows begin with 140 MW and the relaxations, with the magnitude of 10 MW, occur at the last two intervals. The model sets the penalty price adders for the last two segments at the interval one to three. Also, the model defines the penalty price adders for the entire segments at the last interval. Although there is a relaxation begins at the third interval, the anticipated temperature was lower than 95 °C due to the limited transient temperature increase from the second interval to the third interval. In Case C, due to the relaxations, the model sets the penalty price adders for the almost entire segments at all the intervals. The result shows that the determined penalty price adders increase accordingly based on the magnitude of the relaxations.

7.3.3. The Impact of the Duration of the Relaxations

The study defines additional two cases, as presented in Table 7.7, to investigate the impact of the duration of the relaxations on the penalty price determination. Again, the study assumes a summer weather condition with the scheduling time at noon. The Case D and Case E have continuous relaxations at the last three intervals. Table 7.8 and Table 7.9

presents the line temperature estimation and penalty price adder determination results, respectively. The results show that the determined penalty price adders capture the duration of the relaxation properly. In Case D and Case E, the determined penalty price adders increase as the number of consecutive overloading intervals increase.

Table 7.7 Case Study Data (Case D-E, Power Flow, MW)

Interval	1	2	3	4	5
Case D	120	120	170	170	170
Case E	150	150	190	190	190

Table 7.8 Temperature Estimation Results (Case D-E, °C)

Interval		1	2	3	4	5
Case D	Initial	75	75	86	91	93
	Segment 1	87	87	93	95	96
	Segment 2	98	98	103	106	107
	Segment 3	111	111	117	119	120
Case E	Initial	84	84	97	103	106
	Segment 1	92	92	98	100	102
	Segment 2	103	103	109	112	113
	Segment 3	116	116	122	125	127

Table 7.9 Penalty Price Adder Determination Results (Case D-E, $/MWh)

Interval		1	2	3	4	5
Case D	Segment 1	-	-	-	-	176
	Segment 2	277	277	749	967	979
	Segment 3	1,151	1,151	1,177	1,189	1,194
Case E	Segment 1	-	-	476	860	896
	Segment 2	685	685	984	1,007	1,042
	Segment 3	1,173	1,173	1,200	1,224	1,257

7.3.4. The Impact of the Magnitude and Duration of the Relaxations.

Lastly, the study investigates the impact of the magnitude and duration of the relaxations simultaneously. The analysis defines a hypothetical power flow series, Case F, as presented in Table 7.10. To maintain the consistency, the study adopts a summer weather condition with the scheduling time at noon. Table 7.11 and Figure 7.2 presents the penalty price adder determination result. Also, Figure 7.3 presents the final staircase penalty price scheme after adding the penalty price adders in Table 7.11 to the base staircase penalty price scheme. In Table 7.11 and Figure 7.2, the result shows that the proposed online penalty price determination model sets penalty price adders properly while capturing the magnitude and duration of the relaxations. As a result, the result in Figure 7.3 illustrates that the final staircase penalty price scheme is automatically updated based on the impact of the relaxations.

Table 7.10 Case Study Data (Case F, Power Flow, MW)

Interval	1	2	3	4	5	6
Case F	140	140	170	170	150	150
Interval	7	8	9	10	11	12
Case F	150	180	180	190	190	190

Table 7.11 Penalty Price Adder Determination Results (Case F, $/MWh)

Interval		1	2	3	4	5	6
Case F	Segment 1	-	-	-	65	-	-
	Segment 2	474	474	840	977	832	752
	Segment 3	1,162	1,162	1,182	1,191	1,181	1,177
Interval		7	8	9	10	11	12
Case F	Segment 1	-	222	549	866	898	904
	Segment 2	715	980	985	1,013	1,043	1,049
	Segment 3	1,175	1,196	1,201	1,229	1,258	1,262

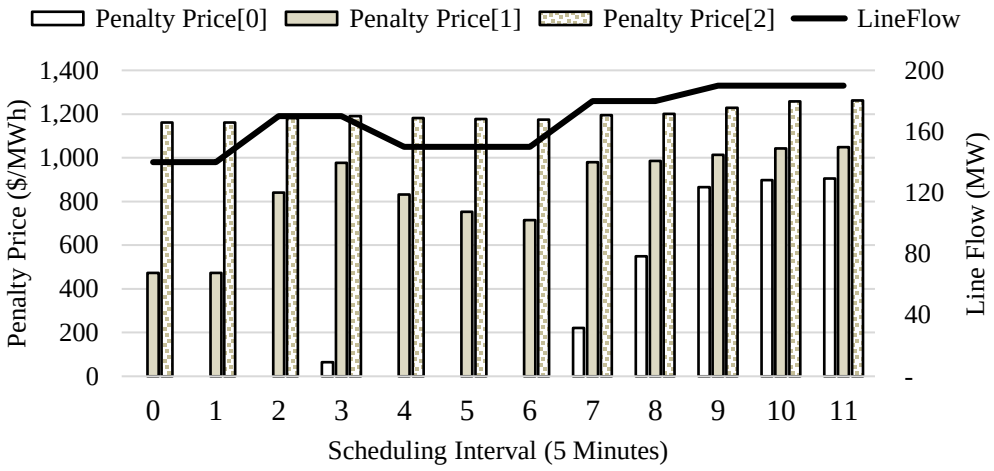

Figure 7.2 Penalty Price Adder Result (Case F).

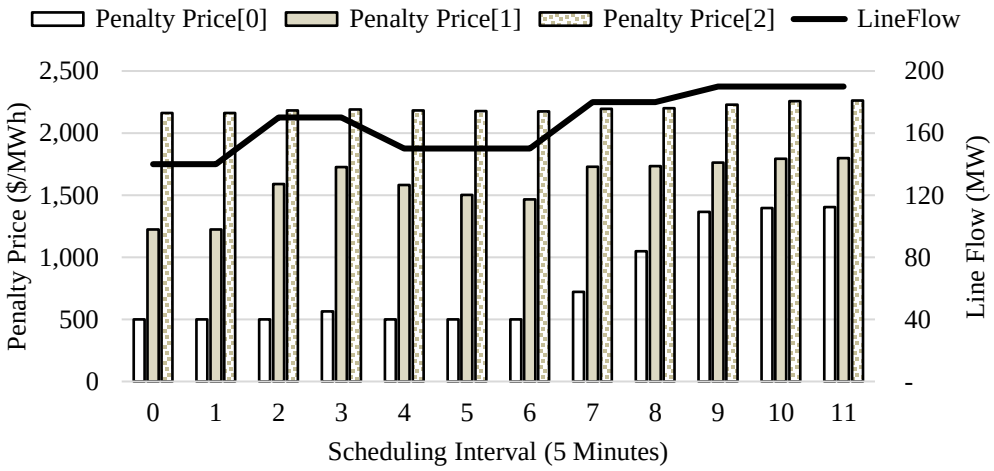

Figure 7.3 Final Penalty Price Result (Case F).

7.4. Conclusions

ISOs employ TCR practices in the market optimization models for various purposes. Such practices can affect the generation fleet as well as market prices. Therefore, it is crucial to set the penalty prices properly. However, the existing industry practices on

determining penalty prices do not have a systematic methodology and rely on operator's judgment and manual intervention. Also, the currently used penalty price schemes cannot capture the impact of the magnitude and duration of the relaxations simultaneously.

This work proposes an online penalty price determination model. The main goal of the proposed model is to update and provide staircase penalty prices to a real-time SCED model at each execution interval. The model considers the magnitude and duration of the relaxations simultaneously; moreover, the model captures the trade-off between relaxing transmission thermal limits and its impact on conductor materials. The numerical analysis results show that the proposed model can provide an automated and systematic mean to set staircase penalty prices on an online basis.

CHAPTER 8. STOCHASTIC LOOK-AHEAD SECURITY CONSTRAINED UNIT COMMITMENT

This chapter presents *ongoing* and *joint* research that investigates a methodology to ensure system reliability through a stochastic optimization approach. This dissertation mainly contains the parts associated with its contribution along with a core description of the whole research approach. The uncertainty and variability associated with the increasing penetration levels of renewable resources pose new challenges to power system reliability. This research proposes to design and develop a stochastic look-ahead commitment (SLAC) tool, which is a stand-alone advisory tool, to handle the uncertainties. The SLAC tool is envisioned to enhance the system flexibility by providing the system operators and market models with operational guidance concerning the uncertainties.

8.1. Background and Motivation

Significant attention has been given to renewable energy technologies, such as wind and solar, to meet the grand challenge of power system sustainability, to achieve power system security, and to improve energy independence. In addition to the frequently changing system operating conditions due to load forecasting deviations and system resource contingencies, the uncertainty and variability associated with the increasing penetration levels of stochastic resources pose new challenges to power system reliability. This research proposes a stochastic optimization based advisory tool, a SLAC tool, to handle the uncertainties effectively for resource scheduling applications.

The inclusion of uncertainty modeling within resource scheduling tools presents two practical barriers: (1) computational complexity of the resulting stochastic optimization problem and (2) market barriers primarily due to the complications associated with pricing in a stochastic market environment. As a result, most of the contemporary power system operational frameworks use deterministic approaches along with various approximations to handle the uncertainties. The *N*-1 reliability requirement, which necessitates the system-wide reserve to cover the loss of any bulk power system element, set forth by the NERC and the WECC, is an example of one such crude approximation. Other instances of such approximations include the 3+5 rule proposed by the National Renewable Energy Laboratory. In addition, most system operators use a zonal reserve model to distribute the reserves across the system. However, with such inherent approximations, there is no guarantee that reserves, which are acquired by the market, will be deliverable without causing security violations in the post-disturbance realization state. Such approximate, deterministic approaches also require expensive OMCs to adjust resource schedules to account for modeling inaccuracies. Moreover, rapidly increasing uncertainties from stochastic resources will make existing industry practices far more inefficient. As a consequence, there is a recent movement in the industry to explicitly model uncertainties, in a limited manner, by approximating the system response in the post-contingency state using factors, such as generator loss distribution factors and zonal reserve deployment factors; a detailed description will be provided in Section 8.2.

This ongoing and joint research attempts to enhance the recent industry practices while avoiding the aforementioned practical barriers by developing a stochastic optimization

based advisory tool. Although the concept of stochastic optimization based resource scheduling approach is not new, the contribution of this work is two-fold: (1) the development of a stochastic optimization algorithm, which is designed to be scalable to realistic systems, and (2) the development of an information translation tool that processes the solution from the stochastic program and generates information to be communicated with system operators and market models. The proposed SLAC tool has two main modules as presented in Figure 8.1. The first module is a two-stage stochastic programming model, for stochastic resource scheduling applications, that leverages statistical information of an ensemble of scenarios and their respective likelihoods. The second module is proposed to be a solution translation tool that processes the output from the first module and generates information to be communicated with system operators and market models.

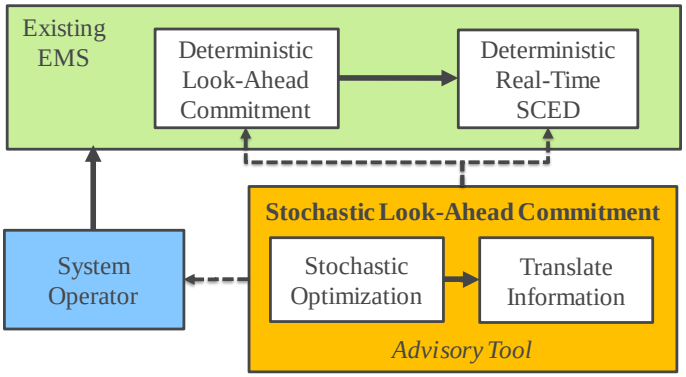

Figure 8.1 Proposed Market Scheduling Framework Incorporated with the SLAC Tool.

Note that the entire SLAC tool development will not be achieved by this dissertation alone but though the team efforts dedicated to the project. As such, this dissertation in-

cludes the core description of the approach but not full confirmation of the approach. Particularly this dissertation mainly focuses on the design and initial implementation of the first module's subproblem. The contribution of this dissertation includes:

(1) Creation of a mathematical formulation for an extensive form of a two-stage stochastic programming model for the SLAC tool.

(2) The use of a horizontal decomposition algorithm, PH, to separate the large stochastic program into smaller subproblems in an attempt to preserve the scalability of the model.

(3) Initial implementation of the PH subproblem along with various heuristic techniques to enhance the computational performance.

(4) Evaluation of the computational performance of the PH subproblem with an actual large-scale PJM test system.

For details associated to the whole confirmation of the proposed SLAC tool, please refer to the ongoing efforts associated with the ARPA-E NODES project led by Arizona State University.[1]

8.2. Recent Industry Movement

System operators manage transmission contingencies in the market by incorporating a set of post-contingency transmission constraints, described by (8.1), for each modeled transmission contingency case.

---

[1] The SLAC tool development is sponsored by the Advanced Research Projects Agency-Energy (ARPA-E) Network Optimized Distributed Energy Sources (NODES) program. The project team for Arizona State University (ASU) is led by Dr. Junshan Zhang with co-investigators Dr. Vijay Vittal, Dr. Anna Scaglione, and Dr. Kory Hedman. The presented SLAC work in this thesis is based on collaborative research efforts with Dr. Kory Hedman, Dr. Jean-Paul Watson of Sandia National Laboratories, Narsi Vempati of Nexant Inc., and ASU PhD students Nikita Singhal and Mehdi Saleh along with MSE student Tarek Ibrahim.

$$|f_{kt} + LODF_{ck} f_{ct}| \leq F_k^{c+} \qquad \forall k \in \Omega^{LC}, t \in T \qquad (8.1)$$

Here, the first component represents the pre-contingency flow on line k and the second component represents the portion of flow redistributed from line c to line k if line c is lost. F_k^{c+} denotes the emergency rating. In other words, present-day resource scheduling models represent transmission line contingencies explicitly without the use of recourse decision variables. Transmission contingency modeling is traditionally done by assuming that the generators will not change their pre-contingency dispatch to a different dispatch set point. This is known as a preventive action approach to ensure system security against transmission contingencies. While this is a sub-optimal policy since generators are capable of ramping their production, this approach is taken as it enables the mathematical program to avoid the need of defining a recourse decision variable (a second-stage decision variable) for the change in the generator's production. The fact that supply does not deviate for transmission contingencies allows for this simplified approach (with the exception of a transmission contingency on a tie-line that would change the overall imports or exports). Furthermore, in order to reduce the computational complexity, such constraints are modeled only for a limited set of frequently congested critical transmission lines (Ω^{LC}).

Although transmission contingencies are handled adequately today, the loss of a generating unit can also constrain the transmission system considerably. ISOs tackle this problem outside the market engine using OMCs or in the market using approximations/nomograms. However, recent literature suggests proposed changes in the market design to accommodate the influence of generator contingencies on transmission lines. For instance, MISO uses post-zonal reserve deployment transmission constraints,

described by (8.2), to model the effect of generator contingencies on set L^c and to implicitly determine their zonal reserve requirements [116].

$$|f_{kt} - PTDF_{zk}^{Trip} P_z^{max} + D_{kt}^{SPIN} \sum_z PTDF_{zk}^{Spin} r_{zt}^{Spin} + D_{kt}^{Supp} \sum_z PTDF_{zk}^{Supp} r_{zt}^{Supp} | \leq F_k^{c+} \qquad \forall k \in \Omega^{LC}, z \in Z, t \in T \tag{8.2}$$

Here, the first component represents the pre-contingency flow, the second component represents the deviation in flow due to the largest contingency event in zone z, and the third and fourth components represent the aggregated impact of zonal reserve (i.e., spinning and supplemental, respectively) deployment on the corresponding inter-zonal link, in the post-contingency state explicitly. In addition, D_{zt}^{SPIN} and D_{zt}^{SUPP} denote the pre-determined zonal reserve deployment factors.

Similarly, CAISO intends to enhance its scheduling models to include generator contingencies and pre-defined remedial action schemes explicitly as in (8.3) [117]. In this case, the post-contingency transmission constraints are defined as follows:

$$|f_{kt} - PTDF_{n(c),k}^{R} p_{g=c,t} + \sum_{\forall g: g \neq c} PTDF_{n(g),k}^{R} GDF_{gt}^{c} p_{g=c,t} | \leq F_k^{c+} \qquad \forall k \in \Omega^{LC}, z \in Z, t \in T \tag{8.3}$$

Here, the first, second, and third components represent the pre-contingency flow, the change in flow due to generator loss, and the change in flow due to reserve response, on set Ω^{LC}, respectively. GDF_{gt}^{c} denotes generator loss distribution factors, analogous to the more familiar participation factors, for generator contingency c and $p_{g=c,t}$ denotes the pre-contingency real power production of the contingency unit. Again, no second-stage recourse decisions are used. For a generator contingency, there is no way to get around the

fact that the generators must deviate away from their pre-contingency dispatch set point to make up for the change in overall production. While that is true, the industry has adopted the previously discussed approaches, which eliminate a second-stage recourse deviation variable from being used, in order to simplify the mathematical program. Instead, they force the post-contingency dispatch to be based on a function of the pre-contingency dispatch and reserve procurement. That is, the post-contingency dispatch is uniquely determined based on a function dependent on the pre-contingency dispatch set point and reserve as opposed to being a decision variable that is optimized. This is analogous to the existing practice within real-time contingency analysis where energy management systems do not run a full-fledged optimal power flow but simply power flows for *N*-1 contingencies; to avoid the unrealistic assumption of an infinite generator (slack bus) that can always provide any amount of generation to make up for the loss of a unit, participation factors are used for generator contingency simulations to adjust the assumed injections for the base-case power flows. Those participation factors are offline, assumed corrective responses for the generators as opposed to optimizing the potential corrective actions to minimize post-contingency violations.

The key issue with such approaches lies in the appropriate determination of participation factors and the associated market pricing implications. This is where the proposed SLAC tool can improve the existing industry practices. For instance, the SLAC tool can determine more appropriate reserve deployment factors (nodal and zonal) and resource participation factors (nodal) than existing practices. Moreover, the tool can provide a guidance regarding ramping products and ancillary services.

8.3. Stochastic Look-Ahead Commitment Model

This section introduces the main design features and the core mathematical formulation of the SLAC tool. The SLAC tool is designed as a supportive tool for intra-day resource scheduling applications by providing operational guidance concerning uncertainties. The SLAC tool has two main modules: (1) a stochastic resource scheduling application and (2) a solution translation tool. This dissertation only focuses on the first module, which is formulated as a two-stage stochastic programming model. The decision variable includes incremental commitment schedule for the fast start units, dispatch set point, awards for the reserve products, and reserve deployment as a recourse decision to address the uncertain events. The model explicitly considers the uncertainties, through a set of scenarios, from the stochastic resources and the transmission and generator contingencies. The model is designed such that both the base case and the renewable scenario cases are feasible with respect to the transmission and the generator contingencies. The generator contingencies are properly addressed by optimizing the recourse decision variable, which defines the amount of activated reserves. However, the transmission contingencies are preventively handled without the use of recourse decision variables; this is analogous to existing industry practices. Figure 8.2 presents an overview of the model; each box inside the base case and the renewable scenario case represents a set of constraints.

The model treats the uncertainties independently; it is assumed that each modeled event can occur simultaneously, and is addressed by its own reserve product. The model includes three reserve products: regulating reserve, spinning reserve, and non-spinning reserve. The regulating reserve will address the load deviations. Within the formulation, the spinning

reserve product is represented as a sum of regular spinning reserve and renewable reserve variable. The regular spinning variable and the non-spinning reserve product will address the generator contingencies. A new 10-minute reserve variable, i.e., a renewable reserve variable, is introduced to address deviations in renewable energy from the corresponding forecasted values. In other words, the based case dispatch set points are linked to the renewable scenarios via the renewable reserve variable and its corresponding ramp capability. While these distinctions are made within the mathematical program in an effort to provide a clear formulation that is efficiently solved, the use of the available reserve capability (the actual activation of reserve) is not subject to this precise separation of the reserve products within this stochastic model, which is how actual operations are handled today.

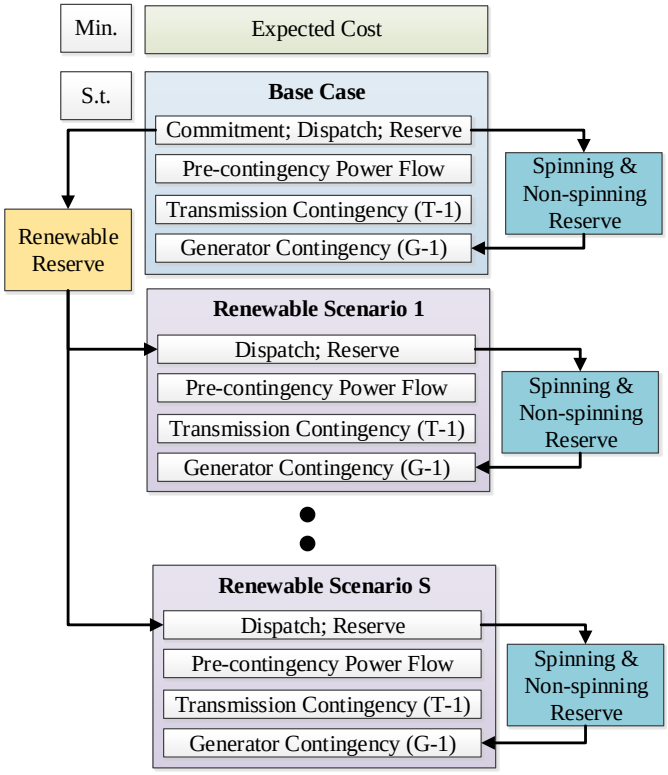

Figure 8.2 Design of the Two-Stage Stochastic Optimization Programming Model for the SLAC Tool.

8.3.1. Extensive Formulation

This section presents an extensive form of a two-stage stochastic programming model formulation. The model is represented as an MILP problem along with a DCOPF based SCUC formulation.

$$Minimize: \ (1-\sum_{\forall s}\pi_s)f^{base}+\sum_{\forall s}\pi_s f_s+\sum_{\forall gt}\left(C_g^{NL}u_{gt}+C_g^{SU}v_{gt}\right) \tag{8.4}$$

Where:

$$f^{base}=\sum_{\forall gt}\Big[\sum_{\forall i}\left(C_{gti}^{op}p_{gti}+C_{wti}p_{wti}\right)+C_{gt}^{reg_{up}}r_{gt}^{reg_{up}}+C_{gt}^{reg_{dn}}r_{gt}^{reg_{dn}}+ C_{gt}^{SP}\left(r_{gt}^{spin_{up}}+r_{gt}^{spin_{dn}}+r_{gt}^{w_{up}}+r_{gt}^{w_{dn}}\right)+C_{gt}^{NS}r_{gt}^{nspin}\Big] \tag{8.5}$$

$$f_s=\sum_{\forall gt}\Big[\sum_{\forall i}\left(C_{gti}^{op}p_{gtis}+C_{wti}p_{wtis}\right)+C_{wt10}p_{wts}^{11}+C_{gt}^{reg_{up}}r_{gts}^{reg_{up}}+C_{gt}^{reg_{dn}}r_{gts}^{reg_{dn}}+ C_{gt}^{SP}\left(r_{gts}^{spin_{up}}+r_{gts}^{spin_{dn}}\right)+C_{gt}^{NS}r_{gts}^{nspin}\Big] \tag{8.6}$$

Subject to:

Generator segments (base case):

$$0\le p_{gti}\le P_{gti}^{+}u_{gt} \qquad \forall g,t,i \tag{8.7}$$

$$p_{gt}=\sum_{\forall i}\left(p_{gti}\right) \qquad \forall g,t \tag{8.8}$$

$$0\le p_{wti}\le P_{wti}^{+} \qquad \forall w,t,i \tag{8.9}$$

$$p_{wt}=\sum_{\forall i}(p_{wti}) \qquad \forall w,t \tag{8.10}$$

$$0\le p_{wt}\le \overline{P_{wt}} \qquad \forall w,t \tag{8.11}$$

Generator reserve (base case):

$$p_{gt}+r_{gt}^{reg_{up}}+r_{gt}^{spin_{up}}+r_{gt}^{w_{up}}\le P_{gt}^{+}u_{gt} \qquad \forall g,t \tag{8.12}$$

$$P_{gt}^{-}u_{gt} + r_{gt}^{reg_{dn}} + r_{gt}^{spin_{dn}} + r_{gt}^{w_{dn}} \leq p_{gt} \qquad \forall g,t \qquad (8.13)$$

$$0 \leq r_{gt}^{reg_{up}} + r_{gt}^{spin_{up}} + r_{gt}^{w_{up}} \leq R_g^{10}u_{gt} \qquad \forall g,t \qquad (8.14)$$

$$0 \leq r_{gt}^{reg_{dn}} + r_{gt}^{spin_{dn}} + r_{gt}^{w_{dn}} \leq R_g^{10}u_{gt} \qquad \forall g,t \qquad (8.15)$$

$$0 \leq r_{gt}^{nspin} \leq R_g^{10}(1 - u_{gt}) \qquad \forall g \in G^{fast},t \qquad (8.16)$$

$$r_{gt}^{nspin} = 0 \qquad \forall g \notin G^{fast},t \qquad (8.17)$$

$$0 \leq r_{gt}^{reg_{up}} \leq R_g^{5}u_{gt} \qquad \forall g \in G^{AGC},t \qquad (8.18)$$

$$0 \leq r_{gt}^{reg_{dn}} \leq R_g^{5}u_{gt} \qquad \forall g \in G^{AGC},t \qquad (8.19)$$

$$r_{gt}^{reg_{up}} = 0 \qquad \forall g \notin G^{AGC},t \qquad (8.20)$$

$$r_{gt}^{reg_{dn}} = 0 \qquad \forall g \notin G^{AGC},t \qquad (8.21)$$

$$r_{gt}^{spin_{up}}, r_{gt}^{spin_{dn}}, r_{gt}^{w_{up}}, r_{gt}^{w_{dn}} \geq 0 \qquad \forall g,t \qquad (8.22)$$

Generator inter-temporal ramping, startup, shutdown (base case):

$$p_{gt} - p_{g,t-1} \leq M_{t-1}R_g^{up}u_{g,t-1} + R_g^{SU}v_{gt} \qquad \forall g,t \qquad (8.23)$$

$$p_{g,t-1} - p_{gt} \leq M_{t-1}R_g^{dn}u_{gt} + R_g^{SD}(v_{gt} - u_{gt} + u_{g,t-1}) \qquad \forall g,t \qquad (8.24)$$

Unit commitment (base case):

$$u_{gt} = \overline{U_{gt}} \qquad \forall g \notin G^{fast},t \qquad (8.25)$$

$$u_{gt} \geq \overline{U_{gt}} \qquad \forall g \in G^{fast},t \qquad (8.26)$$

$$u_{gt} \in \{0,1\} \qquad \forall g,t \qquad (8.27)$$

$$0 \leq v_{gt} \leq 1 \qquad \forall g,t \qquad (8.28)$$

$$v_{gt} \geq u_{gt} - u_{g,t-1} \qquad \forall g,t \qquad (8.29)$$

$$v_{gt} \leq 1 - u_{g,t-1} \qquad \forall g,t \qquad (8.30)$$

$$v_{gt} \leq u_{g,t} \qquad \forall g,t \qquad (8.31)$$

Reserve requirements (base case):

$$\sum_{\forall g}\left(r_{gt}^{reg_{up}}\right) \geq Max\left\{\alpha^{reg_{up}} \sum_{\forall n}(D_{nt}), R_t^{reg_{up}}\right\} \qquad \forall t \qquad (8.32)$$

$$\sum_{\forall g}\left(r_{gt}^{reg_{dn}}\right) \geq Max\left\{\alpha^{reg_{dn}} \sum_{\forall n}(D_{nt}), R_t^{reg_{dn}}\right\} \qquad \forall t \qquad (8.33)$$

$$\sum_{\forall g}\left(r_{gt}^{w_{dn}}\right) \geq \underset{s}{Max}\{\sum_{\forall w}(\overline{P_{wts}})\} - \sum_{\forall w}(p_{wt}) \qquad \forall t \qquad (8.34)$$

$$\sum_{\forall g}\left(r_{gt}^{w_{up}}\right) \geq \sum_{\forall w}(p_{wt}) - \underset{s}{Min}\{\sum_{\forall w}(\overline{P_{wts}})\} \qquad \forall t \qquad (8.35)$$

$$\sum_{\forall g}\left(r_{gt}^{spin_{up}}\right) \geq \frac{1}{2}\left(Max\left\{\underset{g}{Max}\{P_g^+\}, R_t^{cont}\right\}\right) \qquad \forall g,t \qquad (8.36)$$

$$\sum_{\forall g}\left(r_{gt}^{spin_{up}} + r_{gt}^{nspin}\right) \geq Max\left\{\underset{g}{Max}\{P_g^+\}, R_t^{cont}\right\} \qquad \forall g,t \qquad (8.37)$$

Power flow and global power balance (base case):

$$f_{kt} = \sum_{\forall n} PTDF_{k,n}^R\left(\sum_{\forall g \in G^n}\left(p_{gt} - P_{gt}^0\right) + \sum_{\forall w \in W^n}(p_{wt} - P_{wt}^0)\right) \qquad \forall k,t \qquad (8.38)$$

$$F_{kt}^{a-} \leq f_{kt} \leq F_{kt}^{a+} \qquad \forall k,t \qquad (8.39)$$

$$\sum_{\forall g}\left(p_{gt}\right) + \sum_{\forall w}(p_{wt}) = \sum_{\forall n}(D_{nt}) \qquad \forall t \qquad (8.40)$$

Transmission contingencies (base case):

$$F_{kt}^{c-} \leq f_{kt} + LODF_{\ell,k}(f_{\ell t} + F_{\ell t}^0) \qquad \forall k,t,\ell \qquad (8.41)$$

$$f_{kt} + LODF_{\ell,k}(f_{\ell t} + F_{\ell t}^0) \leq F_{kt}^{c+} \qquad \forall k,t,\ell \qquad (8.42)$$

Generator contingencies (base case):

$$F_{kt}^{c-} \leq f_{kt} - PTDF_{k,n(c)}^R p_{g=c,t} + \sum_{\forall n}\left[PTDF_{k,n}^R\left(\sum_{\forall g \in G^n} r_{gtc}\right)\right] \qquad \forall k,t,c \qquad (8.43)$$

$$f_{kt} - PTDF^{R}_{k,n(c)} p_{g=c,t} + \sum_{\forall n}\left[PTDF^{R}_{k,n}\left(\sum_{\forall g \in G^{n}} r_{gtc}\right)\right] \leq F^{c+}_{kt} \qquad \forall k,t,c \qquad (8.44)$$

$$\sum_{\forall g} r_{gtc} = p_{g=c,t} \qquad \forall t,c \qquad (8.45)$$

$$r_{g=c,tc} = 0 \qquad \forall t,c \qquad (8.46)$$

$$-r^{spin_{dn}}_{gt} \leq r_{gtc} \leq r^{spin_{up}}_{gt} + r^{nspin}_{gt} \qquad \forall g,t,c \qquad (8.47)$$

Generator segments (renewable scenario)**:**

$$0 \leq p_{gtis} \leq P^{+}_{gti} u_{gt} \qquad \forall g,t,i,s \qquad (8.48)$$

$$p_{gts} = \sum_{\forall i}\left(p_{gtis}\right) \qquad \forall g,t,s \qquad (8.49)$$

$$0 \leq p_{wtis} \leq P^{+}_{wti} \qquad \forall w,t,i,s \qquad (8.50)$$

$$p_{wts} = \sum_{\forall i}(p_{wtis}) + p^{11}_{wts} \qquad \forall w,t,s \qquad (8.51)$$

$$0 \leq p_{wts} \leq \overline{P_{wts}} \qquad \forall w,t,s \qquad (8.52)$$

$$0 \leq p^{11}_{wts} \leq max\{0, \overline{P_{wts}} - \sum_{\forall i} P^{+}_{wti}\} \qquad \forall w,t,s \qquad (8.53)$$

Generator reserve (renewable scenario):

$$p_{gts} + r^{reg_{up}}_{gts} + r^{spin_{up}}_{gts} \leq P^{+}_{gt} u_{gt} \qquad \forall g,t,s \qquad (8.54)$$

$$P^{-}_{gt} u_{gt} + r^{reg_{dn}}_{gts} + r^{spin_{dn}}_{gts} \leq p_{gts} \qquad \forall g,t,s \qquad (8.55)$$

$$0 \leq r^{reg_{up}}_{gts} + r^{spin_{up}}_{gts} \leq R^{10}_{g} u_{gt} \qquad \forall g,t,s \qquad (8.56)$$

$$0 \leq r^{reg_{dn}}_{gts} + r^{spin_{dn}}_{gts} \leq R^{10}_{g} u_{gt} \qquad \forall g,t,s \qquad (8.57)$$

$$0 \leq r^{nspin}_{gts} \leq R^{10}_{g}\left(1 - u_{gt}\right) \qquad \forall g \in G^{fast},t,s \qquad (8.58)$$

$$r^{nspin}_{gts} = 0 \qquad \forall g \notin G^{fast},t,s \qquad (8.59)$$

$$0 \leq r^{reg_{up}}_{gts} \leq R^{5}_{g} u_{gt} \qquad \forall g \in G^{AGC},t,s \qquad (8.60)$$

$$0 \le r_{gts}^{reg_{dn}} \le R_g^5 u_{gt} \qquad \forall g \in G^{AGC}, t, s \qquad (8.61)$$

$$r_{gts}^{reg_{up}} = 0 \qquad \forall g \notin G^{AGC}, t, s \qquad (8.62)$$

$$r_{gts}^{reg_{dn}} = 0 \qquad \forall g \notin G^{AGC}, t, s \qquad (8.63)$$

$$r_{gts}^{spin_{up}}, r_{gts}^{spin_{dn}} \ge 0 \qquad \forall g, t, s \qquad (8.64)$$

Generator inter-temporal ramping, startup, shutdown (renewable scenario):

$$-r_{gt}^{w_{dn}} \le p_{gts} - p_{gt} \le r_{gt}^{w_{up}} \qquad \forall g, t, s \qquad (8.65)$$

$$p_{gts} - p_{g,t-1,s} \le M_{t-1} R_g^{up} u_{g,t-1} + R_g^{SU} v_{gt} \qquad \forall g, t, s \qquad (8.66)$$

$$p_{g,t-1,s} - p_{gts} \le M_{t-1} R_g^{dn} u_{gt} + R_g^{SD} \left(v_{gt} - u_{gt} + u_{g,t-1}\right) \qquad \forall g, t, s \qquad (8.67)$$

System/zonal reserve modeling (renewable scenario):

$$\sum_{\forall g} \left(r_{gts}^{reg_{up}}\right) \ge max\left\{\alpha^{reg_{up}} \sum_{\forall n}(D_{nt}), R_t^{reg_{up}}\right\} \qquad \forall t, s \qquad (8.68)$$

$$\sum_{\forall g}\left(r_{gts}^{reg_{dn}}\right) \ge max\left\{\alpha^{reg_{dn}} \sum_{\forall n}(D_{nt}), R_t^{reg_{dn}}\right\} \qquad \forall t, s \qquad (8.69)$$

$$\sum_{\forall g} \left(r_{gts}^{spin_{up}}\right) \ge \frac{1}{2}\left(max\left\{\max_g\left\{P_g^+\right\}, R_t^{cont}\right\}\right) \qquad \forall g, t, s \qquad (8.70)$$

$$\sum_{\forall g} \left(r_{gts}^{spin_{up}} + r_{gts}^{nspin}\right) \ge max\left\{\max_g\left\{P_g^+\right\}, R_t^{cont}\right\} \qquad \forall g, t, s \qquad (8.71)$$

Power flow and global power balance (renewable scenario):

$$f_{kts} = \sum_{\forall n} PTDF_{k,n}^R\left(\sum_{\forall g \in G^n}\left(p_{gts} - P_{gt}^0\right) + \sum_{\forall w \in W^n}\left(p_{wts} - P_{wt}^0\right)\right) \qquad \forall k, t, s \qquad (8.72)$$

$$F_{kt}^{a-} \le p_{kts} \le F_{kt}^{a+} \qquad \forall k, t, s \qquad (8.73)$$

$$\sum_{\forall g}\left(p_{gts}\right) + \sum_{\forall w} p_{wts} = \sum_{\forall n}(D_{nt}) \qquad \forall t, s \qquad (8.74)$$

Transmission contingencies (renewable scenario):

$$F_{kt}^{c-} \leq f_{kts} + LODF_{\ell,k}(f_{\ell ts} + F_{\ell t}^{0}) \qquad \forall k,t,\ell,s \qquad (8.75)$$

$$f_{kts} + LODF_{\ell,k}(f_{\ell ts} + F_{\ell t}^{0}) \leq F_{kt}^{c+} \qquad \forall k,t,\ell,s \qquad (8.76)$$

Generator contingencies (renewable scenario):

$$F_{kt}^{c-} \leq f_{kts} - PTDF_{k,n(c)}^{R} p_{g=c,ts} + \sum_{\forall n}\left[PTDF_{k,n}^{R}\left(\sum_{\forall g \in G^{n}} r_{gtcs}\right)\right] \qquad \forall k,t,c,s \qquad (8.77)$$

$$f_{kts} - PTDF_{k,n(c)}^{R} p_{g=c,ts} + \sum_{\forall n}\left[PTDF_{k,n}^{R}\left(\sum_{\forall g \in G^{n}} r_{gtcs}\right)\right] \leq F_{kt}^{c+} \qquad \forall k,t,c,s \qquad (8.78)$$

$$\sum_{\forall g} r_{gtcs} = p_{g=c,ts} \qquad \forall t,c,s \qquad (8.79)$$

$$r_{g=c,tcs} = 0 \qquad \forall t,c,s \qquad (8.80)$$

$$-r_{gts}^{spin_{dn}} \leq r_{gtcs} \leq r_{gts}^{spin_{up}} + r_{gts}^{nspin} \qquad \forall g,t,c,s \qquad (8.81)$$

The objective (8.4) minimizes expected costs of the base case and renewable scenarios along with start up, shut down, and no load costs. The total system costs, including the procurement of operating reserves, are modeled in (8.5)-(8.6). Note that there is no *N*-1 redispatch cost reflected in the objective function. The generator operating restrictions are modeled in (8.7)-(8.13). The allocation of the reserve products is restricted by the ramping limit as well as the physical availability of each unit in (8.14)-(8.22). The model treats the uncertain events independently and assumes that the uncertain events can happen simultaneously. Therefore, the model forces the reserve products to all be collectively below the ramp limit in (8.14)-(8.15). The inter-temporal ramping restrictions are enforced in (8.23)-(8.24). The generator's incremental commitment and start-up constraints are

models as (8.25)-(8.31). A generic system-wide operating reserve requirements are modeled in (8.32)-(8.37). It is assumed that the total regulation reserve procurement must exceed the maximum of a predetermined regulation reserve requirement and a particular portion of the total demand (8.32)-(8.33). The model allocates the renewable reserves such that there is enough room to link the base case and the renewable scenarios in (8.34)-(8.35). Moreover, the model requires that 50 % of the total operating reserve requirement should be fulfilled by the spinning reserves in (8.36). Also, the model ensures that the quantity of the system-wide operation reserve procurement exceeds the capacity of the largest unit in the system (8.37). The network constraints represent the pre-contingency transmission network in (8.38)-(8.39) and the global power balance in (8.40). Note that a delta flow concept is used in (8.38); that is, the model only captures the deviations in power flows due to the changes in dispatch set points. The model manages the transmission contingencies by incorporating a set of preventive post-contingency transmission constraints in (8.41)-(8.42) while assuming that the generators pre-contingency dispatch will not be changed. On the other hand, the model explicitly represent the generator contingencies with a set of corrective post-contingency constraints in (8.43)-(8.47) along with recourse decision variables, r_{gtc}. The model manages the system within the renewable scenarios in (8.48)-(8.81) in a similar manner as that of the base case. The model binds the dispatch between the renewable scenarios to the base case in (8.65). That is, the renewable reserve product, which is acquired to handle the base case to renewable scenario pivot, links the base case and the renewable scenarios.

8.3.2. Progressive Hedging Decomposition

The primary challenge of the extensive form model is its computational complexity. For small-scale applications, the extensive form model can be solved directly; however, when it comes to larger-scale applications, decomposition-based solution methods are generally used to improve the scalability of the model. There are mainly two classes of decomposition techniques: vertical decomposition and horizontal decomposition. Vertical decomposition methods, such as Benders' decomposition, decompose a stochastic model by stages. On the other hand, horizontal decomposition methods, such as PH, decompose a stochastic model by scenario. Watson et al. [28] applied PH to solve a large scale stochastic UC model. Although PH does not guarantee a global optimal solution for non-convex optimization models, the authors showed that PH is an effective heuristic for large-scale mixed integer stochastic programs. This research utilizes PH to preserve the scalability of the model. First, the extensive form model is decomposed into PH subproblems by renewable scenarios and generator contingencies. Therefore, each PH subproblem includes one renewable scenario, one generator contingency, and full transmission contingencies as uncertain events. Figure 8.3 presents an overview of the PH subproblem decomposition.

Each PH subproblem is solved independently. Then the PH algorithm seeks an agreement of the hedging variables, e.g., the first stage decision variables u_{gt}, between solutions from each subproblem by iteratively updating the weights to be added to the objective function of each subproblem. The added weights penalize the lack of agreement of the hedging variables using a sub-gradient estimator and a squared penalty term [29]. Figure 8.4 presents an overview of the PH algorithm.

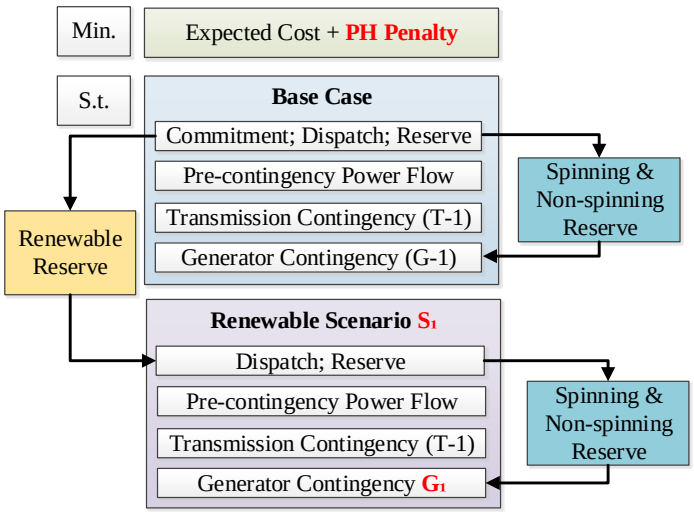

Figure 8.3 Design of the PH Subproblem for the SLAC Tool.

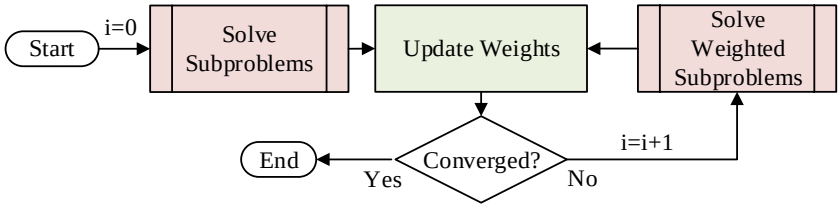

Figure 8.4 PH Algorithm Flowchart.

8.3.3. Progressive Hedging Subproblem Decomposition

The defined PH subproblem is also a stochastic programming problem due to the nature of the chosen horizontal decomposition technique. Although the PH subproblem is relatively easier to solve than the extensive form model, the present PH subproblem is still difficult to solve via direct methods particularly with a large, real-world test system, i.e., the PJM network. Therefore, additional row-decomposition techniques are applied to solve the PH subproblems efficiently. Figure 8.5 presents a solution process for the PH subproblems along with the decomposition technique. First, in the pre-processing stage, the model determines a set of critical transmission lines to be monitored as well as an initial set of

pre- and post-contingency transmission constraints to be loaded to the PH subproblem. A base power flow analysis and contingency analysis are conducted, with a given initial dispatch schedule, to identify those sets. That is, in the beginning, the model starts with the selected initial transmission constraints, instead of considering the whole transmission constraints associated with the monitored lines, and ensures the deliverability with respect to the monitored lines through an iterative process. Second, the model conducts a PTDF cutoff procedure. The power flow constraints, (8.35) and (8.69), only capture deviations in power flows due to changes in dispatch and commitment. This modeling feature provides an efficient way to prescreen PTDF values for each line based on their expected influences on power flow deviations. That is, the model identifies which buses to monitor for power injected by generators relative to their most influential impact on the power flows. Figure 8.6 presents a detailed procedure to determine the expected influences on power flow deviations for each line. Additionally, the model further prescreens PTDF values based on their relative ranking. An iterative PTDF cutoff feasibility test is proposed to determine the number of buses to capture for each line while keeping the accuracy, i.e., the deviations in power flow calculation, within a predetermined threshold, which is assumed as 5 % in this work.

Once the initial subproblem is solved, the model performs a deliverability test, which includes a base power flow analysis and contingency analysis. If any violations are identified, the model adds associated cuts to the master PH subproblem; the whole process will be repeated until the termination criteria are met. The PH subproblem is implemented using the Python optimization modeling objects (PYOMO) software.

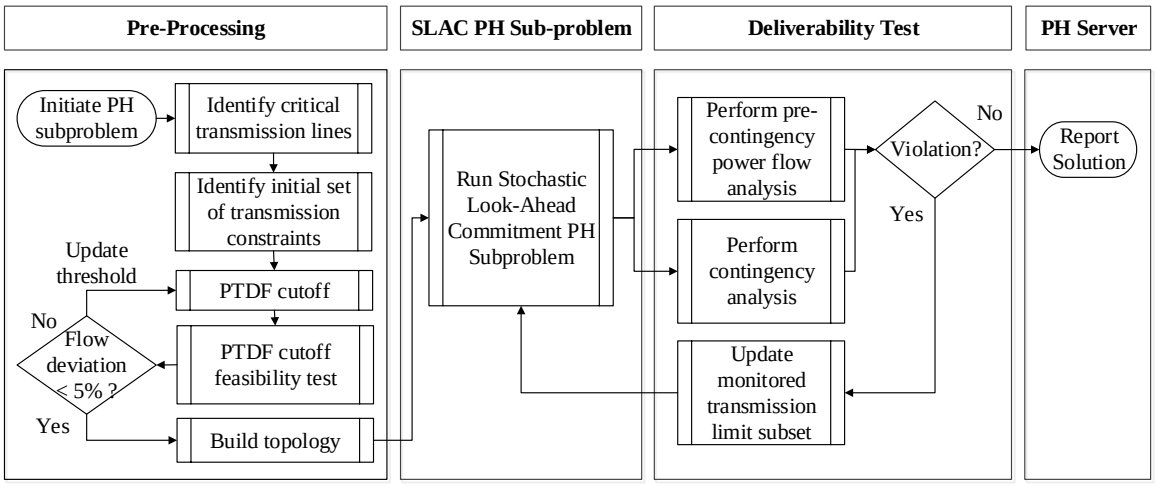

Figure 8.5 PH Subproblem Decomposition Flowchart.

For all branch $k \in K$:
  For all bus $n \in N$:
    $\text{Netinjection}_n = 0$
    For all generator $g \in G^n$:
      If $\overline{U_{gt}} > 0$:
        $\text{Netinjection}_n = \text{Netinjection}_n + Max(P_{gt}^{max} - P_{gt}^0, P_{gt}^0 - P_{gt}^{min}, R_{gt}^{10})$
      Else if $\overline{U_{gt}} = 0$ and $g \in G^{fast}$:
        $\text{Netinjection}_n = \text{Netinjection}_n + Min(P_{gt}^{min} + R_{gt}^{10}, P_{gt}^{max})$
    For all renewable $w \in W^n$
        $\text{Netinjection}_n = \text{Netinjection}_n + Max_{s \in S}(|\overline{P_{wts}} - \overline{P_{wt}}|)$
  $\text{PTDF\_impact}_{nk} = \text{Netinjection}_n \cdot PTDF_{k,n}^R$

Figure 8.6 Expected Impact of Net Injection Calculation Process.

8.4. Numerical Results

This section presents the performance evaluation results of the PH subproblem implementation. The PJM test case, which is a large-scale real-world system, is used to assess the computational performance. This analysis focuses on demonstrating the capability of the model to solve within tight time requirements as well as produce high-quality solutions

with a small optimality gap. PJM provided hourly dispatch set point, system topology, power flow, and market data for one week in July 2013. In this analysis, only two hours of data, Monday 9:00 am to 10:00 am, are utilized. Table 8.1 summarizes the PJM data set.

Table 8.1 PJM Data Set Description

Component	PJM area	Neighboring areas	Total
Zones	30	50	80
Buses	6,460	8,766	15,226
Generators	1,228	1,573	2,801
Generators with Cost Information	919	362	1,281
Renewables with Cost Information	77	1	78
Branches	8,181	12,325	20,506
Max. Load (GW)	82	169	251

Note that the provided market data does not have cost information for all the generators; therefore, only 48 % of the generators are considered as a dispatchable unit in this analysis. The remaining generator's output is assumed to be fixed. In addition, this study only enforces transmission constraints for non-radial lines at or above 138 kV. The lines within the neighboring area, except the inter-tie lines, are also excluded due to the fact that about 80 % of generators in the neighboring area are treated as a non-dispatchable unit; that is, the market model only captures the impact of the generators in the neighboring area on the inter-tie lines. The given initial dispatch set point is used in a pre- and post-contingency analysis to determine a set of critical transmission lines to monitor and an initial set of pre- and post-transmission constraints to be loaded.

Four cases are created to investigate the computational performance of the PH subproblem. Case A has the same time resolution with the given PJM data set. Case B extends the

case A by reducing the time resolution in half. Case C has six time periods; the first four periods have 15 minutes of time resolution, and the last two have 30 minutes of time resolution. Lastly, case D has a total of eight time periods with 15 minutes resolution. Table 8.2 describes the design of the cases along with the problem size information.

Table 8.2 Analysis Design of PJM Data Set

	Case A	Case B	Case C	Case D
Num. Time Period	2	4	6	8
Time Resolution (min)	60	30	15 / 30	15
Num. Variable	69,323	138,239	206,589	276,545
Num. Binary Variable	1,434	2,868	4,302	5,736
Num. Constraint	67,483	136,995	205,971	276,493
Num. Nonzero Coefficient	1,875,355	3,668,409	5,507,373	7,351,019

This analysis investigates various heuristic strategies as a way to enhance the computational performance. First, this study evaluates the advantage of the power flow deviation modeling, which only captures the deviations in power flows in (8.35) and (8.69), that enables a network reduction technique by prescreening PTDF values based on their expected influences on power flow deviations. Second, this analysis includes further PTDF selection strategies based on the magnitude of PTDF values and relative ranking with fixed thresholds. Third, this investigation assesses the effectiveness of the proposed PTDF cutoff threshold determination process, which is introduced in Section 8.3.3 and Figure 8.5, concerning the reduction in run time and the accuracy in power flow calculations. Lastly, this work examines a priority based decomposition technique; a simulation starts with the selected post transmission contingency constraints only in the renewable scenario case with a hope that these constraints dominate pre-contingency and post generator contingency constraints in the base and renewable scenario case. Note that the iterative deliverability

test still ensures the feasibility of the solution. All the simulations are performed on the Intel Xeon 3.60 GHz CPU with 48 GB memory. The chosen optimality gap is 1 %.

Table 8.3 presents the computational performance of case A. The result shows that the network reduction technique alone provides about 55 % reduction in total run time without causing any flow violations, which is a gap in power flow between the full network and the reduced network. In this study, 5 % gap is chosen as a threshold. The additional PTDF cutoff based on the magnitude of PTDF values with a threshold of 0.001 gives further run time reduction. Using more aggressive thresholds, above 0.005, shows more reduction in run time; however, flow violations are reported along with noticeable gaps in objective values. The relative PTDF value ranking approach with a threshold of 1,000 also shows additional reductions in total run time. Similarly, using the thresholds below 500 can reduce the run time while causing flow violations. Utilizing predetermined PTDF cutoff threshold for each line shows a significant reduction in run time without causing any flow violation. Lastly, this study shows that using the priority based decomposition technique combined with the predetermined PTDF cutoff threshold can provide about 78 % reduction in total run time with zero flow violations. Table 8.4 presents the simulation results of case B. The network reduction technique shows about 40 % reduction in total run time. Further PTDF cutoff strategies based on the magnitude of PTDF values and relative ranking with fixed thresholds show similar results; an aggressive cutoff threshold results in a higher reduction in run time along with a lower quality of solution. In case B, the priority based decomposition technique along with the predetermined PTDF cutoff threshold provides 75 % reduction in total run time without causing flow violations above 5 %.

Table 8.3 PH Subproblem Computational Performance (Case A)

	Full Network	Reduced Network								
PTDF Cutoff Method			Value			Rank			Preprocess	Priority based Decomposition
PTDF Cutoff Threshold	-	-	0.001	0.005	0.01	1000	500	250		
Initialize Data	64	16	15	14	14	15	15	15	14	15
Topology Construction	241	91	70	30	20	75	51	32	38	37
Solution Time (Seconds)	174	109	99	56	38	96	76	53	71	55
Total Time (Seconds)	479	216	185	100	72	187	142	100	135	107
Objective ($k/hour)	2,908	2,906	2,902	2,953	3,009	2,909	2,891	2,899	2,898	2,908
Gap (%)	-	0.1	0.2	1.6	3.5	0.0	0.6	0.3	0.3	0.0
Num. Flow Violation (>5 %)	-	0	0	5 (2)	12 (6)	0	10 (5)	13 (7)	0	0

Table 8.4 PH Subproblem Computational Performance (Case B)

	Full Network	Reduced Network								
PTDF Cutoff Method			Value			Rank			Preprocess	Priority based Decomposition
PTDF Cutoff Threshold	-	-	0.001	0.005	0.01	1000	500	250		
Initialize Data	64	15	15	14	14	15	15	14	14	15
Topology Construction	416	173	133	55	35	146	96	62	72	70
Solution Time (Seconds)	528	417	346	243	112	444	282	195	217	169
Total Time (Seconds)	1,007	606	495	312	161	606	393	271	303	254
Objective ($k/hour)	2,960	2,956	2,956	2,977	2,993	2,959	2,922	2,929	2,939	2,942
Gap (%)	-	0.1	0.1	0.6	1.1	0.1	1.3	1.1	0.7	0.6
Num. Flow Violation (>5 %)	-	0	0	7 (2)	17 (3)	0	20 (5)	30 (9)	2 (0)	2 (0)

Table 8.5 presents the analysis results of case C and case D. The proposed priority based decomposition, combined with the predetermined PTDF cutoff threshold, provides run time reduction about 67 % in case C and 70 % in case D. However, there are noticeable gaps in the objective values in both cases along with line flow violations, all below 5 %. This inaccuracy is caused by the fact that the PTDF threshold prescreening process only utilizes the given data set, which has 60 minutes of time resolution.

Table 8.5 PH Subproblem Computational Performance (Case C-D, Second)

	Case C		Case D	
	Full Network	Priority based Decomposition	Full Network	Priority based Decomposition
Initialize Data	129	18	128	18
Topology Construction	592	105	777	142
Solution Time	1,269	517	2,672	8,98
Total Time	1,990	640	3,577	1,058
Objective ($k/hour)	2,994	2,940	3,012	2,963
Gap (%)	-	1.7	-	1.6
Num. Flow Violation (>5 %)	-	5 (0)	-	5 (0)

8.5. Conclusions

Increasing penetration levels of renewable resources combined with existing uncertain nature of power system operations pose new challenges to power system reliability. Introducing stochastic resource scheduling application, which explicitly models the uncertain events, presents two practical barriers including the computational complexity of the model as well as market objections. Thus, existing industry practices rely on a deterministic model or semi-stochastic model, which utilizes deterministic factors to approximate the system response in uncertainty realization state, to handle the uncertainty. This research proposes a stochastic optimization based advisory tool, a SLAC tool, to bridge a gap between the

existing practices and an innovative technology advancement while avoiding the practical barriers.

This dissertation focuses on the derivation of a mathematical formulation for the extensive form two-stage stochastic programming model, the utilization of PH decomposition algorithm, and the initial implementation of the PH subproblem along with investigations on various heuristic strategies to enhance the computational performance. The numerical analysis, which uses a large-scale real-world PJM test case, confirms the performance of the initial implementation of the PH subproblem by demonstrating the capability of the model to solve within tight time limits as well as produce high-quality solutions with a small optimality gap. Although this dissertation alone does not provide a full validation of the entire SLAC tool, the work provides an effective initial implementation of the PH subproblem to be utilized for further progress of the research project.

CHAPTER 9. CONCLUSIONS AND FUTURE WORK

9.1. Conclusions

System planners and operators manage various optimization models, for long-term capacity expansion planning and short-term operation planning, to maintain a reliable and economically efficient delivery of electric energy. Due to the complexities of power systems, most of the present-day power system operational frameworks rely on deterministic approaches along with various approximations. This research investigates the possible room for improvement of the contemporary power system operation practices and proposes innovative methodologies to provide operational guidance to system planners, operators and market models.

The first part of this dissertation focuses on TCR practices, which is already employed by all ISOs in US. Enabling TCR within a market model allows a line flow to exceed its thermal rating for a predefined penalty price. It is important to set the penalty prices properly due to their impact on generation scheduling and market settlements; however, the existing industry practices do not have a systematic methodology in determination of the penalty prices. The primary goal of the first part of this dissertation is to propose systematic penalty price determination methods for TCR based on a reduced service life of an asset from the relaxations.

In Chapter 5, this dissertation investigates the importance and effectiveness of acknowledging the existing operational practice, TCR, within a long-term TEP study. A linearized conductor temperature and degradation effect estimation model is proposed to

properly capture the impact of exercising TCR within a TEP model. First, the chapter introduces a static TEP model that determines optimal conductor size and path for a large wind farm integration while considering TCR. Second, the chapter presents a dynamic TEP model that considers various means, including TCR, to increase transmission capacity while preserving existing ROW. The numerical analysis shows that considering TCR practices with properly determined penalty prices in long-term TEP studies can provide the total planning cost savings.

In Chapters 6 and 7, this dissertation proposes advanced penalty price determination methods. First, in Chapter 6, this work introduces an offline risk-based penalty price determination model for TCR that provides fixed penalty prices based on the degradation risk while considering probabilistic weather condition. The proposed model sets penalty prices for a given look-ahead period while anticipating system operating conditions. Second, in Chapter 7, this study presents a practical penalty price determination model that provides a staircase penalty price to a real-time SCED model on an online basis. The model captures the impact of the magnitude and duration of the relaxations simultaneously. The numerical analysis shows that the proposed models can provide an automated and systematic mean to set penalty prices. Although practicing TCR practices with a proper selection of penalty prices does not guarantee significant cost savings, this work enhances the existing industry practices, which rely on operator's judgments and manual interventions to manage the relaxations, by providing systematic methodologies for setting the penalty prices. Also, the results show that all market participants can achieve benefits by practicing TCR with a proper selection of penalty prices.

The second part of this dissertation introduces an advanced stochastic programming based methodology to handle the uncertainties in power system operations. This ongoing and joint research proposes to design and develop a SLAC tool, which is a stand-alone advisory tool, to connect the existing industry practices and an innovative technology advancement. The SLAC tool is envisioned to enhance the system flexibility by providing system operators with operational guidance concerning the uncertainties. This dissertation contributes to the derivation of a mathematical formulation for the extensive form two-stage stochastic programming model, the utilization of PH decomposition algorithm, and the initial implementation of the PH subproblem along with investigations on various heuristic strategies to enhance the computational performance. The numerical analysis, which uses a large-scale real-world PJM test case, confirms the performance of the initial implementation of the PH subproblem. The results show the capability of the developed model to solve within tight time requirements as well as produce high-quality solutions with a small optimality gap. Also, the results indicate that the proposed decomposition and heuristic techniques can provide 40 % to 77 % reduction in total solution time without causing violations. Although this dissertation alone does not provide a full validation of the entire SLAC tool development, this work provides an effective initial implementation of the PH subproblem to be utilized for further progress of the research project.

9.2. Future Work

All ISOs in the US already employ CR practices for various purposes. This research investigates advanced methodologies to enhance the contemporary industry practices while focusing on TCR. The proposed penalty price determination methods consider the actual

cost, a reduced service life of an asset, of the relaxations by utilizing two IEEE standard models in [30] and [35]. The numerical analysis shows the possible benefit of practicing TCR along with well-defined penalty prices by the proposed models. However, the study only includes analytical simulations; future work can be extended to confirm the feasibility and accuracy of the proposed models through actual experiments. Also, a further investigation on the impact of exercising TCR on the conductor accessories could be useful. Moreover, ISOs employ CR practices on a much broader basis. Future work can further investigate other types of CR practices. For instance, many ISOs relax reserve requirements within the market models while using a fixed price or a reserve demand curve. Future research could make progress in the determination of appropriate penalty prices for the reserve requirement relaxations.

The development of the whole SLAC tool is a work in progress by the team dedicated to the project. Although this dissertation provides a well-functioning initial implementation of the PH subproblem, which is a core part of the SLAC tool, there is still room for improvement. First, the main bottleneck of the computational performance is the communication time between the solver and PYOMO. A reduction in the communication time would noticeably enhance the performance of the PH subproblem. Moreover, future work can investigate various PH heuristic techniques, such as bundling, slamming, forcing solutions, avoiding cycling, and handling the non-converged variables to enhance the overall computational efficiency of the entire PH algorithm.

Lastly, the future work can investigate an effective way to link the developed stochastic program to deterministic market frameworks through the solution translation tool. For instance, the optimized amount of activated reserves can be translated to more appropriate

reserve deployment factors or generation participation factors, which are already used by the industry.

REFERENCES

[1]. A. Wood and B. Wollenberg, Power Generation, Operation, and Control, John Wiley and Sons, 2nd edition, New York, 1996.

[2]. H. T. Yang, P. C. Yang, and C. L. Huang, "Evolutionary programming based economic dispatch for units with non-smooth fuel cost functions," IEEE Transactions on Power Systems, vol. 11, no. 1, pp. 112-118, Feb. 1996.

[3]. F. Li and R. Bo, "DCOPF-based LMP simulation: algorithm, comparison with ACOPF, and sensitivity," IEEE Transactions on Power Systems, vol. 22, no. 4, pp. 1475-1485, Nov. 2007.

[4]. O. W. Akinbode and K. W. Hedman, "Fictitious losses in the DCOPF with a piecewise linear approximation of losses," IEEE Power and Energy Society General Meeting, Vancouver BC, pp. 1-5, Jul. 2013.

[5]. P. Sánchez-Martín, and A. Ramos, "Modeling transmission ohmic losses in a stochastic bulk production cost model," Institute for Research in Technology, Madrid 1997. [Online]. Available: http://www.iit.upcomillas.es/~aramos/papers/losses.pdf

[6]. A. Shapiro and A. Philpott, "A tutorial on stochastic programming," [Online]. Available: http://stoprog.org/stoprog/SPTutorial/TutorialSP.pdf

[7]. Y. M. Al-Abdullah, A. Salloum, K. W. Hedman, and V. Vittal, "Analyzing the impacts of constraint relaxation practices in electric energy markets," IEEE Transactions on Power Systems, vol. 31, no. 4, pp. 2566-2577, Oct. 2015.

[8]. T. Ding, R. Bo, F. Li, Y. Gu, Q. Guo, and H. Sun, "Exact penalty function based constraint relaxation method for optimal power flow considering wind generation uncertainty," IEEE Power Engineering Letters, vol. 30, no. 3, pp. 1546-1547, May 2015.

[9]. X. Guo and J. McCally, "Risk-based constraint relaxation for security constrained economic dispatch," 2015 North American Power Symposium, Charlotte, NC, 2015.

[10]. D. Douglass, "High-temperature, low-sag transmission conductors," Electric Power Research Institute, Palo Alto, CA, Tech. Rep. 1001811, Jun. 2002.

[11]. A. G. Exposito, J. R. Santos, and P. C. Romero, "Planning and operational issue arising from the widespread use of HTLS conductors," IEEE Transactions on Power Systems, vol. 22, no. 4, pp. 1446-1455, Nov. 2007.

[12]. B. J. Pierre and G. T. Heydt, “Increased ratings of overhead transmission circuits using HTLS and compact designs,” North American Power Symposium, Champaign IL, pp. 1-6, Sept. 2012.

[13]. R. Gorur, B. Mobasher, and R. Olsen, “Characterization of composite cores for high temperature-low sag (HTLS) conductors: final project report,” [Online]. Available: http://www.pserc.wisc.edu/documents/publications/reports/2009_reports/gorur_pserc_report_t-33_july2009.pdf

[14]. R. Hemmati, R.-A. Hooshmand, and A. Khodabakhshian, “Comprehensive review of generation and transmission expansion planning,” IET Generation, Transmission and Distribution, vol. 7, no. 9, pp. 955-964, Sept. 2013.

[15]. R. Hemmati, R.-A. Hooshmand, and A. Khodabakhshian, “State-of-the-art of transmission expansion planning: Comprehensive review,” Renewable and Sustainable Energy, vol. 23, pp. 312-319, Mar. 2013.

[16]. J. Chan, B. Clairmont, D. Rueger, D. Childs, and S. Karki, “Demonstration of advanced conductors for overhead transmission lines,” Electric Power Research Institute, Palo Alto, CA, Tech. Rep. CEC-500-2013-030, Jul. 2008.

[17]. J. S. Engelhardt, and S. P. Basu, “Design, installation, and field experience with an overhead transmission dynamic line rating system,” in Proc. 1996 IEEE Transmission and Distribution Conference, Los Angeles CA, pp. 366-370, Sep. 1996.

[18]. B. Clairmont, D. A. Douglass, E. C. Bascom, III, and T. C. Raymond, “Increased power flow guidebook: increasing power flow on transmission and substation circuits,” Electric Power Research Institute, Palo Alto, CA, Tech. Rep. 1010627, Nov. 2005.

[19]. S. Uski-Joutsenvuo and R. Pasonen, “Maximising power line transmission capability by employing dynamic line ratings–technical survey and applicability in Finland,” VTT Technical Research Centre, Finland, Tech. Rep. VTT-R-01604-13, Feb. 2013.

[20]. G. Brennan, “Refurbishment of existing overhead transmission lines,” CIGRE, Tech. Rep. B2-203, 2004.

[21]. S. L. Chen, W. Z. Black, and H. W. Loard Jr., “High-temperature ampacity model for overhead Conductors,” IEEE Transactions on Power Delivery, vol. 17, no. 4, pp. 1136-1141, Oct. 2002.

[22]. C.-P. Cheng, C.-W. Liu, and C.-C. Liu, “Unit commitment by Lagrangian relaxation and genetic algorithms,” IEEE Transactions on Power Systems, vol. 15, no. 2, pp. 707-714, May 2000.

[23]. T. Mitani, Y. Mishima, T. Satoh, and K. Nara, "Security constrains unit commitment by Lagrangian decomposition and tabu search," Proceedings of the 13th International Conference on Intelligent Systems Application to Power Systems, Arlington VA, pp. 440-445, Nov. 2005.

[24]. X. Wang, Y. H. Song, and Q. Lu, "Lagrangian decomposition approach to active power congestion management across interconnected regions," IEE Proceedings on Generation, Transmission, and Distribution, vol. 148, no. 5, Sep. 2001.

[25]. A. Papavasiliou and S. S. Oren, "Multiarea stochastic unit commitment for high wind penetration in a transmission constrained network," Operations Research, vol. 61, no. 3, pp. 578-592, May 2013.

[26]. M. L. Fisher, "The Lagrangian relaxation method for solving integer programming problem," Management Science, vol. 50, no. 12, pp. 1861-1871, Dec. 2004.

[27]. R.T. Rockafellar and R. J-B. Wets, "Scenarios and policy aggregation in optimization under uncertainty," Mathematics of Operations Research, vol. 16, no. 1, pp. 119-147, Feb. 1991

[28]. J.-P. Watson and D. L. Woodruff, "Progressive Hedging innovations for a class of stochastic resource allocation problems," Computational Management Science, vol. 8, no. 4, pp. 335-370, Nov. 2011.

[29]. S. M. Ryan, R. J.-B. Wets, D. L. Woodruff, C. Silva-Monroy, and J.-P. Watson, "Toward scalable, parallel progressive hedging for stochastic unit commitment," IEEE Power and Energy Society General Meeting, Vancouver BC, pp. 1-7, Jul. 2013.

[30]. IEEE standard for calculating the current-temperature of bare overhead conductors, IEEE Standard 738-2006, Jan. 2006.

[31]. R. Stephen, D. Douglas, and M. Gaudry, "Thermal behavior of conductors," CIGRE ELECTRA, No. 144, Oct. 1992.

[32]. N. P. Schmidt, "Comparison between IEEE and CIGRE ampacity standards," IEEE Transactions on Power Delivery, vol. 14, no. 4, pp. 1155-1159, Oct. 1999.

[33]. W. Z. Black and R. L. Rehberg, "Simplified model for steady state and real-time ampacity of overhead conductors," IEEE Transactions on Power Apparatus and Systems, vol. PAS-104, no. 10, pp. 2942-2953, Oct. 1985.

[34]. J. R. Harvey, "Effect of elevated temperature operation on the strength of aluminum conductors," IEEE Transactions on Power Apparatus and Systems, vol. PAS-91, no. 5, pp. 1769–1772, Sept./Oct. 1972.

[35]. IEEE guide for determining the effects of high-temperature operation on conductors, connectors, and accessories, IEEE Standard 1283-2013, Aug. 2013.

[36]. V. T. Morgan, "The loss of tensile strength of hard-drawn conductors by annealing in service," IEEE Transactions on Power Apparatus and Systems, no. 3, pp. 700-709, May 1979.

[37]. Midcontinent Independent System Operator, "Energy and operating reserve markets business practices manual," [Online]. Available at: https://www.misoenergy.org/Library/BusinessPracticesManuals/Pages/BusinessPracticesManuals.aspx

[38]. Monitoring Analytics., "Quarterly state of the market report for PJM: January through June," Monitoring Analytics, Southeastern, PA, Aug. 2016.

[39]. Electric Reliability Council of Texas, "SCED penalty factor," [Online]. Available at: www.ercot.com/content/meetings/natf/keydocs/2010/0809/08_sced_penalty_factor_100809.ppt

[40]. D. B. Patton, P. L. VanSchaick, and J. Chen, "2015 State of the market report for the New York ISO markets," Potomac Economics, Fairfax, VA, May 2016.

[41]. California Independent System Operator, "Business practice manual for market operations," [Online]. Available at: https://www.caiso.com/rules/Pages/BusinessPracticeManuals/Default.aspx

[42]. Southwest Power Pool, "VRL analysis," [Online]. Available at: https://www.spp.org/documents/29222/2014_2015%20vrl%20analysis.pdf

[43]. R. Karki, P. Hu, and R. Billinton, "Adequacy criteria and methods for wind power transmission planning," IEEE Power and Energy Society General Meeting, Calgary AB, pp. 1-7, Jul. 2009.

[44]. G. Latorre, R. D. Cruz, J. M. Areiza, and A. Villegas, "Classification of publications and models on transmission expansion planning," IEEE Transactions on Power Systems, vol. 18, no. 2, pp. 938-946, May 2003.

[45]. Western Electricity Coordinating Council, "Transmission expansion planning," [Online]. Available: http://www.wecc.biz/committees/BOD/TEPPC/

[46]. A. H. El-Abiad and Y. P. Dusonchet, "Discrete optimization and the planning of electric power networks," IEEE Transactions on Circuit Theory, vol. CT-20, no.3, pp. 230-238, May 1973.

[47]. M. El-Metwally and A. Harb, “Transmission planning using admittance approach and quadratic programming,” Electric Machines and Power Systems, vol. 21, no. 1, pp. 69-83, Jan. 1993.

[48]. Z. M. Al-Hamouz and A. S. Al-Faraj, “Transmission expansion planning using nonlinear programming,” in Proc. 2002 IEEE Power Engineering Society Transmission and Distribution Conference, vol. 1, pp. 50-55, Oct. 2002.

[49]. N. Alguacil, A. L. Motto, and A. J. Conejo, “Transmission expansion planning: a mixed-integer LP approach,” IEEE Transactions on Power Systems, vol. 18, no. 3, pp. 1070–1077, Aug. 2003.

[50]. A. Khodaei, M. Shahidehpour, L. Wu, and Z. Li, “Coordination of short-term operation constraints in multi-area expansion planning,” IEEE Transactions on Power Systems, vol. 27, no. 4, pp. 2242-2250, Nov. 2012.

[51]. I. G. Sanchez, R. Romero, J. R. S. Mantovani, and A. Garcia, “Interior point algorithm for linear programming used in transmission network synthesis,” Electric Power Systems Research, vol. 76, no. 1, pp. 9-16, Sep. 2005.

[52]. E. J. de Oliveira, I. C. da Silva, J. L. R. Pereira, and S. Carneiro, “Transmission system expansion planning using a sigmoid function to handle integer investment variables,” IEEE Transaction on Power Systems, vol. 20, no.3, pp. 1616-1621, Aug. 2005.

[53]. S. Binato, M. V. F. Pereira, and S. Granville, “A new Benders decomposition approach to solve power transmission network design problems,” IEEE Transactions on Power Systems, vol. 16, no. 2, pp. 235-240, May 2001.

[54]. R. C. Leou, “A multi-year transmission planning under a deregulated market,” International Journal of Electrical Power & Energy Systems, vol. 33, no. 3, pp. 708–714, Mar. 2011.

[55]. S. Binato, G. C. de Oloveira, and J. de Araujo, “A greedy randomized adaptive search procedure for transmission expansion planning,” IEEE Transactions on Power Systems, vol. 16, no. 2, pp. 247-253, May 2001.

[56]. E. L. da Silva, J. M. A. Ortiz, G. C. de Oliveira, and S. Binato, “Transmission network expansion planning under a tabu search approach,” IEEE Transactions on Power Systems, vol. 16, pp. 62-68, Feb. 2001.

[57]. H. Kim, S. Moon, J. Choi, C. Lee, J. Wang, and R. Billinton, “Transmission system expansion planning of KEPCO system (Youngnam area) using fuzzy set theory,” IEEE Power Engineering Society Summer Meeting 2002, vol. 1, pp. 535-540, Jul. 2002.

[58]. F. F. Wu, F. L. Zheng, and F. S. Wen, “Transmission investment and expansion planning in a restructured electricity market,” Energy, vol. 31, no. 7, pp. 954-966, Jun. 2006.

[59]. California Independent System Operator, “Transmission economic assessment methodology (TEAM),” Jun. 2004. [Online]. Available: http://www.caiso.com/docs/2004/06/03/2004060313241622985.pdf

[60]. G. A. Orfanos, P. S. Georgilakis, and N. D. Hatziargyriou, “Transmission expansion planning of systems with increasing wind power integration,” IEEE Transactions on Power Systems, vol. 28, no. 2, pp. 1355-1362, May. 2013.

[61]. H. Yu, C. Y. Chung, K. P. Wong, and J. H. Zhang, “Expansion planning method with consideration of load and wind farm uncertainties,” IEEE Transactions on Power Systems, vol. 24, no. 3, pp. 1568-1576, Aug. 2009.

[62]. M. Moeini-Aghtaie, A. Abbaspour, and M. F Fotuhi-Firuzabad, “Incorporating large-scale distant wind farms in probabilistic transmission expansion planning—Part I: Theory and algorithm,” IEEE Transactions on Power Systems, vol. 27, no. 3, pp. 1585-1593, Aug. 2012.

[63]. M. Moeini-Aghtaie, A. Abbaspour, and M. F Fotuhi-Firuzabad, “Incorporating large-scale distant wind farms in probabilistic transmission expansion planning—Part II : Case Studies,” IEEE Transactions on Power Systems, vol. 27, no. 3, pp. 1594-1601, Aug. 2012.

[64]. B. Banerjee, D. Jayaweera, and S. M. Islam, “Optimal scheduling with dynamic line ratings and intermittent wind power,” IEEE Power and Energy Society General Meeting, Washington DC, pp. 1-5, Jul. 2014.

[65]. P. Pinson, H. Madsen, H. A. Nielsen, G. Papaefthymiou and B. Klöckl, “From probabilistic forecasts to statistical scenarios of short-term wind power production,” Wind energy, vol. 12, no. 1, pp. 51-62, Sep. 2008.

[66]. J. M. Morales, R. Minguez and A. J. Conejo, “A methodology to generate statistically dependent wind speed scenarios,” Applied Energy, vol. 87, no. 3, pp. 843-855, Mar. 2010.

[67]. N. Gröwe-Kuska, H. Heitsch, and W. Römisch, “Scenario reduction and scenario tree construction for power management problems,” in Proc. IEEEE Power Tech Conf., Bologna, Italy, vol. 3, pp. 23-26, Jun. 2003.

[68]. Z. Zhou, C. Liu, and A. Botterud, “Stochastic methods applied to power system operations with renewable energy: a review,” Technical Report ANL/ESD-16/14 Argonne National Laboratory, Argonne, IL, 2016.

[69]. S. Takriti, J. R. Birge, and E. Long, “A stochastic model for the unit commitment problem,” IEEE Transactions on Power System, vol. 11, no. 3, pp. 1497-1507, Aug. 1996.

[70]. J. M. Arroyo and F. Galiana, “Energy and reserve pricing in security and network-constrained electricity markets,” IEEE Transactions on Power System, vol. 20, no. 2, pp. 634-643, May 2005.

[71]. F. Bouffard, F. D. Galiana, and A. J. Conejo, “Market-clearing with stochastic security- Part I: formulation,” IEEE Transactions on Power System, vol. 20, no. 4, pp. 1818-1816, Nov. 2005.

[72]. F. Bouffard, F. D. Galiana, and A. J. Conejo, “Market-clearing with stochastic security- Part II: case studies,” IEEE Transactions on Power System, vol. 20, no. 4, pp. 1818-1816, Nov. 2005.

[73]. A. Papavasiliou, S. S. Oren, and R. P. O’Neil, “Reserve requirements for wind power integration: a scenario-based stochastic programming framework,” IEEE Transactions on Power System, vol. 26. no. 4, pp. 2197-2206, Nov. 2011.

[74]. J. Wang, M. Shahidephour, and Z. Li, “Security-constrained unit commitment with volatile wind power generation,” IEEE Transactions On Power System, vol. 23, no. 3, pp. 1319-1327, Aug. 2008.

[75]. F. Bouffard and F. D. Galiana, “Stochastic security for operations planning with significant wind power generation,” IEEE Power and Energy Society General Meeting, July 2008.

[76]. H. Wu and M. Shahidehpour, “Stochastic SCUC solution with variable wind energy using constrained ordinal optimization,” IEEE Transactions on Sustainable Energy, vol. 5, no. 2, pp. 379-388, Apr. 2014.

[77]. J. J. Hargreaves and B. F. Hobbs, “Commitment and dispatch with uncertain wind generation by dynamic programming,” IEEE Transactions on Sustainable Energy, vol. 3, no. 4, pp. 724-734, Oct. 2012.

[78]. P. Meibom, R. Barth, B. Hasche, H. Brand, C. Weber and M. O'Malley, “Stochastic optimization model to study the operational impacts of high wind penetrations in Ireland,” IEEE Transactions on Power Systems, vol. 26, no. 3, pp. 1367-1379, Aug. 2011.

[79]. A. Tuohy, P. Meibom, E. Denny and M. O'Malley, “Unit commitment for systems with significant wind penetration,” IEEE Transactions on Power Systems, vol. 24, no. 2, pp. 592-601, May 2009.

[80]. L. Wu, M. Shahidehpour and T. Li, "Cost of reliability analysis based on stochastic unit commitment," IEEE Transactions on Power Systems, vol. 23, no. 3, pp. 1364-1374, May 2008.

[81]. J. Wang, J. Wang, C. Liu and J. P. Ruiz, "Stochastic unit commitment with sub-hourly dispatch constraints," Applied Energy, vol. 105, pp. 418-422, May 2013.

[82]. Y. Yang, R. G. Harley, D. Divan, and T. G. Havetler, "Overhead conductor thermal dynamics identification by using echo state networks," International Joint Conference on Neural Networks, Atlanta GA, pp. 3436-3443, Jun. 2009.

[83]. Aluminum Association, Aluminum electrical conductor handbook, 2nd ed. Washington, DC, 1982.

[84]. H. A. Smolleck and J. P. Sims, "Guidelines for the selection and operation of bare ACSR conductors with regard to current-carrying capacity," Electric Power Systems Research, vol. 5, no. 3, pp. 179-190, Sep. 1982.

[85]. M. M. I. Bhuiyan, P. Musilek, J, Heckenbergerova, and D. Koval, "Evaluating thermal aging characteristics of electric power transmission lines," 23rd IEEE Canadian Conference on Electrical and Computer Engineering, Calgary AB, pp. 1-4, May 2010.

[86]. PJM Overhead Conductor Ad Hoc Committee, "Bare overhead transmission conductor rating," [Online]. Available: http://www.pjm.com/~/media/planning/design-engineering/maac-standards/bare-overhead-transmission-conductor-ratings.ashx

[87]. ALCAN, "Aluminum Conductor Steel Reinforced (ACSR) cables," [Online]. Available: ece.citadel.edu/mckinney/elec403/ACSR.pdf

[88]. 3M, "3M™ Aluminum Conductor Composite Reinforced (ACCR)," [Online]. Available: http://solutions.3m.com/wps/portal/3M/en_US/EMD_ACCR/ACCR_Home/TechnicalInfo/ProductDataSpecs/

[89]. K. Adomah, Y. Mizuno, K. Naito, "Probabilistic assessment of the reduction in tensile strength of an overhead transmission line's conductor with reference to climatic data" IEEE Trans. Power Delivery, vol. 15, no. 4, pp. 1221-1224, Oct. 2000.

[90]. K. W. Hedman, M. Ferris, R. P. O'Neill, E. Fisher, and S. S. Oren, "Co-optimization of generation unit commitment and transmission switching with N-1 reliability," vol. 25, no. 2, pp. 1052-1063, May 2010.

[91]. D. Rajan and S. Takriti, "Minimum up/down polytopes of the unit commitment problem with start-up costs," IBM Research Report, June 2005.

[92]. K. W. Hedman, R. P. O'Neill, and S. S. Oren, "Analyzing valid inequalities of the generation unit commitment problem," 2009 IEEE/PES Power Systems Conference and Exposition, Seattle WA, pp. 1-6, 15-18, Mar. 2009.

[93]. Y. Gu, J. D. MacCalley, and M. Ni, "Coordinating large-scale wind integration and transmission planning," IEEE Transactions on Sustainable Energy, vol. 3, no. 4, pp. 652-659, Oct. 2012.

[94]. R. Fourer, "AMPL models for not linear optimization using linear solvers," presented at the EURO-INFORMS Joint International. Meeting, Rome, Italy, 2013.

[95]. National Renewable Energy Laboratory, "Western wind resource dataset," [Online]. Available: http://wind.nrel.gov/Web_nrel/

[96]. N. Growe-Kuska, H. Heitsch, and W. Romisch, "Scenario reduction and scenario tree construction for power management problems," in Proc. IEEE Power Tech Conference, Bologna, Italy, vol. 3, pp. 23-26, Jun. 2003.

[97]. "Power Systems Test Case Archive," [Online]. Available at: http://www.ee.washington.edu/research/pstca/

[98]. C. Grigg, et al., "The IEEE reliability test system-1996. A report prepared by the reliability test system task force of the application of probability methods subcommittee," IEEE Transactions on Power Systems, vol. 14, no. 3 pp. 1010-1020, 1999.

[99]. Energy Informative Administration, "Short-term energy outlook," [Online]. Available: http://www.eia.gov/forecasts/steo/tables/pdf/2tab.pdf

[100]. Energy Informative Administration, "Uranium marketing annual report," [Online]. Available: http://www.eia.gov/uranium/marketing/?src=Nuclear-f1

[101]. Southwire Company, "ACSR," [Online]. Available at: http://www.southwire.com/products/ACSR.htm

[102]. General Cable, "Bare aluminum conductor," [Online]. Available at: http://www.stabiloy.com/nr/rdonlyres/d83c028b-0d2a-4680-84e7-bc9b44e7129b/0/pbare.pdf

[103]. Commerce Commission New Zealand, "Bunnythorpe-Haywards A and B lines conductor replacement investment proposal - options and costing report," [Online]. Available at: http://www.comcom.govt.nz/regulated-industries/electricity/electricity-transmission/

[104]. Energy Informative Administration, “Annual energy outlook 2014,” [Online]. Available: http://www.eia.gov/forecasts/aeo/MT_electric.cfm

[105]. Trading Economics, “US interest rate,” [Online]. Available: http://www.tradingeconomics.com/united-states/interest-rate

[106]. M. Anvari, F. Razavi, and A. A. Nazari, “Electrical and economic study of applying the ACSS conductor in TREC subtransmission network,” Indian Journal of Science and Technology, vol. 6, no. 1, pp. 65-73, Jan. 2013.

[107]. S. Z. Moghaddam, H. Monsef, and M. Jafari, “A new heuristic method for transmission expansion planning using AHP,” 2011 10th International Conference on Environment and Electrical Engineering, Rome, pp. 1-4, May 2011.

[108]. M. O. Buygi, G. Balzer, H. M. Shanechi, and M. Shahidehpour, “Market-based transmission expansion planning,” IEEE Transactions on Power Systems, vol. 19, pp. 2060-2067, Nov. 2004.

[109]. M. Tim, C. Trevor, and W. Dan, “Capital costs for transmission and Heysubstations - recommendations for WECC transmission expansion planning,” Black and Veatch, Phoenix, AZ, Tech. Rep. 176322, Oct. 2012.

[110]. A. Papalexopoulos, “Theoretical and practical considerations in implementing and using a reliability unit commitment (RUC) in restructured electricity markets,” in IEEE PES General Meeting, pp. 1-2, Montreal, Canada, 2006.

[111]. Y. M. Al-Abdullah, M. Abdi-Khorsand, and K. W. Hedman, “The role of out-of-market corrections in day-ahead scheduling,” IEEE Transactions on Power Systems, vol. 30, no. 4, pp. 1937-1946, Jul. 2015.

[112]. K. W. Hedman and V. Vittal, “Constraint relaxations: analyzing the impacts on system reliability, dynamics, and markets (M-29),” Power Systems Engineering Research Center: Industry Advisor Conference Calls, Sep. 17, 2013 and Apr. 10, 2014.

[113]. H. Wan, J. D. McCalley, and V. Vittal, “Increasing thermal rating by risk analysis,” IEEE Transactions on Power Systems, vol. 14, no. 3, pp. 815-828, Aug. 1999.

[114]. Reliability Standards for the Bulk Electric Systems of North America, NERC Std. BAL-001-1, Feb. 2016.

[115]. University of Arizona, “Arizona meteorological network weather data,” [Online]. Available at: http://ag.arizona.edu/azmet/

[116]. Y. Chen, P. Gribik, and J. Gardner, “Incorporating post zonal reserve deployment transmission constraints into energy and ancillary service co-optimization,” IEEE Transactions on Power Systems, vol. 29, no. 2, pp. 537-549, Mar. 2014.

[117]. CAISO, “Generator contingency and remedial action scheme modeling,” Mar. 2017 [Online]. Available: http://www.caiso.com/Documents/RevisedStrawProposal-GeneratorContingencyRemedialActionScheme.pdf